ANTIFUNGAL ASSESSMENTS, CHEMOGENOMIC AND TRANSCRIPTOMIC ANALYSES, AND STRUCTURE-ACTIVITY RELATIONSHIPS OF BIOACTIVE AURONE COMPOUNDS

By

Fatmah M. Alqahtani

A Dissertation Submitted in Partial Fulfillment of the Requirements for the Degree of Doctor of Philosophy in Molecular Biosciences

Middle Tennessee State University

Fall 2021

Dissertation Committee:

Dr. Mary B. Farone, Chair

Dr. Scott T. Handy

Dr. Anthony L. Farone

Dr. Rebecca L. Seipelt-Thiemann

Dr. Paul C. Kline

Dedicated to my parents, husband, siblings, nephews, and nieces.

ACKNOWLEDGMENTS

First, I would like to thank the King Khalid University (KKU) for providing me a full scholarship to pursue this degree. My deepest appreciation and indebtedness to my advisor Dr. Mary Farone for her guidance, support and encouragement. Also, I would like to extent my gratitude to my committee members for their time and support. My sincere thanks go to the Molecular Biosciences (MOBI) doctoral program and the Tennessee Center for Botanical Medicine Research for providing the research support and to the Biology Department at Middle Tennessee State University (MTSU) for providing the convenient environment during my stay as a doctoral student at MTSU.

DECLARATION

I declare that all the contents presented are my original works performed at Middle Tennessee State University. The materials and results presented in chapter I and II of this dissertation have been published in the following peer-reviewed journals:

1. **Alqahtani FM, Arivett BA, Taylor ZE, Handy ST, Farone AL, Farone MB** (2019) Chemogenomic profiling to understand the antifungal action of a bioactive aurone compound. ***PLoS ONE*** 14(12): e0226068. https://doi.org/10.1371/journal.pone.0226068.

2. **Alqahtani FM, Handy ST, Sutton CL and Farone MB** (2021) Combining Genome-Wide Gene Expression Analysis (RNA-seq) and a Gene Editing Platform (CRISPR-Cas9) to Uncover the Selectively Pro-oxidant Activity of Aurone Compounds Against *Candida albicans*. ***Front. Microbiol.*** 12:708267. doi: 10.3389/fmicb.2021.708267.

ABSTRACT

Candida spp. as commensal colonizers of mucocutaneous surfaces in humans are the major fungal cause of bloodstream infections, resulting in 50,000 deaths every year. Because of the paucity of fundamental antifungal treatments along with the recurrent emergence of resistant strains, the urgency for new antifungal agents with selective and novel targets necessitates the efforts of laboratory research. Complementary to such attempts for identification of novel anti-*Candida* agents, two synthetically aurones, SH1009 and SH9051, have shown significant inhibitory activities against *Candida* spp. The main goal of this research was to assess antifungal activity and mammalian cell cytotoxicity and comprehensively characterize the modes of action for aurones SH1009 and SH9051.

Aurone SH1009 exhibited significant antifungal activity against *Candida* spp., including resistant isolates, with fungistatic pharmacodynamic properties. SH1009 treatment of a pooled genome-wide set of *Saccharomyces cerevisiae* deletion mutants demonstrated a set of sensitive and resistant growth responses in mutants encoding cell cycle-dependent organization of actin cytoskeleton. Accordingly, phenotypic studies revealed cell cycle arrest at the G1 phase in SH1009-treated *Candida albicans* along with abnormally interrupted actin dynamics and enlarged, unbudded cells, validating the chemical genetic interaction and suggesting a novel mode of action for aurone SH1009 as an antifungal.

In vitro cytotoxicity assays using human cell lines showed selective toxicity of SH1009 toward fungal cells and less selectivity in SH9051-treated cells. In an attempt to increase antifungal activity by combining both aurones, antifungal synergy was

detected as an indifferent interaction, suggesting different modes of action for the aurones. To interpret these differences, transcriptome changes in SH1009- and SH9051-treated *C. albicans* were analyzed, revealing common and unique pathways enriched consistently based on the chemical structure of each aurone. A reverse genetic approach coupled with structure-activity relationship analyses demonstrated that trehalose was uniquely responsible for SH1009 resistance. SH9051 uniquely stimulated sulfur amino acid catabolism, and the core chemical structure of both aurones commonly promoted intracellular oxidative stress.

The results of these studies determined a selectively novel molecular target, for aurone SH1009 as a promising antifungal and revealed cellular effects for different functional groups of the aurone, paving the way for future development and investigation.

TABLE OF CONTENTS

LIST OF FIGURES

CHAPTER I

CHAPTERII

LIST OF TABLES

CHAPTER I

LIST OF APPENDICES

CHAPTER I

CHAPTER II

INTRODUCTION

Pathogenic Fungi: A Public Health Threat.

Fungi are a kingdom of eukaryotic organisms of the global tree of life with massive diversity in morphological phenotypes, biochemical properties, and lifestyles, ranging from mushrooms and filamentous fungi to single-cell yeasts and including as many as six million species (American Academy of Microbiology Colloquium Report, 2019). These organisms are ubiquitous on the biosphere and play critical roles to maintain the global ecological equilibrium as mutualists with plants (mycorrhizae) and decomposers (soil and aquatic hyphomycetes), and thereby function as fundamental drivers for organic matter recycling and food web dynamics (Grossart et al., 2019; Jansson & Hofmockel, 2020). Besides the numerous benefits of domesticated fungi to humans, either for their use for the preparation of bread and spiritual beverages through fermentation and as industrial producers of biotechnological products (e.g., enzymes and antibiotics), other fungi can also infect specific hosts and inflict damage.

Pathogenic fungi are known to seriously impact human life indirectly by causing fungal diseases to crops, leading to reduced food supply and directly causing mortality, posing a public health threat. According to recent global estimates, human fungal pathogens affect more than one billion individuals throughout the world, in which 15-30% of these infections are considered serious and cause more than 1.6 million deaths each year, exceeding the mortality rate of malaria by threefold (Bongomin et al., 2017). In 2001, ~ 300 fungal species were linked directly to diseases in human (Taylor et al., 2001); however, by 2018, more than 1500 different fungal species had been identified and isolated from human specimens (Wickes & Wiederhold, 2018). The increase in incidence and prevalence of fungal diseases across the globe is primarily dependent on

the patient's immunity in addition to socio-economic and geo-ecological characteristics. For instance, the epidemiology of cryptococcal meningitis is highly associated with AIDS patients who cannot access anti-retroviral therapy in developing countries, while in developed countries, immunosuppressive chemotherapy of cancer and transplant surgeries are the major drivers of invasive candidiasis and chronic pulmonary aspergillosis (Janbon et al., 2019).

Although several hundred fungal species can infect humans, only a small minority of these pathogenic fungi can severely parasitize on humans (Köhler et al., 2014). *Aspergillus*, *Candida*, *Cryptococcus,* and *Histoplasma* species remain the major systemic human fungal pathogens that cause invasive fungal infections (Bongomin et al., 2017). Unlike these environmental pathogenic fungi (*Aspergillus fumigatus, Cryptococcus neoformans,* and *Histoplasma capsulatum*) that inadvertently cause invasive infections through inhalation of spores or other mucus membrane or skin contact with viable cells, *Candida* spp. naturally exist as a commensal of the human microbiome. By occupying mucocutaneous surfaces of skin, genitourinary, and gastrointestinal tracts, *Candida* spp. are the primary opportunistic human fungal pathogen that could establish invasive infection if the host immune defense system is attenuated (Kim, 2016).

Changes in the Epidemiology of Candidiasis

Candidiasis can include infections that appear as white spots in the mouth and oropharynx (thrush) and other mild mucosal infections such as superficial, esophageal and vulvovaginal candidiasis. In more chronic situations, if the mucosal membranes or gastrointestinal barriers are disrupted by vascular catheters or abdominal surgery, *Candida* can disseminate hematogenously, causing invasive candidiasis infections

(candidemia in the bloodstream) and colonize different organs, causing tissue candidiasis (candida in a sterile site) in which end-organ abscesses may damage the kidney, brain, heart, liver, spleen, bone, and joints. During candidemia, *Candida* may disseminate again and lead to further metastatic infections as a result of secondary candidemia (Kullberg & Arendrup, 2015).

Over the past few decades, the epidemiology of invasive candidiasis has dramatically evolved and is associated with significant morbidity, mortality, and high healthcare costs due to the expanding population of immunosuppressed and hospitalized patients and advances in medical care practices (e.g., intensive care use, chemotherapy, transplantation, and catheterization) (Lamoth et al., 2018). Among various fungal pathogens, *Candida* spp. are still the leading cause of fungal nosocomial (healthcare-associated) bloodstream infections worldwide (Chen et al., 2020; Li et al., 2019; Méan et al., 2008; Singh & Wulansari, 2018) and the fourth leading cause of these infections in USA hospitals (Rajendra, 2017), burdening both the healthcare institutions and costs (Jahagirdar et al., 2018).

The mortality rate of candidemia was estimated as 40% (Rajendra, 2017), but it can increase by as much as 20% if preemptive treatment is delayed more than 12 hours after collecting the initially positive blood culture (Morrell et al., 2005). In fact, a combination of several critical factors such as imprecise diagnosis, inappropriate disease management, scarce expertise and tools in medical mycology, and general condition of the patient can raise the mortality rate to an alarming level (Wickes & Wiederhold, 2018). Mortality rates in particular regions can be much higher; for instance, in South Africa (60%) and Brazil (72%) (Lamoth et al., 2018). The mortality

rate in critically ill patients or patients with candidemia-induced septic shock reached up to 87-90% in the USA (Dimopoulos et al., 2008; Guzman et al., 2011).

Furthermore, a progressive shift from the most common cause species of candidiasis (*C. albicans*) to non-*albicans* spp. has been noted in most medical centers of the world (Lamoth et al., 2018). Among the 150 known *Candida* species, only 14 have caused infections in humans in addition to *C. albicans*. These species include *C. glabrata*, *C. tropicalis*, *C. parapsilosis*, *C. krusei*, *C. guilliermondii*, *C. lusitaniae*, *C. dubliniensis*, *C. pelliculosa*, *C. kefyr*, *C. lipolytica*, *C. famata*, *C. inconspicua*, *C. rugosa*, and *C. norvegensis* (Rajendra, 2017). Some of these emerging species are associated with pathogenic virulence and high mortality rate (Lamoth et al., 2018), in which the most recent example was the newly discovered *C. auris*, which has caused an unusually high death rate due to its multidrug resistance and rapidly expanding global outbreaks (Wickes, 2020).

However, geographical location significantly determines the overall species distribution. In North America and Europe, *C. albicans* had previously dominated as causing the highest proportion of *Candida* infections, but *C. glabrata* has recently become the predominant species. In other different parts of the world, *C. albicans* is yet the most prevalent species, followed by non-*albicans* species such as *C. parapsilosis* in South Europe, South America, and Africa, and *C. tropicalis* in Asia (Lamoth et al., 2018). These epidemiologic changes in the species responsible for invasive candidiasis necessitates public health efforts to understand the pathogenicity of these commensal organisms and, more importantly, develop effective anti-*Candida* therapies.

Candida albicans - SC5314 Pathogenicity as the Model Fungal Pathogen

Candida albicans - SC5314 is a clinical strain that was isolated for the first time from a patient with disseminated candidiasis in 1984 (Gillum et al., 1984), and the first pathogenic fungus that was sequenced completely in 2004 as a diploid organism with 2X 15.845 MB genome size distributed to 8 chromosomes (Chr1-7 and ChrR) (Jones et al., 2004). The availability of a free online database (www.candidagenome.com) of strain SC5314 provides access to genomic sequence data, functional context to genes and proteins, and a set of bioinformatic analysis tools, enabling study of this reference strain at the molecular level (Skrzypek et al., 2018). Despite the obligate diploid state of the majority of commensal and clinical isolates, the highly natural heterozygosity, chromosome translocations and polymorphism of the genome can lead to infrequently discrete isolates in ploidy states, ranging from haploid to tetraploid and aneuploid states. Also, this genomic plasticity drives the abilities of *C. albicans* to transcriptionally regulate genes in order to adapt to diverse host niches, which is the hallmark of *C. albicans* virulence factors and drug resistance (Rajendra, 2017).

C. albicans can asymptomatically exist in the human body (e.g., skin, oral cavity, gastrointestinal, and urogenital tracts) and interacts naturally with nutritional components, competitor microbiota, and the innate immune system. In case of disruption of intact skin or mucosal membrane or deficiency in production of cell surface pattern recognition receptors that are involved in recognition of *Candida* spp. (STAT1, Dectin-1, and CARD9), *C. albicans* can establish more widespread infection primarily by overexpressing adherent cell wall components (Hwp1 and Als3), facilitating adhesion to the host cell. After the adherence step, the germ tube starts to grow from the yeast cell in order to form true hyphae, the most critical virulence factor

of *C. albicans* pathogenicity, which then penetrates epithelial cell lines. These epithelial cells act as a physical barrier and as a first line of defense against invading filamentous growth and can activate the immune system by producing cytokines and chemokines for the recruitment of phagocytosis and antimicrobial secretions (Rajendra, 2017).

This essential step of the immune activation by epithelial cells explains how the immune system can discriminate between commensal and pathogenic *Candida* states. Additionally, it demonstrates that the filamentous, but not the yeast form, can activate inflammation due to the presence of critical pathogen-associated molecular patterns (PAMPs) present on hyphal cells, but absent on yeast cells, namely the mannan fibrils. Besides the role of hyphal growth in the pathogenesis of *C. albicans,* other virulence factors are significant, including secretion of hydrolytic enzymes, biofilm formation, tolerance to host-imposed stress, and the presence of robust metabolic machinery (Höfs et al., 2016).

Noteworthy, the pathogenic ability of this fungus to adhere, switch to filamentous growth, and form biofilm is not only specialized for biotic surfaces, but also for abiotic surfaces, which can lead to contamination of medical devices such as endotracheal tubes, catheters, and pacemakers. As a consequence of this critical characteristic, approximately half of the candidiasis in healthcare-associated infections are caused by *Candida*-contaminated medical devices (Kojic & Darouiche, 2004).

Antifungal Agents and Emergence of Resistance

There are five groups of licensed antifungal agents as defined by their mode of action. Group I: polyenes (amphotericin B) are the oldest fungicidal drug for treating fungal infection and are produced by *Streptomyces* bacteria. The structure binds to

plasma membrane ergosterol, causing high permeability leading to fungal cell death. A defect in the *Candida ERG3* gene can lead to the accumulation of other sterols instead of ergosterol, resulting in amphotericin B resistance. Another group of fungicidal drugs, group II: echinocandins (caspofungin), are more recently introduced antifungal drugs that inhibit β(1,3)-glucan synthase in the cell wall; however, a mutation in the *FKS1* gene, which encodes the catalytic subunit of the β(1,3)-glucan synthase, results in resistance to echinocandins. Group III: azoles (fluconazole) are widely fungistatic-used drugs for treating candidiasis infections. These inhibit lanosterol 14 α-demethylase in the ergosterol biosynthesis pathway which results in disrupting fungal cell membranes. The hyperactivity of transcriptional activators, *TAC1* and *MRR1*, which mediate the expression of drug efflux pumps, decreases the intracellular accumulation of azoles, leading to fluconazole resistance. Group IV: synthetic pyrimidines (5-fluorocytosine) analogues affect fungal pyrimidine metabolism by inhibiting DNA synthesis and disturb protein synthesis. The hypersynthesis of pyrimidines can decrease the antifungal activity of 5-fluorocytosine, resulting in resistant strains. Group V: allylamines (terbinafine) block squalene epoxidase activity in the ergosterol biosynthesis pathway, but the upregulation of genes that encode membrane transport proteins causes an ejection of terbinafine out of the cell (Bondaryk et al., 2013; Prasad et al., 2019).

Despite the availability of antifungal therapy, the number of antifungal drug classes is limited compared to antibacterial therapy, and the range of their targets is narrow, mostly targeting cell wall formation and ergosterol biosynthesis. Additionally, the ongoing resistance mechanisms, such as drug extrusion by active efflux, drug target overexpression or alteration, and regulating tolerance toward the oxidative stress, along

with reports of clinical standard-antifungal drug failures, jeopardize the antifungal therapy field (Alexander et al., 2013; Shor & Perlin, 2015). Therefore, the World Health Organization and Centers for Disease Control and Prevention have placed drug-resistant *Candida* spp. among the threat lists (World Health Organization Meeting Report, 2020).

Answering the question "Is there an emerging need for new antifungals?", not only did the author of an Expert Opinion on Emerging Drugs article epidemiologically justify the urgent need, but the medical mycology community is also crying out for new drugs (Perfect, 2016), emphasizing that the newest class of antifungals (echinocandins) were discovered nearly 50 years ago (Aldholmi et al., 2019). Fortunately, the business climate for pharmaceutical companies is now favoring antifungal design and development. The Generating Antibiotic Incentives Now (GAIN) Act and the American Food and Drug Administration (FDA) have placed the name of *Candida* on their list of qualifying pathogens. Thus, any novel antifungal therapy directed against this species will benefit from incentives, including priority review, eligibility for fast-track description, and additional 7-year marketing exclusivity (Perfect, 2016).

Natural Products as Promising Sources of Antifungal Scaffolds

Bioactive compounds that are derived from a variety of organisms, including bacteria, algae, fungi, plants, or even sponges, have been considered as rich sources for antifungal drug discovery (Aldholmi et al., 2019). The most successful example in the antifungal arena was the isolation of the natural product polyenes (amphotericin B) from *Streptomyces* spp. of bacteria. Another example are the natural products, echinocandins, first described from *Aspergillus nidulans*, and utilized clinically as the semisynthetic caspofungin. These antifungal drugs are currently considered the optimal

drugs to treat fungal systemic infections in immunosuppressed patients because they are the sole therapies with fungicidal capacity and broad spectrum of activity, emphasizing the significance of studying the natural products as under-utilized sources of antifungal medicines.

As a result of a long history of competitive interactions with fungi, plants have evolutionarily evolved novel chemical skeletons with complexities and diversities that are likely associated with anti-fungal bioactivities. These structures include heterocyclic substituents, multiple chiral centers, and polycyclic frameworks (Di Santo, 2010; Vidyasagar, 2016). Flavonoids are one such class of plant-derived chemicals and can act as antioxidants, pigments, and protective agents against ultraviolet light in plants, These compounds are structurally diverse and have therapeutic properties (Treml & Šmejkal, 2016).

The Tennessee Center for Botanical Medicine Research (TCBMR) at Middle Tennessee State University (MTSU) was established in 2011 to investigate botanical chemicals that have medicinal properties. One main branch of ongoing projects in this center was the diversity-oriented synthesis approach on the flavonoid subclass, aurones (2-benzylidenebenzofuran-3-(2H)-ones) to generate various aurone analogues that have since been studied for their utilities as anticancer (Alsaif, 2017), anti-inflammatory (Park et al., 2017), and antifungal treatments (Sutton et al., 2017).

Aurones SH1009 and SH9051 demonstrated significant inhibitory activities as anti-*Candida* agents among the other aurone derivatives. Therefore, the overall goal in the current project was to further assess the antifungal activity and selectivity of SH1009 and SH9051 and to study the modes of action in *C. albicans.* Although both aurones inhibited the pathogenic *C. albicans* efficiently, they exhibited different

selectivity indexes and an indifferent interaction, and in this study were shown to target different metabolic pathways. Both aurones increased the intracellular oxidative stress in *C. albicans,* and the functional groups in aurone SH1009 were shown to selectively target the oxidative stress protectant pathway of trehalose biosynthesis. In contrast, the activity of the functional group of aurone SH9051 deviated from affecting only oxidative stress, and was shown to also target the sulfur amino acid biosynthesis pathway.

OBJECTIVES

MAIN OBJECTIVES

- To assess the inhibitory activity and the selectivity of aurone SH1009 and SH9051 as potential antifungal agents.
- To characterize at the cellular and molecular levels the modes of actions of aurones SH1009 and SH9051 in *Candida albicans*.

SPECIFIC OBJECTIVES

- To assess the antifungal activity of aurone SH1009 against different *Candida* spp. and resistant isolates using antifungal susceptibility testing.
- To characterize the cellular mode of action of aurone SH1009 using chemical genetic interactions in *Saccharomyces cerevisiae*.
    - To identify the enrichment terms of the responsively sensitive and resistant mutants to aurone SH1009 using the haploinsufficiency (HIP) and homozygous (HOP) assays.
    - To validate the HIP-HOP profiles using growth curve assays for the top sensitive and resistant mutants with comparison to wild type *S. cerevisiae*-288C as a reference.
- To investigate the impact of aurone SH1009 on the cell cycle progression in *C. albicans* using flow cytometry.
- To visualize the distributed effects of SH1009 on actin cytoskeleton dynamics in *C. albicans* using confocal microscopy.
- To quantitate the expression of cell cycle and actin organization genes in SH1009-treated *C. albicans* using RT-qPCR.

- To detect the degree of antifungal synergistic interaction on *C. albicans* between aurones SH1009 and SH9051 using checkerboard microdilution method.
- To determine the selectivity indexes of aurone SH1009 and SH9051 using cytotoxicity assays on three different human cell lines.
- To interpret the molecular basis behind the different selectivity indexes of aurone SH1009 and SH9051 in *C. albicans* using RNA sequencing.
    - To identify the transcriptomic changes in the most repressed molecular pathways in SH1009- and SH9051-treated *C. albicans.*
    - To reveal the commonly and uniquely enriched-biological processes between the aurone SH1009- and SH9051-treated *C. albicans* using cross-transcriptomic profiles analysis.
- To validate the molecular targets that play the key role in resisting the aurone treatment in *C. albicans* using reverse-genetics approach.
- To evidence the molecular effects of the structure-activity relationship using quantitative biochemical tests.

CHAPTER I

CHEMOGENOMIC PROFILING TO UNDERSTAND THE ANTIFUNGAL ACTION OF A BIOACTIVE AURONE COMPOUND

Alqahtani FM, Arivett BA, Taylor ZE, Handy ST, Farone AL, Farone MB (2019) Chemogenomic profiling to understand the antifungal action of a bioactive aurone compound. ***PLoS ONE* 14(12): e0226068.**

ABSTRACT

Every year, more than 250,000 invasive candidiasis infections are reported with 50,000 deaths worldwide. The, limited number of antifungal agents necessitates the need for alternative antifungals with potential novel targets. The 2-benzylidenebenzofuran-3-(2H)-ones have become an attractive scaffold for antifungal drug design. This study aimed to determine the antifungal activity of a synthetic aurone compound and characterize its mode of action. Using the broth microdilution method, aurone SH1009 exhibited inhibition against *C. albicans*, including resistant isolates, as well as *C. glabrata*, and *C. tropicalis* with IC_{50} values of 4-29 μM. Cytotoxicity assays using THP-1, HepG2, and A549 human cell lines showed selective toxicity toward fungal cells. The mode of action was characterized using chemical-genetic interaction via haploinsufficiency (HIP) and homozygous (HOP) profiling of a uniquely barcoded *Saccharomyces cerevisiae* mutant collection. Approximately 5300 mutants were competitively treated with SH1009 followed by DNA extraction, amplification of unique barcodes, and quantification of each mutant using multiplexed next-generation sequencing. Barcode post-sequencing analysis revealed 238 sensitive and resistant mutants that significantly (FDR *P* values ≤ 0.05) responded to aurone SH1009. The

enrichment analysis of KEGG pathways and gene ontology demonstrated the cell cycle pathway as the most significantly enriched pathway along with DNA replication, cell division, actin cytoskeleton organization, and endocytosis. Phenotypic studies of these significantly enriched responses were validated in *C. albicans*. Flow cytometric analysis of SH1009-treated *C. albicans* revealed a significant accumulation of cells in G1 phase, indicating cell cycle arrest. Fluorescence microscopy detected abnormally interrupted actin dynamics, resulting in enlarged, unbudded cells. RT-qPCR confirmed the effects of SH1009 in differentially expressed cell cycle, actin polymerization, and signal transduction genes. These findings indicate the target of SH1009 as a cell cycle-dependent organization of the actin cytoskeleton, suggesting a novel mode of action of the aurone compound as an antifungal inhibitor.

INTRODUCTION

Life-threatening fungal infections have been increasing due to the difficulties with diagnosis and treatment that accelerate mortality rates associated with fungal infections, which now exceed deaths caused by malaria (Brown et al., 2012). *Candida albicans* is the most frequently isolated opportunistic fungal pathogen and is implicated in superficial mucosal infections, or candidiasis of the oral cavity and genitalia of humans, particularly in immunocompromised patients (Sardi et al., 2013). In healthy individuals, *Candida* spp. are a commensals of the mucosal surfaces of genitalia, oral cavity, and gastrointestinal tract. However, with the introduction of antibacterial antibiotics as medical therapy in the 1940s, a gradual increase in the number of invasive candidiasis cases has been reported due to antibiotic-associated loss of the bacterial biota and subsequent colonization of *Candida* spp. on epithelial surfaces, a requirement for pathogenesis (Rajendra, 2017). Several risk factors contribute to the pathogenesis

of invasive candidiasis, including organ transplantation, prolonged hospitalization in an intensive care unit, catheterization, and intensive utilization of antibiotics and immunosuppressive agents. These factors could lead *Candida* spp. to colonize mucosal surfaces, resulting in superficial infections. The fungus can also advance to candidemia, or invasion of the bloodstream, and from there disseminate to different organs. Certain virulence factors are attributed to the pathogenicity of *Candida* spp., including adherence to epithelial surfaces, dimorphic growth, biofilm formation, and production of tissue-damaging enzymes (Kullberg & Arendrup, 2015; Liken & Kaufman, 2018).

For treating candidiasis, there are five groups of antifungal agents as defined by their mode of action and for which mechanisms of resistance have been described. Group I: polyenes (amphotericin B) binds to ergosterol in the cell membrane and form pores in it while Group II: echinocandins (caspofungin) inhibit β(1,3)-glucan synthase in the cell wall. Group III: azoles (fluconazole) inhibit lanosterol 14 α-demethylase in the ergosterol biosynthesis pathway. Group IV: synthetic pyrimidines (5-fluorocytosine) inhibit DNA synthesis and disturb protein synthesis, and Group V: allylamines (terbinafine) inhibit squalene epoxidase in the ergosterol biosynthesis pathway (Bondaryk et al., 2013). Resistance mechanisms have been described as cellular determinants that lead to drug extrusion by active efflux, altered drug targets, or drug target overexpression. However, novel drug resistance mechanisms have been recently reported as robust responses that enhance antifungal tolerance by pathways such as regulation of the oxidative or thermal stress responses (Prasad et al., 2019).

Even with treatment by commercially-available antifungal agents, the mortality rate from disseminated candidiasis has surged to ~40-60%, representing a 20-fold increase compared to only two decades ago (Rajendra, 2017). Every year, more than

250,000 invasive candidiasis infections are reported with 50,000 deaths worldwide (Kullberg & Arendrup, 2015). Furthermore, in the USA alone, the cost of combating candidiasis was estimated to be $2-4 billion annually in the year 2000 (Wilson Leslie et al., 2002). Candidiasis has recently been reported as the third-to-fourth most frequent healthcare-acquired infection globally (Wisplinghoff et al., 2014). Although the majority of candidiasis cases in humans are attributed to *C. albicans*, other *Candida* species have not only emerged as causative agents of candidiasis but have also developed resistance to antifungal drugs. These species most often include *C. glabrata*, *C. tropicalis*, *C. parapsilosis*, and *C. krusei* (Rajendra, 2017). The expanding immunosuppressed population, the limited number of fundamental antifungal agents along with their resistances and toxicity issues, and the emergence of non-albicans pathogenic strains all necessitate the need to seek alternative antifungal agents with potential novel targets.

To achieve this goal of seeking alternative antifungals, the exploitation of natural products, particularly those derived from plants, appears to be a promising source for antifungal compound development (Aqil et al., 2010). Because plants have their own fungal pathogens, these interactions between plants and fungi have resulted in the origination of diverse chemical entities within the plants intended to enhance not only their protection from fungal pathogens, but their survival and competitiveness as well (Mishra & Tiwari, 2011). One of the most promising classes of natural products are the secondary metabolites, aurones, which are ubiquitously present in plants. Aurones, or 2-benzylidenebenzofuran-3-(2H)-ones, are structural isomers of flavonoids that naturally occur as yellow-color pigments in plants (Boumendjel, 2003; Kayser et al., 1999; Morimoto et al., 2007). In addition to their roles in pigmentation, aurones

possess a variety of protective roles in the plant, including insect antifeedant (Morimoto et al., 2007), antiparasitic (Kayser et al., 1999), and antifungal activities (Bandgar et al., 2010; Lawrence et al., 2003). Moreover, activities of aurones as anticancer (Huang et al., 2007; Lawrence et al., 2003), antiparasitic (Kayser et al., 1999), antileishmanial (Ferreira et al., 2004; Pare et al., 1991), and antifungal agents have been reported (Lopez-Lazaro et al., 2002). Since the bioactive properties and therapeutic prospective of natural and synthetic aurones are promising, these bioactive compounds can be considered as an attractive scaffold for antifungal drug design and development.

We have previously reported the synthesis and anti-*Candida* activities of non-natural aurone derivatives containing different functional groups, including aurone SH1009 (**Fig. 1**), which exhibited significant inhibition of *C. albicans* when compared to the other derivatives (Sutton et al., 2017). The reported disruption of biofilm formation by aurone SH1009 emphasizes the importance of understanding the SH1009 mode of action. In the present study, the antifungal activity of aurone SH1009 was determined against different standard and clinical *Candida* spp., including resistant isolates, applying a modified synthetic strategy based on an acid-mediated condensation between the appropriate benzofuranone and aldehyde. The mode of antifungal action of aurone SH1009 was characterized using chemogenomic approach in *Saccharomyces cerevisiae* mutant collections and validated in *C. albicans* SC5314.

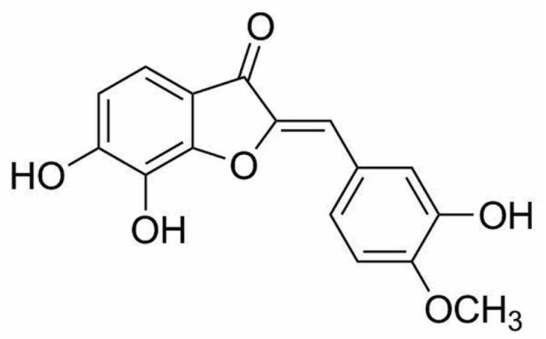

Figure 1: **Chemical structure of aurone SH1009**.

MATERIALS AND METHODS

Materials and Reagents

Candida strains (listed in **Appendix A**) were provided by the Dr. P. David Rogers lab of the University of Tennessee Health Science Center, Memphis, TN. Human cell lines; THP-1 (ATCC, TIB-202), HepG2 (ATCC, HB-8065), and A549 (ATCC, CCL-185) were purchased from the American Type Culture Collection (Manassas, VA, USA). Dulbecco′s Modified Eagle′s Medium, Trypsin-EDTA Solution 1X, Fetal bovine serum (FBS), 100X penicillin/streptomycin solution, Amphotericin B, caspofungin, fluconazole, itraconazole, 5-fluorocytosine, YPD agar and broth, cytochalasin D, 3-(N-morpholino) propanesulfonic acid (MOPS) buffer, and methyl methanesulfonate (MMS) were all purchased form Sigma-Aldrich (St. Louis, MO, USA). RPMI-1640 medium was purchased from Corning Incorporated (Coring, NY, USA). Geneticin selective antibiotic (G-148 sulfate), phosphate buffered saline (PBS), rhodamine phalloidin, propidium iodide, PrestoBlue, and RNaseA enzyme were purchased from Life Technologies Corporation (Carlsbad, CA, USA). 4% Paraformaldehyde was purchased from Alfa Aesar (Ward Hill, MA, USA) and zymolase 20T was purchased from MP Biomedicals, LLC (Solon, OH, USA). The yeast deletion collections (~1,056 heterozygous mutants and ~4,320 homozygous mutants) were purchased from GE Healthcare Life Sciences (Pittsburg, PA, USA) and ThermoFisher Scientific (Waltham, MA, USA), respectively.

Antifungal Susceptibility Testing

Preparation of stock solutions. Aurone SH1009 was synthesized as described in supporting information (**Appendix B**). The powder of SH1009 was dissolved in dimethyl sulfoxide (DMSO) to a high concentration of 20 mM. Two-fold serial

dilutions were prepared at concentrations from 200 to 3.125 μM using RPMI–1640 medium that was buffered previously to pH 7.0 with MOPS and sterilized by filtration. Using 96-wells microtiter plates, 100 μL of each SH1009 concentration was added to respective wells with four replicates for each concentration. Amphotericin B and caspofungin were used as positive controls to ensure 100% growth inhibition of the yeast at concentrations of 16 μg/mL and 8 μg/mL, respectively. In addition, fluconazole, itraconasole, and 5-fluorocytosine were prepared following manufacturer instructions, serially diluted twofold according to CLSI protocol concentrations (Institute, 2008), and used as a reference for some of the strains to confirm their resistance profiles.

Preparation of inocula. Strains for this study (**Appendix A**) were cultured on YPD agar and incubated at 35°C for 24 h. The inoculum suspensions for each strain was prepared according to the CLSI broth microdilution protocol (M27-A3) (CLSI, 2017) (Institute, 2008). The suspension of 5-6 colonies was vortexed in approximately 4 mL of sterile saline solution (0.85% NaCl) and adjusted spectrophotometrically to optical densities at a 530 nm wavelength (OD_{530}) that ranged from 0.12 to 0.15. The inocula were then diluted 1:1000 in RPMI 1640 medium resulting in 1×10^3 to 5×10^3 CFU/mL working concentration. Volumes of 100 μL of each inoculum for each strain were added to the wells of its respective plate. For each isolate, there were drug-free wells and media-control wells with and without 1% DMSO to detect any contamination in the media and for use as an optical blank for optical density and fluorescence measurements.

Inhibition assay. After 48 h of incubation at 35°C, 20 µL of PrestoBlue reagent were added to each microtiter well to a final concentration of 10% after which plates were incubated at 35°C for an additional 60-70 min (Sutton et al., 2017). The minimum inhibitory concentrations (MICs) were defined as the concentration of aurone 1009 that reduced the growth by 90%. The MIC value was determined quantitatively by measuring the fluorescence that results from reducing blue-nonfluorescent resazurin, to red-fluorescent resorufin as a result of metabolic activity of the active cells at 560 nm excitation and 590 nm emission with a SpectraMax M5e spectrophotometer (Molecular Devices, LLC, US). The percentages of yeast growth were calculated by comparing the fluorescent readings of the drug-containing wells with that of the drug-free wells to calculate MIC_{90}. The assay for each strain was performed in duplicate. The IC_{50} values were calculated using GraphPad Prism (GraphPad Software, US).

Cell viability assay. Using 24-well plates, *C. albicans* SC5314 cells were cultured and treated with 200 µM SH1009 in 2 mL of RPMI 1640 medium as described above. After incubation at 35°C for 48 h, 1 mL of SH1009-treated cells, untreated cells, and previously prepared isopropanol-killed cells were washed with PBS. The samples were then diluted to approximately 1 x 10^6 cells/mL in PBS and stained according the live/dead Fungalight Yeast Viability Kit protocol (ThermoFisher, Waltham, MA, USA). Stained cells were investigated for their viability using flow cytometry (Guava Millipore, Burlington, MA, USA) with Guava InCyte Software. To distinguish between live and dead cells in a dot plot, gating the yeast population was determined based on red and green fluorescence levels of isopropanol-killed cells.

Growth rate assay. In 100-well Bioscreen honeycomb plates, *C. albicans* M1:SC5314 cells were cultured and treated with aurone SH1009 (3.125-200 µM) in RPMI 1640

medium as described above. Plates were loaded into the Bioscreen C instrument with Bioscreen software (Growth Curves USA, Piscataway, NJ, USA) at a temperature of 35°C with continuous shaking and 30 min interval measurements at an OD_{530} for 40 h. Growth curves were used to compare growth of untreated-*C. albicans* cells with SH1009-treated cells at different aurone concentrations. Validation of cellular sensitivity and resistance responses of *S. cerevisiae* mutants to SH1009 were also performed with the Bioscreen C instrument as the same manner for *C. albicans* except the media was YPD broth and incubation was at 30°C.

Time-kill assay. A previously described and evaluated antifungal time-kill method was utilized to evaluate the fungicidal activity of aurone SH1009 (Klepser et al., 1998). An initial inoculum of *C. albicans* SC5314 ranging from 0.5 – 1.0 $\times 10^5$ CFU/mL was treated with 5fold the IC_{50} concentration of SH1009 (500 μM). Fluconazole (16 μg/mL) was used as fungistatic control, and Amphotericin B (8 μg/mL) was used as fungicidal control. After incubation at 35°C, 10 μL of each treatment was spread onto YPD agar after 0, 6, 12, 24, and 30 h of treatment and plates were incubated at 35°C for 24 h to determine viable cell numbers. The fungicidal activity was determined as $\geq 3 - \log_{10}$ which is equivalent to 99.9% reduction in CFU/mL from the working concentration 0.25 -0.5$\times 10^5$ CFU/mL.

Cytotoxicity assay

The A549 human lung carcinoma epithelial cell line and human monocytic THP-1 cell line were grown in RPMI-1640 culture medium, while HepG2 human liver carcinoma epithelial cells were grown in DMEM culture medium. Both media were supplemented with 10% FBS and 1% penicillin-streptomycin antibiotics. After maintaining the cell

growth at 37℃ with 5% CO_2 in a humidified incubator until reaching 90% confluency, the A549 and HepG2 cells were trypsinized with 1X trypsin-EDTA and resuspended in fresh medium. The cells were seeded into 96-well microtiter plates at a density of 10,000 viable cells/well and grown overnight, while the suspension THP-1 cells were seeded directly into 96-well microtiter plates at the same density before treatment. The final concentrations of aurone SH1009 were prepared in two-fold serial dilutions (3.125 μM– 200 μM) as described above for the antifungal susceptibility assay. The media containing A549 or HepG2 cells were then replaced after overnight incubation by 200μL of fresh culture media containing the final concentrations of SH1009. The cells were then incubated for additional 24h at 37℃ with 5% CO_2 in a humidified incubator. To evaluate cell viability, each well was treated with 20 μL of PrestoBlue for 3–6h. Metabolically active cells converted the blue non-fluorescent dye resazurin to the pink fluorescent dye resorufin, which can be measured by plate reader as described above in antifungal inhibition assay. Triton X-100 (1%, v/v) was used as a positive control to give a complete loss of cell viability. Percentages of cell viability were calculated as follows: [(negative control value–treated value) × 100]/negative control value. The assay for each cell line was performed in triplicate. The CC50 values were calculated using GraphPad Prism (GraphPad Software, USA).

Chemogenomics Profiling in *Saccharomyces cerevisiae*

Combination of individual mutants into a single pool. The yeast deletion collections were obtained as individual mutants in 96-well plates that had been stored at −80°C. Both the HIP deletion pool and HOP deletion pool were created separately as previously described (Pierce et al., 2007; Piotrowski et al., 2015). The 96-well plates of mutant stocks were thawed completely, after which a 96-well transfer pin was used

to transfer a small volume of mutants to a Nunc Omni Tray containing YPD agar with geneticin antibiotic. Between transfers, the 96-well transfer pin was sterilized with ethanol and flamed three times. After growing the cells for 48 h at 30°C, the missing and slow growing mutants were recorded and two times the cell mass of these mutants were added separately. Working in a sterile hood, each tray was flooded with ~10 mL of YPD broth and all formed colonies were gently scraped by sterile cell spreader. The resuspended colonies were transferred into a sterile 1000 mL flask with a sterile stir bar. The suspension was mixed for 5 min on a stir plate to obtain an homogenized pool. The concentration of the freshly prepared pool was adjusted to 125-250 cells/mutant/µL by centrifugation at 500 × *g*. Once the concentration was adjusted, sterile glycerol was added to 15% (vol/vol) and 200 µL aliquots of the pool were stored in PCR strip tubes at −80°C.

Pooled competition with aurone SH1009. Before exposing the pooled deletion mutants to SH1009, the inhibitory concentration for roughly 20% of the *S. cerevisiae* S288C wild type parent strain of these mutants was determined (500 µM) as previously described (Piotrowski et al., 2015). Using 96-well plates, 8 wells were filled with 198 µL of SH1009 diluted in YPD broth at concentration 500 µM with no more than 1% of DMSO. For the positive control, 8 wells were filled with 198 µL of MMS diluted in YPD broth at concentration 0.01 µg/mL. For the negative control, 8 wells were filled with 198 µL of YPD broth with 1% DMSO only. Two aliquots that were prepared from the previous step of the HOP deletion pool (~4,320 mutants), representing nonessential genes, and HIP deletion pool (~1,056 mutants), representing essential genes, were thawed completely. A 2 µL volume at a concertation of 125-250 cells/mutant/µL of the non-essential deletion pool were added to every 12 wells containing SH1009, MMS,

and 1% DMSO. In the same manner, 2 µL of the essential deletion pool at a concertation of 125-250 cells/mutant/µL were added to every remaining 12 wells of SH1009, MMS, and 1% DMSO. After a 48h incubation at 30°C, cells from each well were harvested independently by pipetting up and down and centrifuging at ~20,000 *x g* for 3 min. The supernatant was removed and the pellet was processed for genomic DNA extraction.

Construction of the DNA library. Pellets of 24 samples were resuspended individually in 125 µL of Zymolyase solution and incubated for 1 h at 37°C. The DNA was extracted from all 24 samples according to Maxwell 16 LEV Plant DNA Kit manual (Promega Corporation, Madison, WI, USA). To amplify the UPTAG unique 20 bp DNA barcodes as previously described (Piotrowski et al., 2015), 24 PCR reactions were prepared independently, such that there was one PCR reaction for each sample in a total volume of 25 µL as follows: 21.5 µL of Taq mix, 0.5 µL of reverse common primer at 0.5 µM, 0.5 µL of indexed primer at 0.5 µM (for each sample, a distinct indexed primer was used (**Appendix C**), and 2.5 µL of genomic DNA at ~ 100 ng. PCR conditions were as follows: 5 min at 95°C for an initial denaturation, followed by 30 cycles of 1 min at 95°C, 30 s at 55 °C, 45 s at 68°C, then, 10 min at 68°C for a final extension. After PCR reactions, 25 µL of all PCR products were pooled together from individual PCR tubes into one tube library. This library was purified by separation on a 2% TAE agarose gel for 50 min at 120V. The desired band (267 bp) containing the amplified UPTAG DNA barcodes was cut and purified from the gel using a QIAGEN Quick Gel Extraction Kit (QIAGEN, Germantown, MD, USA). The library was diluted to 1:5,000, 1:10,000, and 1:20,000 and quantified with the KAPA Library Quantification Kit (KAPA Biosystems, Wilmington, MA, USA) and Bio-Rad CFX96 real-time PCR system (Hercules, CA, USA). After quantifying the correct

concentration of the library, the library was prepared as a DNA template at the final concentration 15 nM with a 5% Spike-In of PhiX control according to the MiSeq System Denature and Dilute Library Guide (Illumina, San Diego, CA, USA). The Illumina MiSeq sequencer was used to run the DNA template for 1 × 50 cycles to yield a cluster density of 700–900 k/mm^2.

Post-sequencing data analysis. The Illumina sequencer generated a Fastq file that was converted to Fasta file using a converter tool due to the ease of manipulating the Fasta file. In order to process and analyze sequence reads, Perl scripts were created (Tisdall, 2001). Two raw-count files for HIP-HOP profiles were imported into excel sheet (Microsoft Corporation, US) to normalize the absolute counts and calculate fitness scores, Z-scores, *P*-values, and FDR values following calculations previously reported (Pierce et al., 2007). The raw sequence reads were deposited in Sequence Read Archive (SRA) under project number PRJNA491750. Enrichment analysis of KEGG pathway and gene ontology (GO) analysis was conducted using hypergeometric testing through ClueGo software to find the significantly enriched KEGG/GO terms using GO categories in the *Saccharomyces cerevisiae*-S288C as a background. To visualize the interactive annotation network between significant genes, ClueGO and CluePedia apps (Bindea et al., 2013; Bindea et al., 2009) along with Cytoscape (Cytoscape Consortium, US) were used.

Flow cytometry

C. albicans SC5314 cells were grown at 30°C until reaching exponential phase, diluted to ~1.2-3×10^6 CFU/mL, and treated with SH1009 at the IC_{50} concentration followed by incubation for an additional 3 h. After harvesting by centrifugation, supernatants were discarded and pellets were washed with PBS and then fixed with cold 70% ethanol at -

20°C for 2 h. Fixed cells were washed in PBS and resuspended in 500 uL of PBS containing 20 μg/mL RNase and incubated at 37°C for 2 h. 200 μL of PBS containing 20 μg/mL propidium iodide (PI) were added to the treated cells. Using the Millipore Guava flow cytometer, 5000 events were counted, and the fluorescent intensity of PI measured. After acquiring the data using Guava PCA-96 software, the data was gated to exclude debris or aggregates. Experiments were performed in triplicate using cytochalasin D, which has been reported to arrest the cell cycle (Heng & Koh, 2010), as a positive control.

Confocal microscopy

C. albicans SC5314 cells were grown at 35°C until reaching exponential phase, then diluted to ~ 1.2-3×10^6 CFU/mL. Aurone SH1009 was added at the IC_{50} concentration and cells were incubated for 3 h. Cells were fixed by addition of 4% paraformaldehyde and subsequently incubated for 2 h at room temperature. After pelleting and washing the cells with PBS, cells were incubated with 1% Triton-X100 for 1 h at room temperature. Rhodamine Phalloidin (RP) was added to the cells followed by incubation in the dark at 4°C for 1 h. After two PBS washes, cells were imaged using confocal microscopy (Zeiss, Thornwood, NJ, USA) at 60x magnification. Cells was assessed for actin distribution by considering that the actin is depolarized if more than five patches were observed in the mother cell (Helliwell et al., 1998). Approximately 100 cells were counted per experiment in triplicate experiments. The *S. cerevisiae CDC42*Δ mutant was used as a positive control.

RT-qPCR

After growing *C. albicans* SC5314 cells at 30°C in YPD broth until reaching exponential phase, the culture was treated with aurone SH1009 at the IC_{50} concentration

followed by incubation for additional 1.5, 3, and 6 h. After harvesting the cells by centrifugation, the RNA was extracted according to the instructions of the Maxwell 16 LEV Plant RNA Kit. Total RNA from treated and untreated samples were normalized to 1 µg. cDNA was constructed by following the manufacturer protocol of SuperScript IV First-Strand Synthesis System kit (ThermoFisher, Waltham, MA, USA) using 10 ng of RNA. The RT-qPCR was preformed using 2× iQ SYBR green supermix (Bio-Rad, Hercules, CA, USA) under the recommended cycle conditions. All reactions were performed in triplicate using listed primer pairs (**Appendix D)**. Transcript levels were normalized to the expression level of the housekeeping gene GAPDH and compared to the untreated sample using $\Delta\Delta C_T$ method (Schmittgen & Livak, 2008).

RESULTS

Aurone SH1009 is inhibitory for *Candida* spp.

To assess the antifungal activity of aurone SH1009 against *Candida* strains (listed in **Appendix A**), antifungal susceptibility testing was performed using the Clinical Laboratory Standards Institute (CLSI) broth microdilution protocol (M27-A3) (Institute, 2008). SH1009 exhibited promising antifungal activity against all *Candida* spp. tested (**Table 1**). *C. albicans* strains M2, M3, M5, and M7 are all fluconazole resistant and, as such, represent a serious risk for patients since fluconazole is the principle antifungal drug for treating candidiasis (Sardi et al., 2013). In this study, fluconazole had no inhibitory activity on these isolates even at high concentrations (MIC > 64 µg/mL), while the IC_{50} of aurone SH1009 is considerably lower [11, 12, 4, and 8 µM) for *C. albicans* M2, M3, M5, and M7 strains, respectively. Similarly, another aggressive, multi-drug resistant isolate, *C. albicans* ATCC 64124, exhibited resistance to a high concentrations of amphotericin B (16 µg/mL), caspofungin (4 µg/mL), and fluconazole (64 µg/mL), although 5-fluorocytosine was inhibitory (MIC < 1 µg/mL).

This strain was also sensitive to SH1009 (IC_{50} = 21 µM). Although *C. albicans* is recovered from at least 50% of candidiasis cases, *C. glabrata* has recently emerged as responsible for approximately 25% of cases in the last two decades, and tends to infect elderly populations (Pfaller & Diekema, 2007). Exposure of *C. glabrata* to SH1009 resulted in inhibition with a low concentration of aurone (IC_{50} < 3.125 µM), suggesting it could be a successful treatment, especially since the development of *C. glabrata* resistance to caspofungin and lower susceptibility to fluconazole have been reported (Silva et al., 2012). *C. tropicalis*, a causative agent in 10-20% of candidiasis cases in the USA and 35-40% of cases in tropical regions, was also susceptible to SH1009 (Rajendra, 2017). Because aurone SH1009 is not affected by the resistance mechanisms of these isolates with known resistances to antifungals, the compound presents new possibilities for further exploration as a potential antifungal agent.

Table 1: The IC_{50} (inhibitory concentration that causes 50% inhibition) and $MIC_{90\%}$ (minimal inhibitory concentration that causes 90% inhibition) of aurone SH1009 for different *Candida* spp.

Strains	IC_{50}**(µM)**	$MIC_{90\%}$**(µM)**
C. albicans ATCC 90028	**11±0.345**	**18.75±6.25***

C. albicans ATCC 90029	**13±1.125**	**25±0**
C. albicans M1: SC5314	**16±2.4**	**25±9.375**
C. albicans M2: ScTAC1R34A a	**11±0.725**	**18.75±6.25**
C. albicans M3: ScMRR1R34A a	**12±0.14**	**25±0**
C. albicans M4: Gu2	**11±0.13**	**12±0**
C. albicans M5: Gu5 a	**4±1.159**	**9.375±3.125**
C. albicans M6: F1	**10±0.54**	**12±1.3**
C. albicans M7: F5 a	**8±0.676**	**12.5±0**
C. albicans ATCC 64124 b	**21±7.125**	**50±0**
C. glabrata ATCC 66032	**<3.125±0**	**<3.125±0**
C. tropicalis ATCC 750	**29±25.7**	**62.5±37.5**

a Resistant to fluconazole.
b Resistant to amphotericin B, caspofungin, and fluconazole except 5-fluorocytosine at high concentration.
*Mean±SEM.

Although SH1009 was inhibitory, the aurone was not fungicidal even at the highest concentration of aurone tested (200 μM), as indicated by colony growth on solid media. Therefore, a more sensitive cell viability assay, compatible with yeast cells, was

required to more precisely measure viable cell number after treatment. Along with flow cytometry, the live/dead Fungalight Yeast Viability Kit was used to quantitate viability after SH1009 treatment. After 48 h of treatment with a high SH1009 concentration (200 μM), *C. albicans* SC5314 strain (**Fig. 2A**) revealed two divided subpopulations after gating for the stained cells in the dot plot graphs. When compared to isopropanol-treated cells (**Fig. 2B**), a significant fraction (**Fig. 2D**) of SH1009-treated cells clustered in the upper-left quadrant, indicating the bioactivity of SH1009 in eliminating *C. albicans* SC5314 growth. In contrast, the viable cells in the SH1009-treated sample (**Fig. 2A**) were reduced by approximately half compared to the untreated-cells sample (**Fig. 2C**).

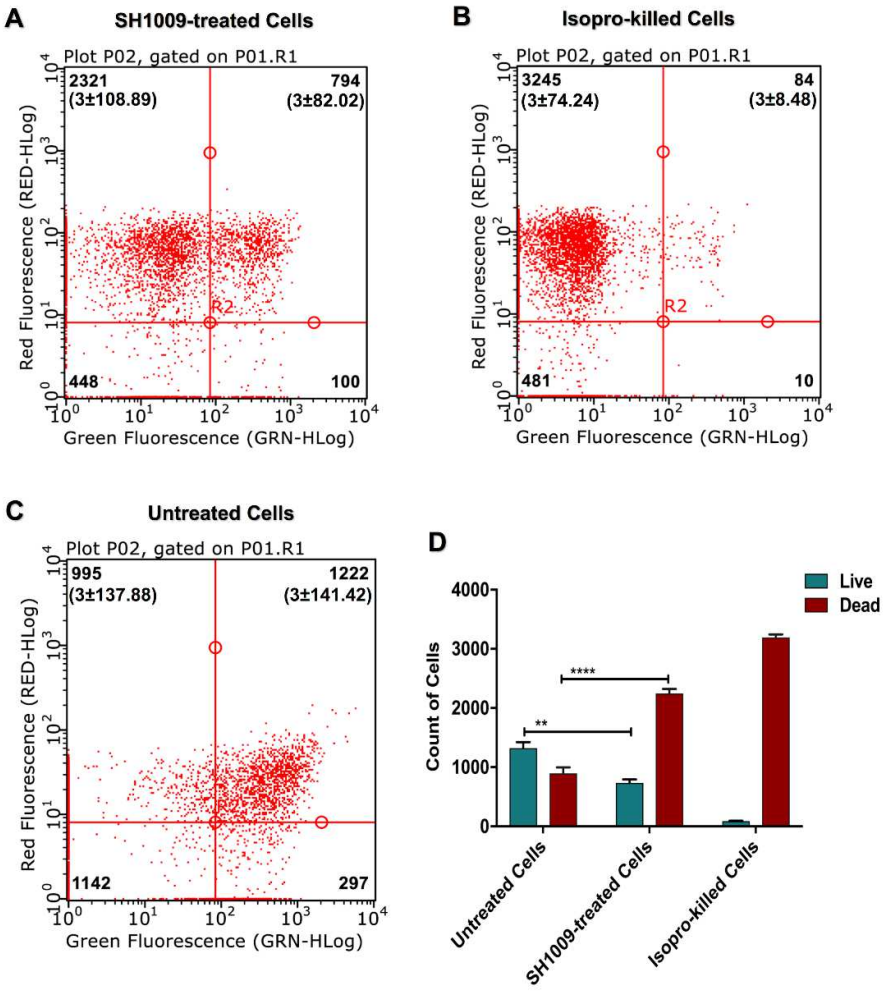

Figure 2: Cell viability assay of aurone SH1009-treated *C. albicans*. *C. albicans* SC5314 cell suspensions were stained with SYTO® 9 dye (green fluorescence) and Propidium Iodide (red fluorescence) and analyzed using the Millipore Guava flow cytometer and InCyte software system. For each dot plot A) 200 µM aurone SH1009-treated cells, B) isopropanol-killed cells, and C) untreated cells, the upper-left quadrants show the count of dead cells and the upper-right quadrants show the count of live cells. D) Significance was calculated using two-way ANOVA to compare the cell viability of two population groups (live and dead) between untreated and SH1009-treated cells. *P* values (**** $P < 0.0001$), (** $P < 0.01$), (n=3±SD).

Growth of SH1009-treated *C. albicans* SC5314 was monitored at 30-min intervals over a 46 h incubation using dilutions of the aurone. A representative set of growth curves of *C. albicans* SC5314 is given in **Fig. 3A**. The curves indicate that there is no regrowth of *C. albicans* SC5314 in the presence of SH1009 above 12.5 μM. Additionally, inhibition of *C. albicans* SC5314 by SH1009 is highly dose dependent. The potency of any bioactive-compound is usually measured by the concentration of compound that inhibits 50% (IC_{50}) of a fixed-pathogenic inoculum in a dose–response assay *in vitro*. However, dose–response curve slope is another clinically independent criterion that can be used as an indicator of the expected therapeutic effectiveness (Webb et al., 2015). Typically, a dose–response curve with a particularly steep slope (Hill coefficient >1) indicates that a small increase in concentration of a drug above the IC_{50} causes extraordinarily high-level inhibition. SH1009 exhibited a steeper dose-response IC_{50} curve in inhibition of *C. albicans* SC5314 as is indicated by the higher slope factor (~2.241) (**Fig. 3B**). The steep slope of the IC_{50} curve reflects the growth curve results for treated cells, in that there is significant loss of viability with aurone concentrations above the IC_{50} concentration of 16.28 μM. This predicts a possible therapeutic potency for SH1009 with a selective 50% inhibitory concentration required to inhibit *C. albicans* SC5314 cells ($0.5\text{-}2.5\times10^3$ CFU/mL).

A time-kill assay was employed to investigate the killing kinetics of aurone SH1009 against *C. albicans* SC5314 along with fluconazole and amphotericin B treatments (**Fig. 3C**). As expected, amphotericin B affected the growth curve at 8 μg/mL after 2 h, regardless of the initial inoculum of *C. albicans* SC5314 cells ($0.5 - 0.25\times10^5$ CFU/mL), demonstrating fungicidal activity. Treatment with SH1009 at a concentration of 5fold the IC_{50} (500 μM) reduced the growth of the yeast similarly to

fluconazole (16 μg/mL) with no significant differences until 12 h of incubation, indicating fungistatic activity. Given the initial inoculum, the SH1009 treatment yielded an approximate > 3 $\log_{10}$ decrease in CFU/mL after each time point of treatment compared with untreated culture, exhibiting a significant reduction (*P* value <0.0001) in the colony count. This reduction in the CFU/mL resulted in no appreciably significant increase in growth rate after SH1009 treatment over 24 h, whereas the untreated culture recorded > 4.4 $\log_{10}$ significant increase in the CFU/mL between 0 and 24 h. These results indicate a fungistatic activity which might be less desirable for immunosuppressed patients to remedy opportunistic infections. Consequently, we measured the cytotoxicity of SH1009 for three different human cell lines.

Toxicity assays to determine the cytotoxic concentration of aurone that reduced cell viability by 50% (CC_{50}) were carried out based on the reduction of resazurin to resorufin by metabolically active cells as a sensitive method for detecting viable cells [26]. The CC50 values for THP-1, HepG2, A549 cells after 24 h treatment with two-fold serial dilutions of SH1009 (3.125–200 μM) were 140, 168, and >200 μM, respectively (**Table 2**). Selectivity index (SI) values were calculated to correlate the antifungal activity of aurone SH1009 against *C. albicans* SC5314 cells (IC_{50} = 16.28 μM) with the CC_{50} concentration for the human cell lines. The CC_{50}/ IC_{50} ratio was an ~8.6->12-fold difference in the concentrations that resulted in 50% loss of cell viability, suggesting a selectivity of SH1009 for the pathogenic yeast cells over human cells. Treatment of *C. albicans* SC5314 cells with SH1009 at 25 μM resulted in a significant reduction (*P* < 0.001) in cell viability when compared to the untreated control group, while treatment of human cell lines with the same concentration resulted in no appreciably significant reduction with 70% cell viability for THP-1 cells and 100%

viability for both HepG2 and A549 cells. With increasing SH1009 concentrations, the cell viability of *C. albicans* SC5314 was reduced significantly ($P < 0.01$), compared to the cell viability of human cells (**Fig 3D**). These results indicate that aurone SH1009 has a selective toxicity for *C. albicans* cells. To assist with assessing the therapeutic potential of aurone SH1009 as an antifungal, we next sought to determine the bioactivity of the compound by defining its mode of toxicity.

Table 2: The CC_{50} (cytotoxicity concentration of aurone SH1009 that causes 50% cell viability loss) ± the SEM and the selectivity index (SI) as a ratio between the CC_{50} for the mammalian cells divided by the IC_{50} against *C. albicans* SC5314.

Human cell line	**CC_{50}(µM)**	**SI**
THP-1 (ATCC, TIB-202)	**140±4.5**	**8.6**
HepG2 (ATCC, HB-8065)	**168±7.6**	**10.31**
A549 (ATCC, CCL-185)	**>200±0**	**>12**

*Mean±SEM.

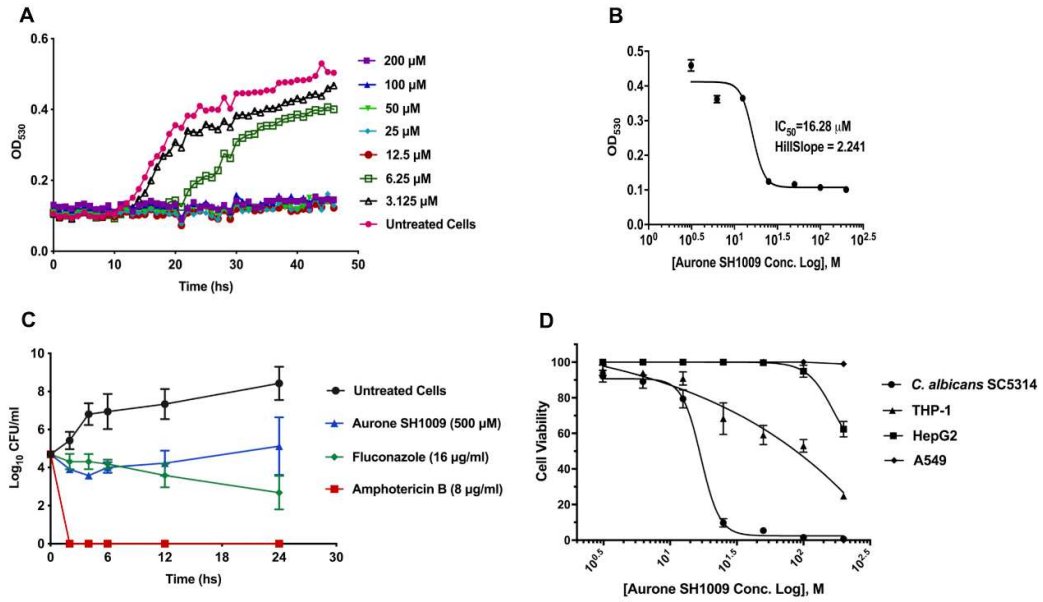

Figure 3: Aurone SH1009 exhibited dose-dependent inhibition of growth. A) Growth curves of *C. albicans* SC5314 strain (2.5-0.5×10^3 CFU/mL) in dilutions of SH1009 (3.125 µM – 200 µM) in RPMI-1640 medium using the Bioscreen C growth curve instrument to measure the OD_{530} every 30 min for 46 hours at 35°C. **B)** Graphing the nonlinear regression of OD_{530} readings using GraphPad Software to calculate the IC_{50} value after transforming the molar concentrations of the aurone SH1009 into the logarithmic form. **C)** Time-kill plot of *C. albicans* SC5314 cells (0.5 - 0.25×10^5 CFU/mL) treated with 5fold the IC_{50} concentration of SH1009 (16.28 µM), fluconazole (0.5 µg/mL) and amphotericin B (0.25 µg/mL) with incubation at 35°C for indicated time points. Colony forming units (CFU) were determined by plating 10 µL of each treatment onto YPD agar plates at each timepoint. **D)** Cytotoxic effects of aurone SH1009 for *C. albicans* SC5314 and THP-1, HepG2, and A549 human cell lines are presented as dose-response curves by graphing the nonlinear regression of the cell viability using GraphPad Software to calculate the CC_{50} values after transforming the molar concentrations of the aurone SH1009 into logarithmic form.

Chemogenomic profiling of aurone SH1009-treated yeast cells identifies roles for genes involved in the cell cycle, cell division, and the actin cytoskeleton

Chemogenomic profiling was used to characterize the mode of action for aurone SH1009. Haploinsufficiency profiling (HIP) and homozygous profiling (HOP) allow for paralleled assessment of the sensitivity and resistance of the pooled genome-wide set of *S. cerevisiae* deletion mutants. First, two pools of *S. cerevisiae* heterozygous (HIP) and homozygous (HOP) deletion mutant collections were treated with aurone SH1009 at the concentration (~ 500 uM) that inhibited the growth of the wild type *S. cerevisiae*-S288C (1.25×10^9 cells /mL) by 20% for 48 h. After purifying genomic DNA from the mutants, the synthetic UPTAG DNA barcodes (20 bp) were amplified using uniquely indexed primers to distinguish each sample. Because each mutant is uniquely identified with DNA barcode, multiplexed-next generation sequencing as a highly robust technique was employed to quantitate the abundance of each mutant.

Haploinsufficiency profiling was performed on ~1056 heterozygous mutants that are essential for growth and express only 50% of gene dosage because one functional copy of that particular gene in the diploid organism has been deleted. Whereby, the identification of the direct target of a certain bioactive compound can be identified in the presence of that compound as the mutant that has a large fitness defect compared to the other mutants that do not encode the drug target. Conversely, homozygous profiling was performed on ~4244 of homozygous mutants that are non-essential for growth and express 0% of gene dosage because both copies of the particular gene are deleted in the diploid organism. With the HOP assay, it is possible to suppress drug sensitivity due to the complete loss-of-function alleles, allowing identification of pathways that confer the drug sensitivity or identification of the direct target of drugs following the principle that deletion of drug target will render the cells

insensitive to the compound (Hoon et al., 2008).

The post-sequencing data analysis of the aurone-treated deletion mutants revealed 3923 mutants, which included 3,133 mutants from the homozygous deletion pool (non-essential genes) and 790 mutants from the heterozygous deletion pool (essential genes), representing ~ 75% of the mutant population with usable read counts and 0.90 correlation between samples, indicating high sample quality and agreement. The chemical-genetic interaction of the positive control methyl methanesulfonate (MMS), a well-characterized antifungal agent that damages DNA (Chang et al., 2002), demonstrated a highly significant enrichment (*P* value < 0.001) for cellular response to DNA damage stimulus, confirming a successful HIP-HOP assay procedure and accurate post-sequencing data analysis. The chemical-genetic interaction identified 238 gene deletion mutants that were significantly responsive to aurone SH1009 (FDR *P* values ≤ 0.05) for both HIP-HOP profiles (**Fig. 4A** and **4B**). The sensitive and resistant genes with that *P* value (approximately ≥ 1.5 fold change) for HIP and HOP independently were used for gene ontology (GO) enrichment analysis using ClueGO (Bindea et al., 2009) and Yeast Gene Ontology Slim Term Mapper at *Saccharomyces* Genome Database (SGD) (Harris et al., 2004) .

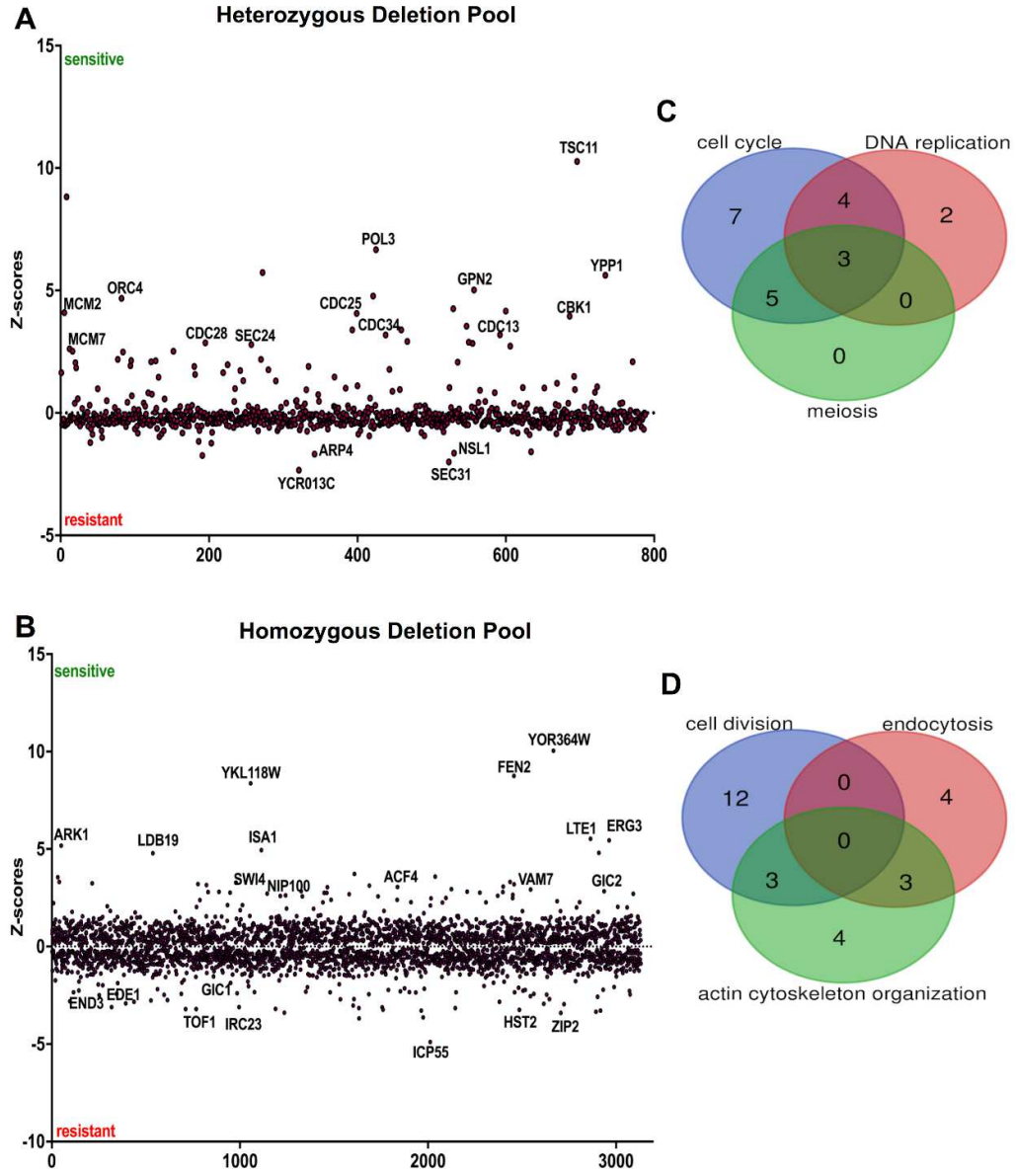

Figure 4: Chemical-genomic analysis of aurone SH1009. A) Z-score plot of heterozygous deletion pool (HIP profile) for essential genes, and **B)** Z-score plot of homozygous deletion pool (HOP profile) for non-essential genes where the sensitive mutants have positive scores and the resistant mutants have negative scores. **C)** and **D)** Number of mutants whose sensitivities or resistances were affected by aurone SH1009 (FDR $P \leq 0.05$, fold change ≥ 1.5) clustered by significant biological responses and represented in the Venn diagram for HIP and HOP profiles, respectively.

For essential genes (HIP profile), GO enrichment ($P < 0.0001$) for mutants that have deleted genes encoding cell cycle proteins were found (e.g. *CDC28*Δ, *CDC34*Δ, *CDC25*Δ, *CDC13*Δ, *ORC4*Δ, *MCM2*Δ, *MCM7*Δ, *CBK1*Δ, and *RFC1*Δ) (**Fig. 4C)**. Moreover, two other biological responses involved in the cell cycle showed a significant GO enrichment ($P < 0.00$). These included genes for meiosis-yeast (*ORC4*Δ, *MCM2*Δ, *MCM7*Δ, *APC4*Δ, *APC1*Δ, *CDC28*Δ, and *CDC5*Δ) and DNA replication (*POL3*Δ, *MCM2*Δ, *MCM7*Δ, *RFC3*Δ and *RFC1*Δ). For non-essential genes (HOP profile), among both sensitive and resistant mutants, GO enrichment ($P < 0.0098$) detected sensitive mutants (*ARK1*Δ, *NIP100*Δ, *GIC1*Δ, *SLK19*Δ, *KIP3*Δ, and *ACF4*Δ) and resistant mutants (*BOI2*Δ, *EDE*Δ, *END3*Δ, and *GIC2*Δ) with deleted genes that are associated with actin cytoskeleton organization (**Fig. 3D)**. Also, mutants that are associated with cell division were significantly enriched from the HOP profile (*LDB19*Δ, *SLK19*Δ, *LTE1*Δ, *ZIP2*Δ, *BUB1*Δ, *ELM1*Δ, *TOF1*Δ, *TOF2*Δ, *SWI4*Δ, *CSM3*Δ, *CLB3*Δ, and *CLN2*Δ). Lastly, there was an enrichment of deletion mutants for the biological response of endocytosis, which also relates to the actin cytoskeleton, that included mutants that were among the top 10 sensitive in the HOP profile (*FEN2*Δ, *LTE1*Δ, *LDB19*Δ, and *ARK1*Δ).

For several phenotypes described above, the cell cycle pathway appeared to be the primary target pathway that was significantly enriched by SH1009 treatment for the essential genes profile and non-essential genes profile, separately. To obtain a broader view of the changes in growth patterns of heterozygous and homozygous mutants after SH1009 treatment, the significantly responsive mutants from both HIP-HOP profiles were combined and used for the enrichment analysis. For all 238 deleted protein-coding genes with (FDR P values ≤ 0.05 and fold change ≥ 1.5) from both profiles, the

clustered analysis of KEGG pathways and gene ontology terms that significantly enriched (FDR P values ≤ 0.05) were plotted for the number of genes that are associated with each term in a histogram (**Fig. 5**). Notably, both the profiles for the 80 essential genes (HIP-profile) and 158 non-essential genes (HOP-profile) are largely clustered in the significantly enriched category. These significantly responsive genes were mapped to six pathways in the KEGG pathway database, with the cell cycle pathway as the most significantly enriched pathway ($P < 0.0001$) along with other pathways that are completely overlapped with cell cycle pathway (meiosis and DNA replication). For gene ontology categories, within the biological process category 18 terms were enriched in differentially sensitive or resistant mutants, including cell division, cytoskeleton organization, and regulation of endocytosis. Also, the nucleotide-binding, aminoacyl-tRNA ligase activity, and DNA-binding terms were significantly enriched in the molecular function category. Nucleus, cytoskeleton, cellular bud, as well as the site of polarized growth terms were significantly enriched in the cellular component category.

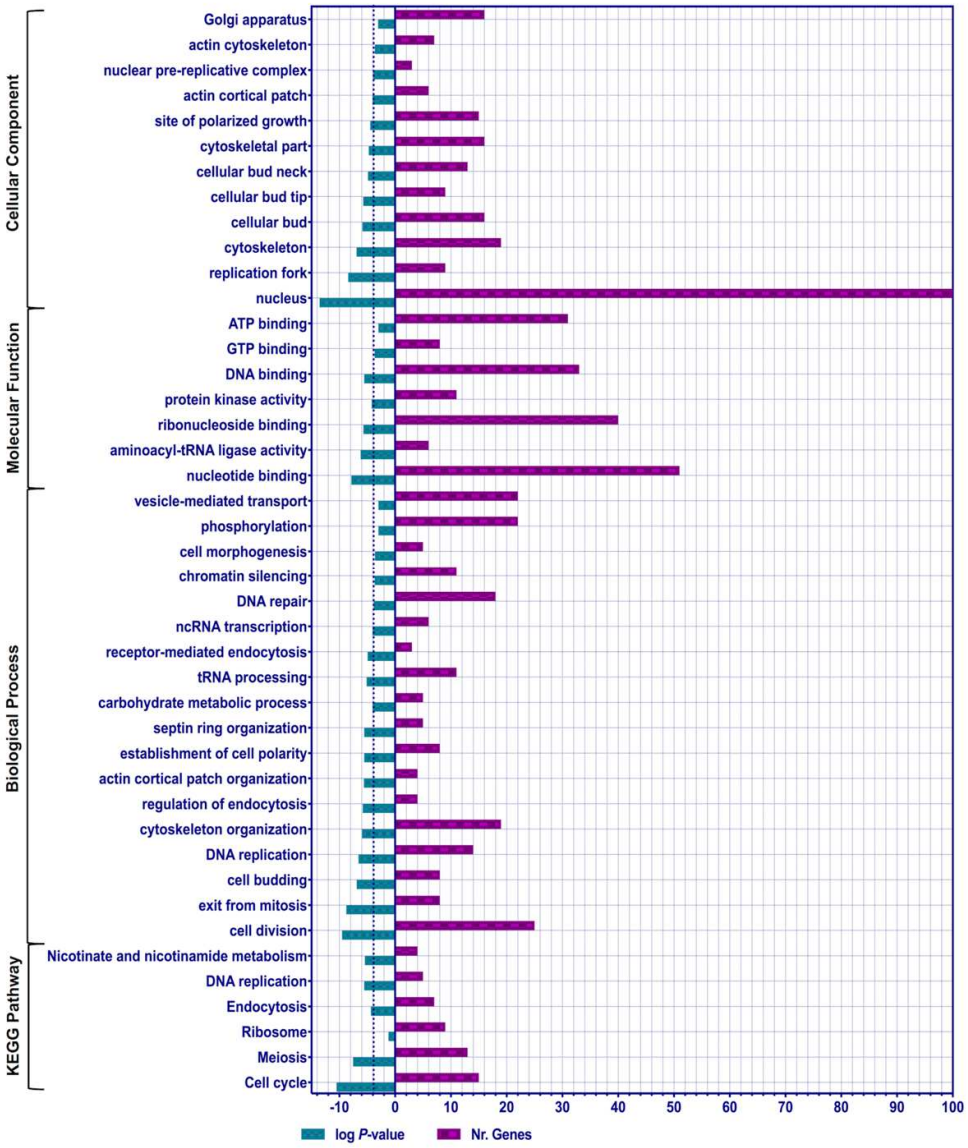

Figure 5: Functional categories of KEGG pathway and gene ontology (biological process, molecular function, and cellular component) enrichment analysis. There are ~238 differentially responsive mutants with FDR ≤ 0.05 and fold change ≥ 1.5 from heterozygous deletion pool (HIP) and homozygous deletion pool (HOP) profiles. Purple bars represent the number of genes, 80 essential genes from HIP-profile and 158 non-essential genes from HOP-profile, that are clustered in each KEGG/GO term. Green bars show the significance of each category as log *P*-values that are calculated by hypergeometric calculation through ClueGo software using GO categories in the *Saccharomyces cerevisiae*-S288C as a background with an FRD < 0.05 as a cutoff significant value for all the plotted categories. The threshold-dotted line depicts the highly significant KEGG/GO categories with $P < 0.01$.

In order to gain insight into the chemical-genetic interaction of genes targeted by aurone SH1009 and visualize the connections between targeted biological responses and pathways identified by both the HIP and HOP profiles, ClueGO and CluePedia along with Cytoscape software were used to extract and map non-redundant biological responses for a large set of functionally clustered genes using GO terms and KEGG pathway (**Appendix E**), simultaneously (Bindea et al., 2013; Bindea et al., 2009). **Fig. 6A** depicts the functional annotation network of clustered essential and non-essential genes. This overlapped network revealed relatively connected biological categories that started from the highest significantly enriched pathway (cell cycle) to the less significant pathways (meiosis, DNA replication, endocytosis, and RNA biogenesis). When focusing on the cell cycle pathway only (**Fig. 6B**), the non-essential genes (HOP profile) were strongly clustered with the essential genes (HIP profile) for significantly enriched biological processes associated with actin cytoskeleton organization and endocytosis. Eight clustered genes for actin cytoskeleton and endocytosis were found among the top 20 sensitive mutants of both the HIP and HOP profiles, implicating cell-cycle-dependent organization of the actin cytoskeleton and endocytosis as targets of aurone SH1009. Additionally, the most significantly enriched molecular function for the SH1009-responsive mutants was the nucleotide-binding protein. The annotation network revealed 51 nucleotide-binding proteins that significantly responded to aurone SH1009; 31 of these genes encode proteins that act as ATP-binding proteins, while the other 10 encode GTP-binding proteins. Taken together, the functional enrichment analysis of the deletion pool of essential and non-essential genes illustrates that aurone SH1009 treatment might target nucleotide binding proteins, leading to a series of cellular defects that belong to cell cycle pathway, actin cytoskeleton organization, and endocytosis.

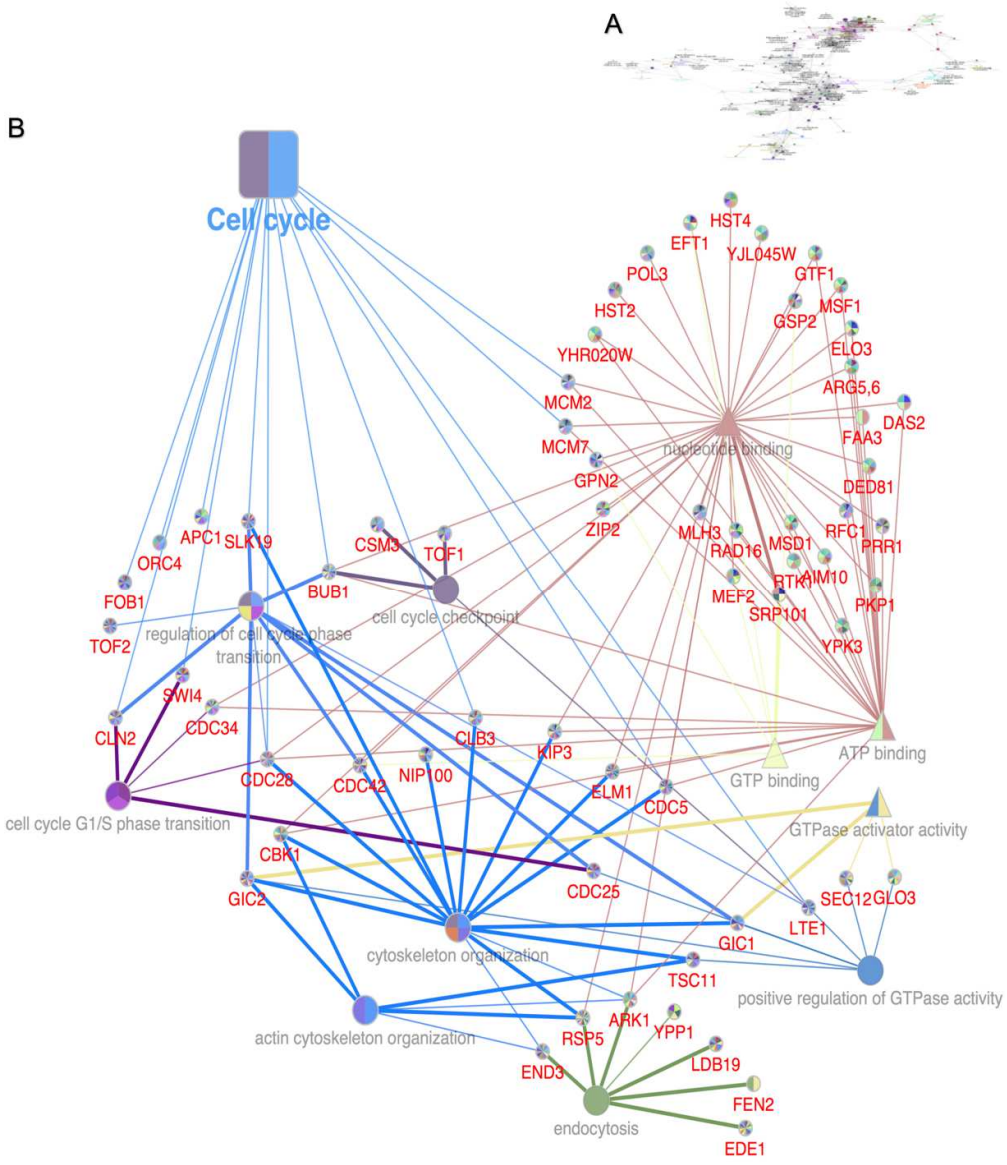

Figure 6: Interactively functional annotation network of 238 differentially responsive mutants. **A)** The functionally grouped network of KEGG pathway and gene ontology terms that are presented as nodes and linked to each other based on the similarity of their associated genes using ClueGo app along with Cytoscape software. **B)** Magnification of the highest significant node revealed the most significant node as the cell cycle pathway ($P < 0.000$). The square node represents the KEGG pathway, the circle nodes represent biological processes, and triangle nodes represent molecular function, while the colors denote clustered genes associated with the biological category and the size of node represents the *P* values (0.05 as cutoff value). CluePedia app shows the genes for each node where the thickness of edges reflects the GO evidence code (thick line is based on experimental evidence whereas thin line is inferred from electronic annotation).

Before assessing biological responses to the aurone, growth curves were used to confirm the sensitivity or resistance responses of the individual mutants to SH1009 (Ericson et al., 2010). Twelve mutants that had more than or equal to a 2-fold change and were also involved in the suggested biological responses from both HIP and HOP profiles were tested individually using dilutions (3.125 μM –200 μM) of SH1009. The differences in the log-phase of the growth between the wild type *S. cerevisiae*-S288C and the mutants treated with SH1009 was compared. **Fig. 7** and **(Appendix F)** depict the growth curves of individual *S. cerevisiae* deletion mutants for confirmation of the growth patterns of the HIP and HOP profiles.

The individual, heterozygous sensitive strains *TSC11*Δ, *YPP1*Δ, *CDC42*Δ, *CDC25*Δ, *CDC28*Δ, and *RSP5*Δ from chemical-genetic profiling all showed reduced growth with SH1009 treatment when compared to the log-phase growth of *S. cerevisiae*-S288C wild type, which supports results from chemical-genetic interaction analysis (**Fig. 7A**). For the homozygous mutant strains, the same cellular effects were observed with decreased growth for sensitive mutants (*LTE1*Δ, *FEN2*Δ, and *ARK1*Δ) and increased growth for resistant mutants (*CLN2*Δ, *LIN1*Δ, and *ZIP2*Δ) in the presence of SH1009 when compared to the wild type *S. cerevisiae*-S288C (**Fig. 7B)**. Additionally, the growth of each mutant in the IC_{50} concentration of SH1009 (16 μM) was compared independently to the growth of *S. cerevisiae*-S288C to assess significant differences between the growth of each mutant and the wild type. All mutants demonstrated significant differences in growth from the wild type ($P \leq 0.05 – 0.0001$), confirming their expected growth patterns as sensitive or resistant mutants to the aurone SH1009 and supporting the enrichment analysis results since these mutants harbor deletions of genes that are associated with cell cycle progression (*CDC25*Δ, *CDC28*Δ,

*CLN2*Δ, *LIN1*Δ, and *ZIP2*Δ), actin cytoskeleton organization (*TSC11*Δ, *CDC42*Δ, *RSP5*Δ, *LTE1*Δ, and *ARK1*Δ), and endocytosis (*TSC11*Δ, *YPP1*Δ, *FEN2*Δ, and *RSP5*Δ) (**Fig. 7C**). Once we confirmed the growth patterns of individual *S. cerevisiae* mutants to aurone SH1009, *C. albicans* was treated with the aurone to detect phenotypic changes associated with the suggested biological responses in the pathogen.

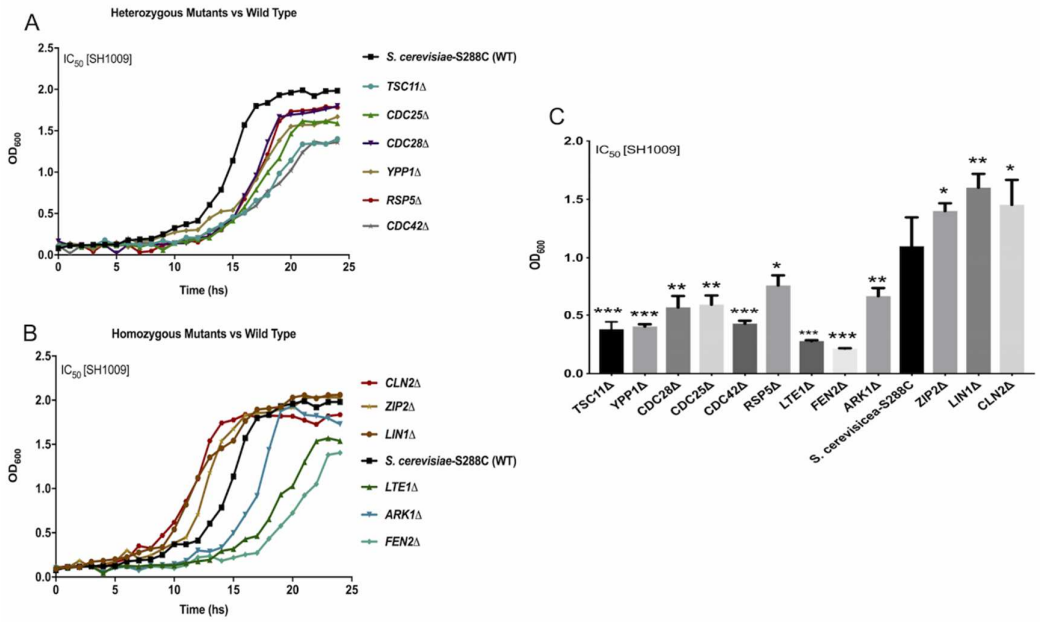

Figure 7: Growth curves of SH1009-treated *S. cerevisiae*-S288C and mutants validate chemical-genetic interaction. A) and **B)** The growth curves of the heterozygous mutants (HIP) and homozygous mutants (HOP), respectively, comparing to the wild type *S. cerevisiae*-S288C under the IC_{50} concentration of aurone SH1009 treatment (16 µM) in YPD broth using the Bioscreen C growth curve instrument, and reading the OD_{600} at 30 min intervals for 25 h during incubation at 30°C. **C)** Individual significance comparisons of the growth of each mutant and wild type *S. cerevisiae*-S288C during exponential phase in the IC_{50} concentration of aurone SH1009 are presented as mean±SEM using Dunnett's multiple comparisons test for heterozygous and homozygous mutants. *P* values (* $P \leq 0.05$) (** $P \leq 0.001$) (*** $P \leq 0.0001$).

Aurone SH1009 blocks cell cycle progression in *Candida albicans*

Cell cycle was the most significantly enriched pathway in the chemical-genetic interaction analysis (**Fig. 5** and **6**). The other enriched pathways, meiosis and DNA replication, also contribute to the cell cycle pathway. Accordingly, if aurone SH1009 targets cell cycle gene-encoded proteins, the distribution of cell cycle phases in the fungal cell population during exponential phase should be altered compared to the normal distribution, indicating cell cycle arrest. For these experiments, changes in DNA content throughout different cell cycle phases was assessed by flow cytometry, which allows quantitative single cell detection. By labeling cellular DNA with propidium iodide (PI), the cells can be quantitatively discriminated in different phases of the cell cycle based on the fluorescence intensity, which is proportional to specific cell cycle phase (Rosebrock, 2017). Since G1 phase cells have a single copy of the genome, thus having the lowest amounts of DNA, whereas S phase cells are actively involved in DNA replication and will have increased amounts of DNA, and G2/M cells have two times the nuclear DNA of G1 phase cells, flow cytometric analyses of propidium iodide-stained nuclei can effectively differentiate G0/G1, S, and G2/M populations.

Before treating *C. albicans* SC5314 cells with SH1009 or cytochalasin D (CytoD) as a positive control for cell cycle arrest, a sample of early exponential culture was harvested and processed as described in the Materials and Methods to ensure cells were actively growing. The histogram in **Fig. 8A**. indicates a rapidly dividing culture by having a significant fraction of cells (~70%) in the S phase. The histogram depicts an optimal flow-cytometric distribution for an actively growing yeast culture in rich media during early exponential phase, and was compatible with previous observations (Rosebrock, 2017; Slater et al., 1977). After an additional 3 h of incubation without treatment, the untreated *C. albicans* SC5314 cells were still dividing with

approximately similar cell cycle-distributed phases before three additional hours of incubation (**Fig. 8B**). However, contrary to the cell cycle progression in untreated samples, the cell cycle distribution for *C. albicans* SC5314 cells that were incubated for 3 h with the SH1009 IC_{50} concentration were distinctly perturbed (**Fig. 8C**). There was a significant decrease in the fraction of cells in the S phase (46.88% compared to 70% in untreated cells, $P < 0.001$) and a significant increase in the proportion of cells in the G1 phase (46% compared to 16.53%, $P < 0.0001$), indicating accumulating cells in G1 phase (**Fig. 8E**). As expected, 3 h of treatment with CytoD, an anticancer drug that inhibits the assembly and disassembly of actin subunits, led to a delay in the progression of G1 phase (Heng & Koh, 2010). The DNA histogram revealed fewer cells in S phase and more in the G1 phase (52.68%, 39.17.0% and 2.13% in G0/G1, S and G2/M phases, respectively) (**Fig. 8D)**.

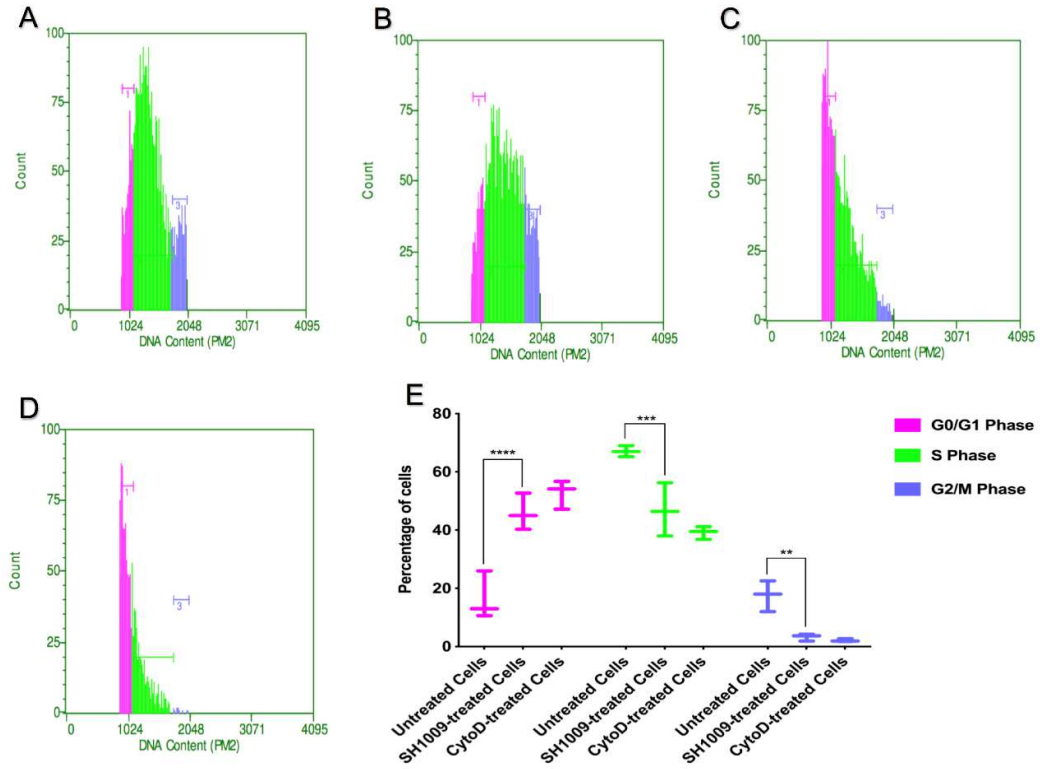

Figure 8: Flow-cytometric analysis of the effects of aurone SH1009 on cell cycle progression in *C. albicans* SC5314. DNA histogram plots showing the percentages of cells in G0/G1 phase (pink peak on left), S phase (green center peak) and G2/M phase (blue peak on right) as a percentage of the total count of cells that were stained with Propidium Iodide (red fluorescence) and analyzed using the Millipore Guava flow cytometer and the Guava PCA-96 software system. A) Untreated cells at 0 time, B) untreated cells after 3 h of additional incubation, C) aurone SH1009-treated cells after 3 h of treatment with IC_{50} SH1009 concentration (16 µM), and **D)** CytoD-treated cells after 3 h of treatment (25 µM) as a positive control. **E)** The significance comparison, *P* values (**** $P \leq 0.0001$), (*** $P \leq 0.001$), (** $P \leq 0.01$) from a two-way ANOVA used to compare three population groups of G0/G1, S, and G2/M phases between untreated cells and SH1009-treated cells.

The accumulation of SH1009-treated cells in G1 phase implies that aurone SH1009 arrests cell cycle progression, supporting the chemical-genetic interaction results in which the most significantly responsive mutants to SH1009 essentially possess deletions for cell cycle-encoding proteins. The chemical-genetic analysis showed that homozygous deletion strain *CLN2*Δ, which lacks the G1 cyclin gene, was resistant to SH1009 (**Fig. 7B**), and heterozygous deletion strain *CDC28*Δ, cyclin-dependent kinase (CDK), was sensitive to SH1009 (**Fig. 7A**). In *S. cerevisiae,* cyclin Cln2 activates CdcC28 in late G1 phase, resulting in regulation of actin cytoskeleton polarization, which is crucial for bud emergence and G1 to S phase transition during cell cycle progression (Park & Bi, 2007). Therefore, we next sought to determine whether aurone SH1009 affected the disruption of the actin cytoskeleton.

Aurone SH1009 perturbs actin cytoskeleton dynamics in *C. albicans*

The chemical-genetic interaction analysis indicated that cell-cycle-dependent organization of the actin cytoskeleton and endocytosis are targets of aurone SH1009 due to highly significant growth perturbation of 18 heterozygous and homozygous deletion mutants annotated as involved in actin cytoskeleton organization and endocytosis (**Fig 6B**). Fluorescent staining of actin and confocal laser scanning microscopy were used to visualize the effects of SH1009 on polarization of the actin cytoskeleton. SH1009-treated and untreated *C. albicans* SC5314 cells along with the *S. cerevisiae CDC42*Δ heterozygous deletion strain with a deletion for an actin-regulatory gene were examined microscopically for phenotypes indicative of disruption of actin distribution. In late G1 phase of the cell cycle of budding yeast, the actin patches should normally be assembled in the tip of the small-growing bud with clear actin cables that are polarized from the bud tip towards the mother cell. Actin cables serve as tracks to transport mRNAs, proteins, mitochondria, and ribosomes from the mother cell to the

daughter cell. Actin patches are clustered in the secretion and endocytosis sites for critical roles in plasma membrane invagination during endocytosis (Mishra et al., 2014) and cell wall remodeling through orienting the polarized secretion of cell wall constituents and enzymes towards the actin patches, promoting bud emergence (Irazoqui & Lew, 2004; Kopecká et al., 2015).

The images in **Fig. 9** depict typical actin polarization for untreated *C. albicans* SC5314 cells during exponential phase in which ~76.47% of cells were observed with red-fluorescent actin patches concentrated in the buds along with polarized-apical cell growth. However, after 3 h of SH1009 treatment, *C. albicans* cells appeared abnormally round and enlarged compared to untreated cells, indicating depolarized growth (**Fig. 9**, DIC panel). In addition, only ~34.17% of SH1009-treated cells retained actin patches in the buds while the remaining had actin patches that were scattered randomly in both the mother cell and buds, signifying actin depolarization. In addition, SH1009-treated cells displayed a distinctively distorted actin assembly resulting in a considerable number of large aggregates of the actin (**Fig. 9**, Actin panel). This phenotype was previously associated with endocytic mutants such as, but not limited to, *ARK1*Δ (Ayscough, 2005), *END3*Δ (Gourlay & Ayscough, 2005), and *RPS5*Δ (Kamińska et al., 2002). In growth curve studies with SH1009-individually treated deletion mutants, these strains were either sensitive (*ARK1*Δ and *RPS5*Δ) or resistant (*END3*Δ) to SH1009 (**Fig. 7A** & **7B**) and were also identified in our chemical-genetic interaction analysis (**Fig. 6B**). A previous study that investigated the composition of the actin clumps using immune-electron microscopy detected an accumulation of endocytic vesicles surrounded with actin filaments and a mixture of actin patches and endocytic proteins, suggesting a failure to mature the endocytic vesicles properly as a consequence of the

inability to disassemble the actin-associated endocytic complexes (Sekiya-Kawasaki et al., 2003).

The actin distribution in the *S. cerevisiae CDC42*Δ deletion mutant was also investigated due to its sensitivity to SH1009 (**Fig. 7A**). In the majority of *S. cerevisiae CDC42*Δ mutant cells, there was an accumulation of large, round, unbudded cells with distributed actin patches (**Fig. 9**, DIC panel), which supports previous reports (Park & Bi, 2007). The depolarized growth as well as the abnormal distribution of the actin patches in SH1009-treated *C. albicans* cells support inhibition of cell cycle arrest by preventing G1 phase progression (**Fig. 8D**). In yeast cells, it has been evidenced in several studies that failure in rearrangement of actin patches at the bud site in G1 phase will prevent the emergence of the bud and arrest the cell cycle at G1 phase (Howell & Lew, 2012; Ushinsky et al., 2002). These findings are compatible with previous observations that have established a definitive link between intact actin cytoskeleton organization and cell cycle progression (Heng & Koh, 2010).

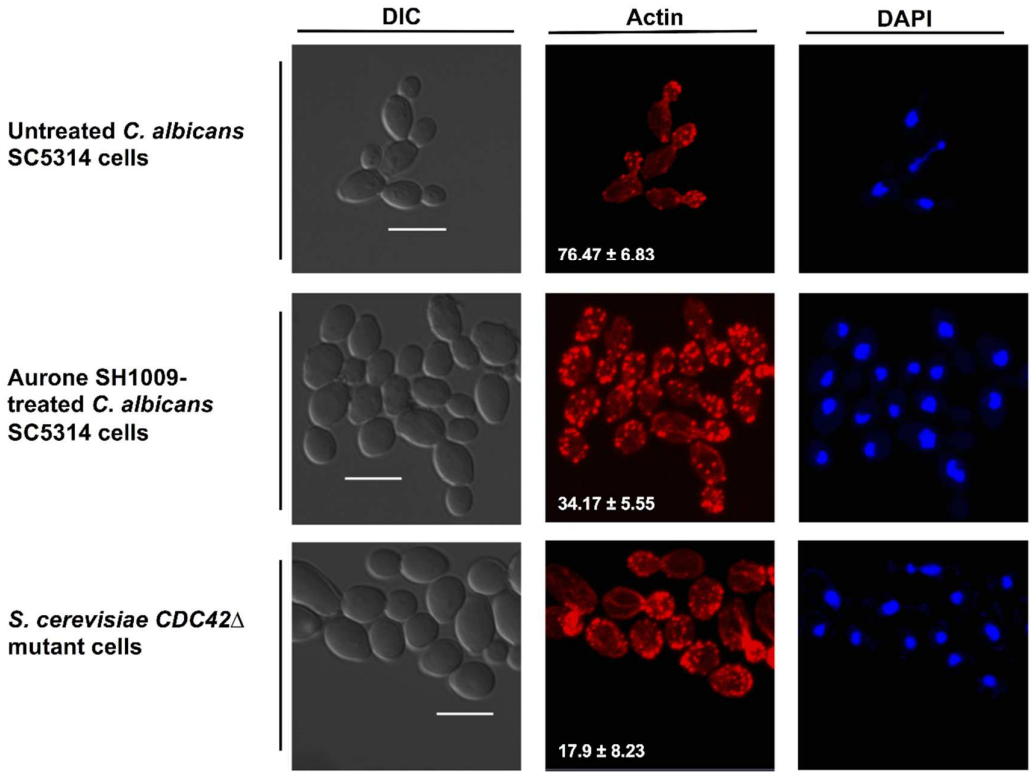

Figure 9: Actin cytoskeleton dynamics in aurone SH1009-treated yeast cells. *C. albicans* SC5314 and *S. cerevisiae CDC42*Δ mutant cells were fixed and the actin was stained with red-fluorescent rhodamine phalloidin (RP) and nuclear DNA was stained with blue-fluorescent DAPI. Scale bar = 5 µm. Quantitative data represent the percentage of cells that retained a polarized actin cytoskeleton as comparison between aurone SH1009-treated and untreated *C. albicans* SC5314 cells Means±SEM. (*P* value< 0.01).

Aurone SH1009 alters *C. albicans* expression of genes involved in the cell cycle, actin polarization, and endocytosis

To study changes in gene expression in response to aurone SH1009, quantitative reverse transcription-PCR was employed to confirm mRNA abundance of a set of *C. albicans* SC5314 genes homologous to the *S. cerevisiae*-S288C genes in the heterozygous and homozygous deletion mutants identified as significantly enriched in pathways from the chemical-genetic interaction analysis (**Fig. 5**). The cell cycle-associated genes were the most responsive to aurone SH1009. Successful cell cycle progression requires expression of checkpoint genes that guarantee sequential execution of certain cellular processes. For instance, before chromosome segregation, chromosomal DNA must first be replicated. These processes are ordered by activation and inactivation of (CDK) Cdc28, an ATP-binding protein, which complexes with activating subunits called cyclins (Howell & Lew, 2012). *HGC1*, is a *C. albicans* gene homologous to *S. cerevisiae* G1 cyclin gene *CLN2*, encoding a G1 cyclin that binds with Cdc28 to form a cyclin-CDK complex with a central role in G1/S transition during the cell cycle (Wang, 2016; Zheng & Wang, 2004). SH1009-treated *C. albicans* SC5314 results in a ~2.3 and 4.9-fold respective downregulation of *CDC28* and *HGC1* gene expression after 1.5 h of treatment (**Fig. 10**), supporting a role for SH1009 in arresting the *C. albicans* cell cycle in G1 phase (**Fig. 8C**).

Binding of Cdc28 to Hgc1 is an important regulator step for controlling cell cycle progression. This complex regulates polarity by phosphorylating and blocking Rga2 (a negative regulator of Cdc42), thus activating Cdc42 (GTP-binding protein), leading to sustained actin polarization and hyphal growth (Zheng et al., 2007). Failure in the relocation of Cdc42 by the Cdc28-Hgc1 complex to either the bud site or hyphal tip in late G1 phase results in a haphazard distribution of actin cytoskeleton and

subsequently accumulation of unbudded, enlarged cells (Park & Bi, 2007; Ushinsky et al., 2002). The *S. cerevisiae CDC42*Δ deletion mutant was hypersensitive to aurone SH1009 treatment (>70% inhibition) at concentration 16 μM (**Fig. 7A**). In SH1009-treated *C. albicans* SC5314, *CDC42* expression was downregulated two-fold (**Fig. 10**), which would confirm the downstream effect of SH1009 on expression of *CDC28* and *HGC1*.

Cdc28 also controls the cell cycle by regulation of DNA replication. The *MCM2* gene encodes an ATP-binding protein that is a part of the pre-replicative complex known as mini-chromosome maintenance, consisting of proteins Mcm2-7, which acts as a helicase to unwind DNA and initiate DNA replication (Tye, 1999). In *S. cerevisiae*, after assembly of the MCM2-7 complex in G1 phase, MCM2-7 requires phosphorylation at the end of G1 by a Cdc28-kinase complex in order to recruit DNA polymerase and initiate DNA replication (Enserink & Kolodner, 2010). SH1009 treatment resulted in a significant five-fold decrease in MCM2 by 1.5 h after treatment (**Fig. 10**), which could represent an additional downstream effect of SH1009 on Cdc28. Mmc2 is also an ATP-binding protein and, along with 12 other proteins enriched by chemical-genetic interaction analysis, contains the widely-distributed P-loop motif, supporting nucleotide-binding proteins as potential targets for SH1009 (Saraste et al., 1990).

In addition to *CDC28,* other genes that encode for nucleotide-binding proteins with roles in signal transduction pathways were identified in deletion mutants with differential sensitivities to aurone SH1009. The *C. albicans CDC25* and *RAS1* genes were downregulated by ~3-fold and 2-fold, respectively (**Fig. 10**). *CDC25* encodes a GTP-binding protein that acts as a guanine nucleotide exchange factor and is the

upstream activator of the Ras/cAMP signaling pathway, responsible for activating the GTP-binding protein, Ras1, which then activates the cAMP synthesis required for cell cycle progression (Toda et al., 1985; Weeks & Spiegelman, 2003). Additionally, Ras1 activation of cAMP synthesis leads to maintenance of the hyphal growth, a virulence factor in systemic candidiasis, by regulating the G1 cyclin Hgc1 which binds to Cdc28 to localize Cdc42 to the hyphal tip (Zheng & Wang, 2004). As evidenced by a previous study, SH1009 was the only aurone compound that disrupted the biofilm formation (Sutton et al., 2017), which would require inhibiting hyphal growth as a key component of biofilm formation.

In contrast to decreased expression of *RAS1* transcripts, *RAS2* transcripts were upregulated 2-fold after 3 h of SH1009 treatment (**Fig. 10**). *RAS2* encodes a GTPase in *C. albicans*, and a previous study has shown cAMP levels in a *RAS1*Δ mutant declined 20-fold yet increased by ~10% in a *RAS2*Δ mutant, indicating an antagonistic activity of *C. albicans* Ras2 on the cAMP levels through an unknown mechanism. In *S. cerevisiae*, both Ras1 and Ras2 are required for activating cAMP synthesis. However, unlike in *S. cerevisiae* in which Ras1 and Ras2 have been well studied and share sequence homology, *C. albicans RAS2* has poor sequence homology with *S. cerevisiae RAS* sequences (Zhu et al., 2009). Although the response of *RAS2* to SH1009 is unclear due to the lack of studies on *C. albicans* Ras2 activity or its interaction with other members of the Ras/cAMP signaling pathway, the upregulation of transcripts may be a response to downregulation of upstream molecules affected by SH1009.

Another transcriptional upregulation in SH1009-treated *C. albicans* was increased expression of *TSC11* after 1.5 h of aurone treatment (**Fig. 10**). *TSC11* encodes a GTP-binding protein characterized as regulating actin cytoskeletal dynamics during

polarized growth and endocytosis (deHart et al., 2003; Schmidt et al., 1996). The increased expression of *TSC11* could be a detoxification mechanism for *C. albicans* to counter the negative effects of SH1009 on actin cytoskeletal dynamics and endocytosis. Previous studies reported phenotypes of *TSC11*Δ mutants (also known as *AVO3* or *RICTOR* in mammals) as having abnormal actin polarization (Ho et al., 2005), reduced endocytosis rate (Grahammer et al., 2017), and arrested cell cycle progression (Hietakangas & Cohen, 2008). Another gene involved in endocytosis exhibiting altered expression in response to SH1009 was *ERG3* which was downregulated 3-fold (**Fig. 10**). *ERG3* is involved in the ergosterol biosynthesis pathway, and gene deletion has been documented as attenuating the endocytosis rate (Heese-Peck et al., 2002). Reduced expression of *ERG3* could also be attributed to the upstream effects of SH1009 on the RAS/cAMP signaling pathway that positively regulates the expression of the *ERG* gene family (Bahn et al., 2007).

Gene expression of *RPS4a,* which encodes a 40S ribosomal protein, decreased 2-fold with SH1009 treatment (**Fig. 10**). A genome-wide study of haploinsufficient *C. alibcans* deletion mutants that were fractionated for abnormal cell size revealed genes associated with ribosome biogenesis and cell cycle, suggesting a correlation between ribosome biogenesis rate and size-dependent cell cycle progression (Chaillot et al., 2017). In *S. cerevisiae*, repressing the synthesis of this conserved gene, *RPS4a*, results in arresting G1 phase or a significantly prolonged G1 phase, along with the phenotype of increased cell size (Thapa et al., 2013), which could explain the enlarged cell phenotype observed microscopically in SH1009-treated *C. albicans* cells (**Fig. 9)**.

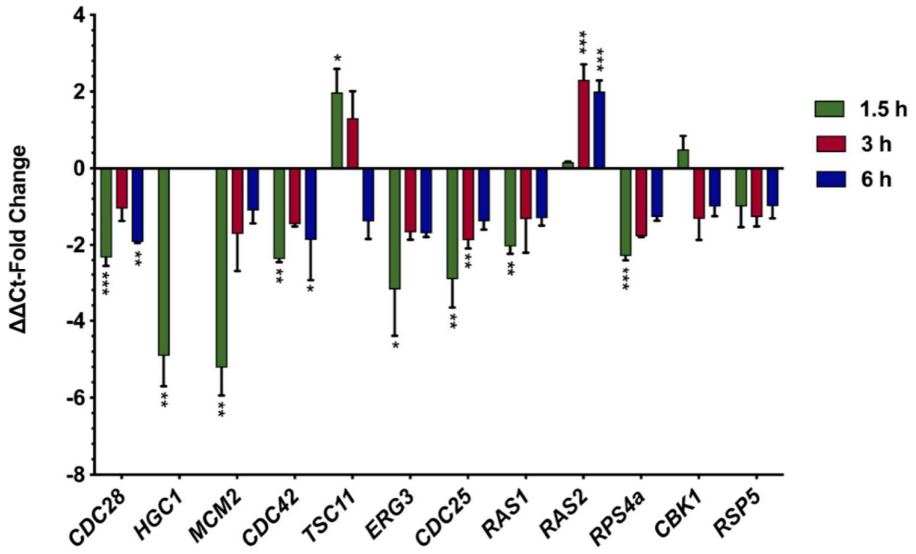

Figure 10: Expression of genes in aurone SH1009-treated *C. albicans* SC5314. The relative gene expression of normalized transcript levels of treated samples was calculated by comparison to normalized transcript levels of untreated samples ($\mathbf{2}^{-\Delta\Delta Ct}$) for cell cycle- and actin cytoskeleton-associated genes at indicated time points of treatment. The data are means from two biological replicates, each with three technical replicates. The fold changes that are ≥ 1.8 with *P* values ≤ 0.05 (* $P \leq 0.05$), (** $P \leq 0.001$), (*** $P \leq 0.0001$) were considered significant for upregulation (positive scores) or downregulation (negative scores).

DISCUSSION

In this study, we investigated *in vitro* antifungal activity of the bioactive compound, aurone SH1009, against widely used CLSI reference resistance tester strains and additional strains of *Candida* spp. using the CLSI broth microdilution method (Wayne, 2002). Aurone SH1009 was not only inhibitory for susceptible strains, but was also inhibitory for resistant-clinical isolates. The clinical isolates, *C. albicans* M4: Gu2 and *C. albicans* M6: F1 were isolated initially as fluconazole-susceptible strains from two HIV-infected patients who were suffering from recurrent oropharyngeal candidiasis. After a two-year period of fluconazole treatment, the last isolates in each series were fluconazole-resistant counterparts known as *C. albicans* M5: Gu5 and *C. albicans* M7: F5 (Franz et al., 1998). *C. albicans* M5 and M7 have acquired gain of function mutations, leading to homozygous alleles for the transcriptional factors *MRR1* and *TAC1* which have been documented for overexpressing the *CDR1*/*2* (Candida Drug Resistance) and *MDR1* (Multi-Drug Resistance) genes for azole-efflux pumps, respectively (Coste et al., 2009). Additionally, *C. albicans* M2: ScTAC1R34A and *C. albicans* M3: ScMRR1R34A are fluconazole-resistant strains that have been mutated in *C. albicans* SC5314 background to encode $MRR1^{P683S}$ and $TAC1^{G980E}$ homozygous activating alleles, respectively. As a consequence of these mutations, the expression of efflux pumps are induced, causing a reduction in intracellular accumulation of azoles and ultimately high fluconazole resistance (Sasse et al., 2011; Schubert et al., 2011).

Loss-of-heterozygosity events as genetic alterations are commonly associated with fluconazole resistance, reflecting the capacity of *C. albicans* to generate adaptive-homozygous mutations, which is attributed to the extraordinary plasticity of the *C. albicans* genome (Ford et al., 2015; Pais, Galocha, Viana, et al., 2019). Aurone SH1009

exhibited considerably low IC_{50} values in the inhibition of these fluconazole-resistant isolates, indicating that the highly expressed efflux pumps could be modulated by aurone SH1009. The efflux pumps *CDR1*/*2* are mainly ATP-binding cassette (ABC) transporter proteins that harness the energy from ATP hydrolysis in order to extrude drug out of the yeast cell (Prasad et al., 2019). In fact, as consistent with previous studies on cancer cells, aurones selectively inhibited the pumping action of these transporters by binding with the C-terminal nucleotide-binding domain of P-glycoprotein which belongs to the ATP-binding cassette (ABC) superfamily (Boumendjel et al., 2002; Sim et al., 2011). The modulatory effect of aurones on drug-efflux pumps allows the intracellular accumulation of the compound and its associated toxicity, which reverses the resistance mechanism and renders the resistant cells as susceptible again, making these bioactive compounds attractive candidates as reversal agents to control drug resistance (Pradines, 2018).

Multidrug resistant isolate *C. albicans* ATCC 64124 is known as Darlington's strain, the name of the patient suffering from chronic mucocutaneous candidiasis (Ryley et al., 1984). Darlington strain, 64124, is defined as resistant to all antifungal agents except 5-fluorocytosine at high concentration (Basso et al., 2018). The resistance mechanisms toward multiple classes of antifungal agents of Darlington's strain have not been studied, but evidence of the evolution of multidrug resistance has been published recently, demonstrating the capacity of clinical *C. albicans* isolates to adapt during long-term antifungal treatment (Jensen et al., 2015). Multidrug resistance is recognized as a multistep process resulting from a gradual accumulation of mutations during long-term antifungal treatment. Briefly, the resistance began with fluconazole treatment that causes an activation mutation in *TAC1*, followed by caspofungin

exposure that leads to a mutation in *FKS1*. Then, amphotericin B treatment causes a loss of function mutation in *ERG2*. Consequently, the final strain was a multidrug resistant strain that acquired all the three mutations and exhibited resistance to three classes of the standard antifungal drugs (Prasad et al., 2019).

Unlike *C. albicans* that acquires the resistance, *C. glabrata* is resistant to azole drugs due to ~67 gain of function mutations in the transcriptional factor *CgPDR1* gene, resulting in overexpression of *CgCDR1/2*-encoded efflux pumps (Ferrari et al., 2009). This could account for the dramatic increase in *C. glabrata* infections since the introduction of azole drugs in the 1980s, identifying *C. glabrata* as the second most common non-*albicans* cause of candidiasis. Drug resistance of *C. glabrata* has not only been found for azoles, but also for all known antifungal drugs, posing a serious challenge to antifungal therapy for the organism (Pais, Galocha, & Teixeira, 2019). Our results indicated that aurone SH1009 effectively inhibited *Candida* spp. growth and exhibited acceptable pharmacodynamics properties (time- and concentration-dependent killing) that were similar to fluconazole, as a valuable estimation for a prospective antimicrobial agent (Pfaller et al., 2004).

After establishing SH1009 antifungal activity, we proceeded to characterize the antifungal mechanism. Studying the mode of action of a new drug is a critical prerequisite to improve therapeutic action and avoid unwanted side effects, but it has been a challenge in drug discovery due to the high consumption of cost and time. However, since the first yeast deletion collection was created in 2002 (Giaever et al., 2002), chemogenomic profiling has been proven as a powerful system for characterizing the mode of action and molecular targets of several drugs (Parsons et al., 2004), as well as thousands of additional bioactive molecules (Hoepfner et al., 2014;

Lee et al., 2014). A considerable number of studies have been recently reviewed the broad spectrum of biological activities of aurone compounds as anticancer agents identified using phenotype-based approaches, exploiting the existing knowledge of a given cellular process inhibited by aurones, including inhibition of CDKs, DNA scissoring, histone deacetylase, topoisomerase, ATP-binding cassette transporter, and tubulin polymerization (Alsayari et al., 2019). In contrast, here, a genetic-based approach was applied to comprehensively reveal all the biological effects of aurone treatment as a potential antimicrobial. The chemogenomic approach that was used in this study is a reverse-genetics technique that allows for comprehensive identification of gene products that functionally interact with bioactive molecules by exposing previously constructed libraries of *S. cerevisiae* mutants to the condition of interest, which in this study was exposure to the novel aurone SH1009. These yeast mutants harbor deletions of the majority (96%) of the yeast genome with only one mutant per deletion-gene. Due to nearly complete coverage of the yeast genome, this approach guarantees unbiased results because it completely maps all targets (biological responses) simultaneously under the term of interconnected pathways of eukaryotic cell (Pierce et al., 2007).

In this study, chemogenomic profiling of *S. cerevisiae* mutants with aurone SH1009 identified roles for genes involved in cell cycle, DNA replication, cell division, actin cytoskeleton, and endocytosis. Enrichment analysis for biological responses in heterozygous and homozygous mutants was first performed separately to confirm significant responses in each pool. The responses were then combined to map the functional annotation network of KEGG pathways, biological responses, and molecular functions simultaneously using GO enrichment analysis to find that the top responsive

heterozygous and homozygous mutants clustered for actin cytoskeleton and endocytosis processes. GO enrichment analysis was also used to map the cell cycle pathway as the most significantly enriched pathway, also encompassing the other enriched biological processes and revealing nucleotide-binding proteins as the molecular function of the most of significantly enriched genes.

Nucleotide-binding proteins play a central role in a variety of pivotal cellular processes, including cell signaling, proliferation, cytoskeletal assembly, protein synthesis, and apoptosis (Xiao & Wang, 2016). The low number of GTP-binding proteins that were identified in this study could be attributed to a relatively low abundance of GTP-binding proteins in nature compared to ATP-binding proteins (Xiao et al., 2013). Nevertheless, because purine nucleoside triphosphates share a similar structure, some ATP-binding proteins may utilize GTP as the phosphate donor and vice versa (Jakobi & Traugh, 1995). In this respect, aurone SH1009 might possess an affinity for the same binding site in different but related nucleotide-binding proteins, hence, affecting a broader spectrum of cellular processes. The functional enrichment of genes encoding nucleotide-binding proteins during analysis of the deletion pool of essential and non-essential genes suggests that aurone SH1009 potentially interacts with nucleotide-binding proteins, leading to a series of cellular defects impacting the cell cycle, actin cytoskeleton, and endocytosis. The benzofuranone ring of SH1009 may dictate the biological activity due to mimicry of adenine, subsequently, inhibiting the activity of ATP-dependent proteins (Sicheri et al., 1997).

Our chemical genetic interaction and enrichment analysis also suggest that treatment with aurone SH1009 targets nucleotide-binding proteins, producing alterations in cell cycle, actin cytoskeleton organization, and endocytosis in *S.*

cerevisiae. These phenotypic changes in response to SH1009 were confirmed in *C. albicans* SC5314 using cell sorting analysis by flow cytometry, which delineated increased populations of cells in G1 phase after 3 h of aurone SH1009 treatment. In *S. cerevisiae*, heterozygous mutants with gene deletions for proteins affecting the cell division cycle (*CDC5*Δ, *CDC34*Δ, *CDC42*Δ, *CDC25*Δ, and *CDC13*Δ) that sensitively responded to aurone SH1009 are all controlled by the master regulator of the cell cycle, (CDK) Cdc28, a catalytic kinase that couples with activating subunits such as Clb3 and Cln2 (Suryadinata et al., 2010), the genes for which both responded to SH1009 as homozygous-resistant mutants. Also, the accumulation of SH1009-treated *C. albicans* cells in G1 phase implies that the cells are in cell cycle arrest and do not yet engage in DNA synthesis, also supporting the chemical-genetic interaction results in which DNA replication mutants *POL3*Δ, *MCM2*Δ, *MCM7*Δ, *RFC1*Δ, *RFC3*Δ, and *ORC4*Δ from the HIP profile were sensitive to SH1009. In *C. albicans*, gene expression during different cell cycle stages has been previously characterized using microarray technology (Cote et al., 2009). This study reported expression of several genes that are required for G1/S transition and some of these genes are identified as sensitive or resistant mutants from our chemical-genetic profiles, including *POL3* for DNA polymerase subunit, *RFC1* and *RFC2* for DNA replication factor elements, *TOF1* gene for a DNA replication checkpoint, *CSM3* gene for accurate chromosome segregation, *SWI4* transcription factor for activation of G1 transition (**Fig. 6**).

Our results are also in agreement with a prior study reporting that aurones arrest the cell cycle via targeting (CDK) protein Cdc28, making aurones a promising candidate for cancer therapy (Boumendjel, 2003). Among different aurone derivatives synthesized as potential anticancer agents, aurone compounds that possess a methoxy

group at position 4 on ring B, like aurone SH1009, were found to produce an enhanced antiproliferative activity by significantly arresting the cell cycle at G2/M phase (Alsayari et al., 2019). In our study, fluorescent imaging was performed to detect actin cytoskeleton depolarization as a consequence of aurone SH1009 perturbation of rearrangement of actin patches in the bud site at the end of G1 phase, leading to cell cycle arrest at G1 phase. These phenotypic findings support the chemogenomic responses of *S. cerevisiae* genes *CDC28*Δ, *CLN2*Δ, and *CDC42*Δ to SH1009, because it has been well characterized that the G1 cyclin Cln2 binds to Cdc28 to localize Cdc42 to promote actin polarization and G1/S phase transition (Park & Bi, 2007).

Chemogenomic profiling does have limitations; for instance, cellular mechanisms affected by SH1009 were identified using growth as a sole endpoint measurement, potentially resulting in selection for false positive sensitivities due to slow growth of some deletion mutants or, in the worst scenario, loss of indispensable mutants. Another limitation is that responses in *S. cerevisiae* differ from responses in *C. albicans* because of the ability of *C. albicans* to produce true hyphae and differences in sensitivity and resistance to antifungals. To confirm specific gene responses in *C. albicans,* relative levels of mRNA of genes identified as differentially responsive were quantified in *C. albicans* SC5314. A sizable subset of genes that function in cell cycle progression was differentially regulated in response to SH1009, leading to a potentially hierarchal pathway beginning with Cdc25 and Ras1 that regulate G1 cyclin Hgc1, which binds to Cdc28 in order to localize Cdc42*,* leading to actin polarization and cell cycle progression. Cdc25 and Ras1 regulate the RAS/cAMP signaling pathway which controls Erg3 maintenance of normal endocytosis rates. The transcriptional changes in the genes for these molecules support the biological responses observed in phenotypic

studies.

Two genes, *CBK1* and *RSP5*, identified by chemogenomic profiling in *S. cerevisiae*, did not demonstrate significant differential expression to SH1009 treatment in *C. albicans* in spite of their respective documented roles in polarized growth (Song et al., 2008) and organized actin patches with normal endocytosis (Kamińska et al., 2002). *CBK1*Δ mutant was among the top 20 sensitive heterozygous deletion mutants (**S2 Table**), and the *RSP5*Δ mutant was confirmed using growth curves for its sensitivity to SH1009 (**Fig. 7A**). Failure to detect changes in gene expression could be related to the timing of expression or discordance between regulation and gene expression. In *S. cerevisiae,* the *TSC11*Δ mutant was hypersensitive to SH1009, however, this gene was transcriptionally upregulated in *C albicans*, which could indicate a difference in survival responses between the two yeasts. This highlights that although this study has validated chemical-genetic interaction using *S. cerevisiae* mutant collections to characterize the mode of action for a novel bioactive aurone compound against *C. albicans*, chemical-genetic interaction studies could also be used to elucidate potential differences in drug responses between organisms.

CONCLUSION

In summary, we investigated aurone SH1009 for antifungal activity, human cell line cytotoxicity, and pharmacodynamics properties. Aurone SH1009 exhibited promising selectively fungistatic-inhibitory activity against *Candida* spp., particularly resistant isolates, highlighting the possibility of a broad-spectrum property for aurone SH1009 against other pathogenic fungi. We also provided the first, comprehensive genome-wide study of haploinsufficiency and homozygous screening in *S. cerevisiae* for a bioactive aurone compound. Chemical-genetic interaction analysis predicted that

SH1009 targets cell cycle-dependent organization of the actin cytoskeleton and endocytosis, suggesting a novel mode of action for this aurone compound. Phenotypic studies for these significantly enriched biological responses were completed in *C. albicans* demonstrating G1 phase-arrested cells with abnormal, depolarized actin cytoskeleton. Differential expression of genes, identified by chemical-genetic interaction, in response of SH1009 *in C. albicans* coincided with enrichment of cells in G1 phase and actin depolarization producing a model that offers a significant improvement in understanding the mechanism for toxicity. The current study provides experimental frameworks for future mechanistic studies that could be used to investigate the bioactivity of a large number of aurone compounds using chemical-genetic interaction and phenotypic-based methods.

References

Alsayari, A., Muhsinah, A. B., Hassan, M. Z., Ahsan, M. J., Alshehri, J. A., & Begum, N. (2019). Aurone: A biologically attractive scaffold as anticancer agent. *Eur J Med Chem*, *166*, 417-431. https://doi.org/10.1016/j.ejmech.2019.01.078

Aqil, F., Zahin, M., Ahmad, I., Owais, M., Sajjad, M., Khan, A., Bansal, S., & Farooq, S. (2010). *Antifungal Activity of Medicinal Plant Extractsand Phytocompounds: A Review*. Springer-Verlag Berlin Heidelberg.

Ayscough, K. R. (2005). Coupling actin dynamics to the endocytic process in Saccharomyces cerevisiae. *Protoplasma*, *226*(1-2), 81-88. https://doi.org/10.1007/s00709-005-0107-5

Bahn, Y. S., Molenda, M., Staab, J. F., Lyman, C. A., Gordon, L. J., & Sundstrom, P. (2007). Genome-wide transcriptional profiling of the cyclic AMP-dependent signaling pathway during morphogenic transitions of Candida albicans. *Eukaryot Cell*, *6*(12), 2376-2390. https://doi.org/10.1128/EC.00318-07

Bandgar, B. P., Patil, S. A., Korbad, B. L., Biradar, S. C., Nile, S. N., & Khobragade, C. N. (2010). Synthesis and biological evaluation of a novel series of 2,2-bisaminomethylated aurone analogs as anti-inflammatory and antimicrobial agents. *Eur. J. Med. Chem.*, *45*(7), 3223-3227. https://doi.org/10.1016/j.ejmech.2010.03.045

Bassilana, M., Hopkins, J., & Arkowitz, R. A. (2005). Regulation of the Cdc42/Cdc24 GTPase module during Candida albicans hyphal growth. *Eukaryot Cell*, *4*(3), 588-603. https://doi.org/10.1128/EC.4.3.588-603.2005

Basso, V., Garcia, A., Q. Tran, D., Schaal, J., Tran, P., Ngole, D., Aqeel, Y., Tongaonkar, P., Ouellette, A., & Selsted, M. (2018). *Fungicidal Potency and Mechanisms of -Defensins against Multidrug-Resistant Candida Species* (Vol. 62). https://doi.org/10.1128/AAC.00111-18

Bindea, G., Galon, J., & Mlecnik, B. (2013). CluePedia Cytoscape plugin: pathway insights using integrated experimental and in silico data. *Bioinformatics*, *29*(5), 661-663. https://doi.org/10.1093/bioinformatics/btt019

Bindea, G., Mlecnik, B., Hackl, H., Charoentong, P., Tosolini, M., Kirilovsky, A., Fridman, W.-H., Pages, F., Trajanoski, Z., & Galon, J. (2009). ClueGO: a Cytoscape plug-in to decipher functionally grouped gene ontology and pathway annotation networks. *Bioinformatics*, *25*(8), 1091-1093. https://doi.org/10.1093/bioinformatics/btp101

Bondaryk, M., KurzAtkowski, W., & Staniszewska, M. (2013). Antifungal agents commonly used in the superficial and mucosal candidiasis treatment: mode of action and resistance development. *Postepy Dermatol Alergol*, *30*(5), 293-301.

Boumendjel, A. (2003). Aurones: A subclass of flavones with promising biological potential. *Current Medicinal Chemistry*, *10*(23), 2621-2630. https://doi.org/10.2174/0929867033456468

Boumendjel, A., Beney, C., Deka, N., Mariotte, A. M., Lawson, M. A., Trompier, D., Baubichon-Cortay, H., & Di Pietro, A. (2002). 4-Hydroxy-6-methoxyaurones with high-affinity binding to cytosolic domain of P-glycoprotein. *Chem Pharm Bull (Tokyo)*, *50*(6), 854-856.

Brown, G. D., Denning, D. W., Gow, N. A. R., Levitz, S. M., Netea, M. G., & White, T. C. (2012). Hidden killers: human fungal infections. *Sci. Transl. Med.*, *4*(165), 165rv113, 110 pp. https://doi.org/10.1126/scitranslmed.3004404

Chaillot, J., Cook, M. A., Corbeil, J., & Sellam, A. (2017). Genome-Wide Screen for Haploinsufficient Cell Size Genes in the Opportunistic Yeast. *G3 (Bethesda)*, *7*(2), 355-360. https://doi.org/10.1534/g3.116.037986

Chang, M., Bellaoui, M., Boone, C., & Brown, G. W. (2002). A genome-wide screen for methyl methanesulfonate-sensitive mutants reveals genes required for S phase progression in the presence of DNA damage. *Proceedings of the National Academy of Sciences*, *99*(26), 16934-16939. https://doi.org/10.1073/pnas.262669299

CLSI. (2017). Reference method for broth dilution antifungal susceptibility testing of yeasts. In (CLSI standard M27 4th ed.): Wayne, PA: Clinical and Laboratory Standards Institute.

Coste, A., Ferrari, S., & Sanglard, D. (2009). Antifungal drug resistance mechanisms in fungal pathogens from the perspective of transcriptional gene regulation. *FEMS Yeast Research*, *9*(7), 1029-1050. https://doi.org/10.1111/j.1567-1364.2009.00578.x

Cote, P., Hogues, H., & Whiteway, M. (2009). Transcriptional analysis of the Candida albicans cell cycle. *Mol. Biol. Cell*, *20*(14), 3363-3373. https://doi.org/10.1091/mbc.E09-03-0210

deHart, A. K., Schnell, J. D., Allen, D. A., Tsai, J. Y., & Hicke, L. (2003). Receptor internalization in yeast requires the Tor2-Rho1 signaling pathway. *Mol Biol Cell*, *14*(11), 4676-4684. https://doi.org/10.1091/mbc.e03-05-0323

Enserink, J. M., & Kolodner, R. D. (2010). An overview of Cdk1-controlled targets and processes. *Cell Div*, *5*, 11. https://doi.org/10.1186/1747-1028-5-11

Ericson, E., Hoon, S., St. Onge, R. P., Giaever, G., & Nislow, C. (2010). Exploring gene function and drug action using chemogenomic dosage assays. *Methods Enzymol.*, *470*(Guide to Yeast Genetics (2nd Edition)), 233-255. https://doi.org/10.1016/s0076-6879(10)70010-0

Ferrari, S., Ischer, F., Calabrese, D., Posteraro, B., Sanguinetti, M., Fadda, G., Rohde, B., Bauser, C., Bader, O., & Sanglard, D. (2009). Gain of function mutations in CgPDR1 of Candida glabrata not only mediate antifungal resistance but also enhance virulence. *PLoS pathogens*, *5*(1), e1000268-e1000268. https://doi.org/10.1371/journal.ppat.1000268

Ferreira, E. O., Salvador, M. J., Pral, E. M. F., Alfieri, S. C., Ito, I. Y., & Dias, D. A. (2004). A new heptasubstituted (E)-aurone glucoside and other aromatic compounds of Gomphrena agrestis with biological activity. *Zeitschrift Fur Naturforschung C-a Journal of Biosciences*, *59*(7-8), 499-505.

Ford, C. B., Funt, J. M., Abbey, D., Issi, L., Guiducci, C., Martinez, D. A., Delorey, T., Li, B. Y., White, T. C., Cuomo, C., Rao, R. P., Berman, J., Thompson, D. A., & Regev, A. (2015). The evolution of drug resistance in clinical isolates of Candida albicans. *eLife*, *4*, e00662-e00662. https://doi.org/10.7554/eLife.00662

Franz, R., Kelly, S. L., Lamb, D. C., Kelly, D. E., Ruhnke, M., & Morschhäuser, J. (1998). Multiple molecular mechanisms contribute to a stepwise development of fluconazole resistance in clinical Candida albicans strains. *Antimicrob Agents Chemother*, *42*(12), 3065-3072.

Giaever, G., Chu, A. M., Ni, L., Connelly, C., Riles, L., Veronneau, S., Dow, S., Lucau-Danila, A., Anderson, K., Andre, B., Arkin, A. P., Astromoff, A., El Bakkoury, M., Bangham, R., Benito, R., Brachat, S., Campanaro, S., Curtiss, M., Davis, K., Deutschbauer, A., Entian, K.-D., Flaherty, P., Foury, F., Garfinkel, D. J., Gerstein, M., Gotte, D., Gueldener, U., Hegemann, J. H., Hempel, S., Herman,

Z., Jaramillo, D. F., Kelly, D. E., Kelly, S. L., Koetter, P., LaBonte, D., Lamb, D. C., Lan, N., Liang, H., Liao, H., Liu, L., Luo, C., Lussier, M., Mao, R., Menard, P., Ooi, S. L., Revuelta, J. L., Roberts, C. J., Rose, M., Ross-Macdonald, P., Scherens, B., Schimmack, G., Shafer, B., Shoemaker, D. D., Sookhai-Mahadeo, S., Storms, R. K., Strathern, J. N., Valle, G., Voet, M., Volckaert, G., Wang, C.-y., Ward, T. R., Wilhelmy, J., Winzeler, E. A., Yang, Y., Yen, G., Youngman, E., Yu, K., Bussey, H., Boeke, J. D., Snyder, M., Philippsen, P., Davis, R. W., & Johnston, M. (2002). Functional profiling of the Saccharomyces cerevisiae genome. *Nature (London, U. K.)*, *418*(6896), 387-391. https://doi.org/10.1038/nature00935

Gillum, A. M., Tsay, E. Y. H., & Kirsch, D. R. (1984). Isolation of the Candida albicans gene for orotidine-5′-phosphate decarboxylase by complementation of S. cerevisiae ura3 and E. coli pyrF mutations. *Molecular and General Genetics MGG*, *198*(1), 179-182. https://doi.org/10.1007/BF00328721

Gourlay, C. W., & Ayscough, K. R. (2005). Identification of an upstream regulatory pathway controlling actin-mediated apoptosis in yeast. *J Cell Sci*, *118*(Pt 10), 2119-2132. https://doi.org/10.1242/jcs.02337

Grahammer, F., Helmstaedter, M., Osenberg, D., Kuhne, L., Kretz, O., Wanner, N., Huber Tobias, B., Ramakrishnan Suresh, K., Larionov Alexey, A., Syed, M., Theilig, F., Rinschen Markus, M., Benzing, T., Khatib, H., Roerden, M., Artunc, F., Sass Jorn, O., & Jouret, F. (2017). mTOR Regulates Endocytosis and Nutrient Transport in Proximal Tubular Cells. *J Am Soc Nephrol*, *28*(1), 230-241.

Greig, J. A., Sudbery, I. M., Richardson, J. P., Naglik, J. R., Wang, Y., & Sudbery, P. E. (2015). Cell cycle-independent phospho-regulation of Fkh2 during hyphal growth regulates Candida albicans pathogenesis. *PLoS Pathog*, *11*(1), e1004630. https://doi.org/10.1371/journal.ppat.1004630

Harris, M. A., Clark, J., Ireland, A., Lomax, J., Ashburner, M., Foulger, R., Eilbeck, K., Lewis, S., Marshall, B., Mungall, C., Richter, J., Rubin, G. M., Blake, J. A., Bult, C., Dolan, M., Drabkin, H., Eppig, J. T., Hill, D. P., Ni, L., Ringwald, M., Balakrishnan, R., Cherry, J. M., Christie, K. R., Costanzo, M. C., Dwight, S. S., Engel, S., Fisk, D. G., Hirschman, J. E., Hong, E. L., Nash, R. S., Sethuraman, A., Theesfeld, C. L., Botstein, D., Dolinski, K., Feierbach, B., Berardini, T., Mundodi, S., Rhee, S. Y., Apweiler, R., Barrell, D., Camon, E., Dimmer, E., Lee, V., Chisholm, R., Gaudet, P., Kibbe, W., Kishore, R., Schwarz, E. M., Sternberg, P., Gwinn, M., Hannick, L., Wortman, J., Berriman, M., Wood, V., de la Cruz, N., Tonellato, P., Jaiswal, P., Seigfried, T., White, R., & Gene Ontology, C. (2004). The Gene Ontology (GO) database and informatics resource. *Nucleic acids research*, *32*(Database issue), D258-D261. https://doi.org/10.1093/nar/gkh036

Heese-Peck, A., Pichler, H., Zanolari, B., Watanabe, R., Daum, G., & Riezman, H. (2002). Multiple functions of sterols in yeast endocytosis. *Mol Biol Cell*, *13*(8), 2664-2680. https://doi.org/10.1091/mbc.e02-04-0186

Helliwell, S. B., Howald, I., Barbet, N., & Hall, M. N. (1998). TOR2 is part of two related signaling pathways coordinating cell growth in Saccharomyces cerevisiae. *Genetics*, *148*(1), 99-112.

Heng, Y. W., & Koh, C. G. (2010). Actin cytoskeleton dynamics and the cell division cycle. *Int J Biochem Cell Biol*, *42*(10), 1622-1633. https://doi.org/10.1016/j.biocel.2010.04.007

Hietakangas, V., & Cohen, S. M. (2008). TOR complex 2 is needed for cell cycle progression and anchorage-independent growth of MCF7 and PC3 tumor cells. *BMC Cancer*, *8*, No pp given. https://doi.org/10.1186/1471-2407-8-282

Ho, H.-L., Shiau, Y.-S., & Chen, M.-Y. (2005). Saccharomyces cerevisiaeTSC11/AVO3 participates in regulating cell integrity and functionally interacts with components of the Tor2 complex. *Curr Genet*, *47*(5), 273-288.

Hoepfner, D., Helliwell, S. B., Sadlish, H., Schuierer, S., Filipuzzi, I., Brachat, S., Bhullar, B., Plikat, U., Abraham, Y., Altorfer, M., Aust, T., Baeriswyl, L., Cerino, R., Chang, L., Estoppey, D., Eichenberger, J., Frederiksen, M., Hartmann, N., Hohendahl, A., Knapp, B., Krastel, P., Melin, N., Nigsch, F., Oakeley, E. J., Petitjean, V., Petersen, F., Riedl, R., Schmitt, E. K., Staedtler, F., Studer, C., Tallarico, J. A., Wetzel, S., Fishman, M. C., Porter, J. A., & Movva, N. R. (2014). High-resolution chemical dissection of a model eukaryote reveals targets, pathways and gene functions. *Microbiol. Res.*, *169*(2-3), 107-120. https://doi.org/10.1016/j.micres.2013.11.004

Hoon, S., St. Onge, R. P., Giaever, G., & Nislow, C. (2008). Yeast chemical genomics and drug discovery: an update. *Trends Pharmacol. Sci.*, *29*(10), 499-504. https://doi.org/10.1016/j.tips.2008.07.006

Howell, A. S., & Lew, D. J. (2012). Morphogenesis and the cell cycle. *Genetics*, *190*(1), 51-77. https://doi.org/10.1534/genetics.111.128314

Huang, W., Liu, M. Z., Li, Y., Tan, Y., & Yang, G. F. (2007). Design, syntheses, and antitumor activity of novel chromone and aurone derivatives. *Bioorganic & Medicinal Chemistry*, *15*(15), 5191-5197. https://doi.org/10.1016/j.bmc.2007.05.022

Institute, C. a. L. S. (2008). Reference method for broth dilution antifungal susceptibility testing of yeasts. *Approved Standard-Third Edition M27-A3*, *28*.

Irazoqui, J. E., & Lew, D. J. (2004). Polarity establishment in yeast. *Journal of Cell Science*, *117*(11), 2169-2171. https://doi.org/10.1242/jcs.00953

Jakobi, R., & Traugh, J. A. (1995). Analysis of the ATP/GTP binding site of casein kinase II by site-directed mutagenesis. *Physiol Chem Phys Med NMR*, *27*(4), 293-301.

Jensen, R. H., Astvad, K. M. T., Silva, L. V., Sanglard, D., Jørgensen, R., Nielsen, K. F., Mathiasen, E. G., Doroudian, G., Perlin, D. S., & Arendrup, M. C. (2015). Stepwise emergence of azole, echinocandin and amphotericin B multidrug resistance in vivo in Candida albicans orchestrated by multiple genetic alterations. *The Journal of antimicrobial chemotherapy*, *70*(9), 2551-2555. https://doi.org/10.1093/jac/dkv140

Kamińska, J., Gajewska, B., Hopper, A. K., & Zoładek, T. (2002). Rsp5p, a new link between the actin cytoskeleton and endocytosis in the yeast Saccharomyces cerevisiae. *Mol Cell Biol*, *22*(20), 6946-6948.

Kayser, O., Kiderlen, A. F., Folkens, U., & Kokodziej, H. (1999). In vitro leishmanicidal activity of aurones. *Planta Medica*, *65*(4), 316-319. https://doi.org/10.1055/s-1999-13993

Klepser, M. E., Ernst, E. J., Lewis, R. E., Ernst, M. E., & Pfaller, M. A. (1998). Influence of test conditions on antifungal time-kill curve results: proposal for standardized methods. *Antimicrob Agents Chemother*, *42*(5), 1207-1212.

Kopecká, M., Yamaguchi, M., & Kawamoto, S. (2015). Effects of the F-actin inhibitor latrunculin A on the budding yeast Saccharomyces cerevisiae. *Microbiology*, *161*(7), 1348-1355. https://doi.org/doi:10.1099/mic.0.000091

Kullberg, B. J., & Arendrup, M. C. (2015). Invasive candidiasis. *N. Engl. J. Med.*, *373*(15), 1445-1456. https://doi.org/10.1056/NEJMra1315399

Lawrence, N. J., Rennison, D., McGown, A. T., & Hadfield, J. A. (2003). The total synthesis of an aurone isolated from Uvaria hamiltonii: Aurones and flavones as anticancer agents. *Bioorganic & Medicinal Chemistry Letters*, *13*(21), 3759-3763. https://doi.org/10.1016/j.bmcl.2003.07.003

Leach, M. D., & Cowen, L. E. (2014). Membrane fluidity and temperature sensing are coupled via circuitry comprised of Ole1, Rsp5, and Hsf1 in Candida albicans. *Eukaryot Cell*, *13*(8), 1077-1084. https://doi.org/10.1128/EC.00138-14

Lee, A. Y., St. Onge, R. P., Proctor, M. J., Wallace, I. M., Nile, A. H., Spagnuolo, P. A., Jitkova, Y., Gronda, M., Wu, Y., Kim, M. K., Cheung-Ong, K., Torres, N. P., Spear, E. D., Han, M. K. L., Schlecht, U., Suresh, S., Duby, G., Heisler, L. E., Surendra, A., Fung, E., Urbanus, M. L., Gebbia, M., Lissina, E., Miranda, M., Chiang, J. H., Aparicio, A. M., Zeghouf, M., Davis, R. W., Cherfils, J., Boutry, M., Kaiser, C. A., Cummins, C. L., Trimble, W. S., Brown, G. W., Schimmer, A. D., Bankaitis, V. A., Nislow, C., Bader, G. D., & Giaever, G. (2014). Mapping the Cellular Response to Small Molecules Using Chemogenomic Fitness Signatures. *Science (Washington, DC, U. S.)*, *344*(6180), 208-211. https://doi.org/10.1126/science.1250217

Liken, H. B., & Kaufman, D. A. (2018). Candida. In J. B. Cantey (Ed.), *Neonatal Infections: Pathophysiology, Diagnosis, and Management* (pp. 33-49). Springer International Publishing. https://doi.org/10.1007/978-3-319-90038-4_4

Lopez-Lazaro, M., Martin-Cordero, C., Toro, M. V., & Ayuso, M. J. (2002). Flavonoids as DNA topoisomerase I poisons. *J. Enzyme Inhib. Med. Chem.*, *17*(1), 25-29. https://doi.org/10.1080/14756360290011744

Lu, H., Yao, X. W., Whiteway, M., Xiong, J., Liao, Z. B., Jiang, Y. Y., & Cao, Y. Y. (2015). Loss of RPS41 but not its paralog RPS42 results in altered growth, filamentation and transcriptome changes in Candida albicans. *Fungal Genet Biol*, *80*, 31-42. https://doi.org/10.1016/j.fgb.2015.03.012

Mishra, B. B., & Tiwari, V. K. (2011). Natural products: An evolving role in future drug discovery. *European Journal of Medicinal Chemistry*, *46*(10), 4769-4807. https://doi.org/10.1016/j.ejmech.2011.07.057

Mishra, M., Huang, J., & Balasubramanian, M. K. (2014). The yeast actin cytoskeleton. *FEMS Microbiology Reviews*, *38*(2), 213-227. https://doi.org/10.1111/1574-6976.12064

Mitra, S., Gómez-Raja, J., Larriba, G., Dubey, D. D., & Sanyal, K. (2014). Rad51-Rad52 mediated maintenance of centromeric chromatin in Candida albicans. *PLoS Genet*, *10*(4), e1004344. https://doi.org/10.1371/journal.pgen.1004344

Morimoto, M., Fukumoto, H., Nozoe, T., Hagiwara, A., & Komai, K. (2007). Synthesis and insect antifeedant activity of aurones against Spodoptera litura larvae. *Journal of Agricultural and Food Chemistry*, *55*(3), 700-705. https://doi.org/10.1021/jf062562t

Nailis, H., Coenye, T., Van Nieuwerburgh, F., Deforce, D., & Nelis, H. J. (2006). Development and evaluation of different normalization strategies for gene expression studies in Candida albicans biofilms by real-time PCR. *BMC Mol Biol*, *7*, 25. https://doi.org/10.1186/1471-2199-7-25

Pais, P., Galocha, M., & Teixeira, M. C. (2019). Genome-Wide Response to Drugs and Stress in the Pathogenic Yeast Candida glabrata. In I. Sá-Correia (Ed.), *Yeasts in Biotechnology and Human Health: Physiological Genomic Approaches* (pp. 155-193). Springer International Publishing. https://doi.org/10.1007/978-3-030-13035-0_7

Pais, P., Galocha, M., Viana, R., Cavalheiro, M., Pereira, D., & Teixeira, M. C. (2019). Microevolution of the pathogenic yeasts Candida albicans and Candida glabrata during antifungal therapy and host infection. *Microbial cell (Graz, Austria)*, *6*(3), 142-159. https://doi.org/10.15698/mic2019.03.670

Pare, P. W., Dmitrieva, N., & Mabry, T. J. (1991). PHYTOALEXIN AURONE INDUCED IN CEPHALOCEREUS-SENILIS LIQUID SUSPENSION-CULTURE. *Phytochemistry*, *30*(4), 1133-1135. https://doi.org/10.1016/s0031-9422(00)95189-6

Park, H. O., & Bi, E. (2007). Central roles of small GTPases in the development of cell polarity in yeast and beyond. *Microbiol Mol Biol Rev*, *71*(1), 48-96. https://doi.org/10.1128/MMBR.00028-06

Parsons, A. B., Brost, R. L., Ding, H., Li, Z., Zhang, C., Sheikh, B., Brown, G. W., Kane, P. M., Hughes, T. R., & Boone, C. (2004). Integration of chemical-genetic and genetic interaction data links bioactive compounds to cellular target pathways. *Nat. Biotechnol.*, *22*(1), 62-69. https://doi.org/10.1038/nbt919

Pfaller, M. A., & Diekema, D. J. (2007). Epidemiology of invasive candidiasis: a persistent public health problem. *Clin. Microbiol. Rev.*, *20*(1), 133-163. https://doi.org/10.1128/cmr.00029-06

Pfaller, M. A., Sheehan, D. J., & Rex, J. H. (2004). Determination of fungicidal activities against yeasts and molds: lessons learned from bactericidal testing and the need for standardization. *Clin Microbiol Rev*, *17*(2), 268-280.

Pierce, S. E., Davis, R. W., Nislow, C., & Giaever, G. (2007). Genome-wide analysis of barcoded Saccharomyces cerevisiae gene-deletion mutants in pooled cultures. *Nat. Protoc.*, *2*(11), 2958-2974. https://doi.org/10.1038/nprot.2007.427

Piotrowski, J. S., Simpkins, S. W., Li, S. C., Deshpande, R., McIlwain, S. J., Ong, I. M., Myers, C. L., Boone, C., & Andersen, R. J. (2015). Chemical Genomic Profiling via Barcode Sequencing to Predict Compound Mode of Action. *Methods Mol. Biol. (N. Y., NY, U. S.)*, *1263*(Chemical Biology), 299-318. https://doi.org/10.1007/978-1-4939-2269-7_23

Pradines, B. (2018). P-Glycoprotein-Like Transporters in Leishmania: A Search for Reversal Agents: Consequences, Molecular Mechanisms and Possible Treatments. In (pp. 319-340). https://doi.org/10.1007/978-3-319-74186-4_14

Prasad, R., Nair, R., & Banerjee, A. (2019). Emerging Mechanisms of Drug Resistance in Candida albicans. In I. Sá-Correia (Ed.), *Yeasts in Biotechnology and Human Health: Physiological Genomic Approaches* (pp. 135-153). Springer International Publishing. https://doi.org/10.1007/978-3-030-13035-0_6

Rajendra, P. (2017). *Candida albicans : Cellular and Molecular Biology* (2nd ed.). Springer Nature.

Rosebrock, A. P. (2017). Analysis of the Budding Yeast Cell Cycle by Flow Cytometry. *Cold Spring Harb Protoc*, *2017*(1). https://doi.org/10.1101/pdb.prot088740

Ryley, J. F., Wilson, R. G., & Barrett-Bee, K. J. (1984). Azole resistance in Candida albicans. *Sabouraudia*, *22*(1), 53-63.

Saraste, M., R. Sibbald , P., & Wittinghofer, A. (1990). The P-loop — a common motif in ATP- and GTP-binding proteins. *Trends in Biochemical Sciences*, *15*(11), 430-434.

Sardi, J. C. O., Scorzoni, L., Bernardi, T., Fusco-Almeida, A. M., & Giannini, M. J. S. M. (2013). Candida species: current epidemiology, pathogenicity, biofilm formation, natural antifungal products and new therapeutic options. *J. Med. Microbiol.*, *62*(1), 10-24. https://doi.org/10.1099/jmm.0.045054-0

Sasse, C., Schillig, R., Dierolf, F., Weyler, M., Schneider, S., Mogavero, S., Rogers, P. D., & Morschhäuser, J. (2011). The transcription factor Ndt80 does not contribute to Mrr1-, Tac1-, and Upc2-mediated fluconazole resistance in Candida albicans. *PloS one*, *6*(9), e25623-e25623. https://doi.org/10.1371/journal.pone.0025623

Schmidt, A., Kunz, J., & Hall, M. N. (1996). TOR2 is required for organization of the actin cytoskeleton in yeast. *Proc Natl Acad Sci U S A*, *93*(24), 13780-13785.

Schmittgen, T. D., & Livak, K. J. (2008). Analyzing real-time PCR data by the comparative CT method. *Nat. Protoc.*, *3*(6), 1101-1108. https://doi.org/10.1038/nprot.2008.73

Schubert, S., Barker, K. S., Znaidi, S., Schneider, S., Dierolf, F., Dunkel, N., Aïd, M., Boucher, G., Rogers, P. D., Raymond, M., & Morschhäuser, J. (2011). Regulation of efflux pump expression and drug resistance by the transcription factors Mrr1, Upc2, and Cap1 in Candida albicans. *Antimicrobial agents and chemotherapy*, *55*(5), 2212-2223. https://doi.org/10.1128/AAC.01343-10

Sekiya-Kawasaki, M., Groen, A. C., Cope, M. J., Kaksonen, M., Watson, H. A., Zhang, C., Shokat, K. M., Wendland, B., McDonald, K. L., McCaffery, J. M., & Drubin, D. G. (2003). Dynamic phosphoregulation of the cortical actin cytoskeleton and endocytic machinery revealed by real-time chemical genetic analysis. *J Cell Biol*, *162*(5), 765-772. https://doi.org/10.1083/jcb.200305077

Sicheri, F., Moarefi, I., & Kuriyan, J. (1997). Crystal structure of the Src family tyrosine kinase Hck. *Nature*, *385*(6617), 602-609.

Silva, S., Negri, M., Henriques, M., Oliveira, R., Williams, D. W., & Azeredo, J. (2012). Candida glabrata, Candida parapsilosis and Candida tropicalis: biology, epidemiology, pathogenicity and antifungal resistance. *FEMS Microbiol. Rev.*, *36*(2), 288-305. https://doi.org/10.1111/j.1574-6976.2011.00278.x

Sim, H. M., Loh, K. Y., Yeo, W. K., Lee, C. Y., & Go, M. L. (2011). Aurones as Modulators of ABCG2 and ABCB1: Synthesis and Structure–Activity Relationships. *ChemMedChem*, *6*(4), 713-724. https://doi.org/10.1002/cmdc.201000520

Slater, M. L., Sharrow, S. O., & Gart, J. J. (1977). Cell cycle of Saccharomycescerevisiae in populations growing at different rates. *Proc Natl Acad Sci U S A*, *74*(9), 3850-3854.

Song, Y., Cheon, S. A., Lee, K. E., Lee, S. Y., Lee, B. K., Oh, D. B., Kang, H. A., & Kim, J. Y. (2008). Role of the RAM network in cell polarity and hyphal morphogenesis in Candida albicans. *Mol Biol Cell*, *19*(12), 5456-5477. https://doi.org/10.1091/mbc.e08-03-0272

Suryadinata, R., Sadowski, M., & Sarcevic, B. (2010). Control of cell cycle progression by phosphorylation of cyclin-dependent kinase (CDK) substrates. *Bioscience Reports*, *30*(4), 243-255. https://doi.org/10.1042/bsr20090171

Sutton, C. L., Taylor, Z. E., Farone, M. B., & Handy, S. T. (2017). Antifungal activity of substituted aurones. *Bioorg. Med. Chem. Lett.*, *27*(4), 901-903. https://doi.org/10.1016/j.bmcl.2017.01.012

Thapa, M., Bommakanti, A., Shamsuzzaman, M., Gregory, B., Samsel, L., Zengel, J. M., & Lindahl, L. (2013). Repressed synthesis of ribosomal proteins generates protein-specific cell cycle and morphological phenotypes. *Mol Biol Cell*, *24*(23), 3620-3633. https://doi.org/10.1091/mbc.E13-02-0097

Tisdall, J. (2001). *Beginning Perl for Bioinformatics* (First Edition ed.). O'REILLY.

Toda, T., Uno, I., Ishikawa, T., Powers, S., Kataoka, T., Broek, D., Cameron, S., Broach, J., Matsumoto, K., & Wigler, M. (1985). In yeast, RAS proteins are controlling elements of adenylate cyclase. *Cell*, *40*(1), 27-36.

Tye, B. K. (1999). MCM proteins in DNA replication. *Annu Rev Biochem*, *68*, 649-686. https://doi.org/10.1146/annurev.biochem.68.1.649

Ushinsky, S. C., Harcus, D., Ash, J., Dignard, D., Marcil, A., Morchhauser, J., Thomas, D. Y., Whiteway, M., & Leberer, E. (2002). CDC42 is required for polarized growth in human pathogen Candida albicans. *Eukaryot Cell*, *1*(1), 95-104.

Wang, Y. (2016). Hgc1-Cdc28-how much does a single protein kinase do in the regulation of hyphal development in Candida albicans? *J Microbiol*, *54*(3), 170-177. https://doi.org/10.1007/s12275-016-5550-9

Wayne, P. (2002). Reference method for broth dilution antifungal susceptibility testing of yeasts, approved standard. *CLSI document M27-A2*.

Webb, N. E., Montefiori, D. C., & Lee, B. (2015). Dose-response curve slope helps predict therapeutic potency and breadth of HIV broadly neutralizing antibodies. *Nat Commun*, *6*, 8443. https://doi.org/10.1038/ncomms9443

Weeks, G., & Spiegelman, G. B. (2003). Roles played by Ras subfamily proteins in the cell and developmental biology of microorganisms. *Cell Signal*, *15*(10), 901-909.

Wilson Leslie, S., Reyes Carolina, M., Stolpman, M., Speckman, J., Allen, K., & Beney, J. (2002). The direct cost and incidence of systemic fungal infections. *Value Health*, *5*(1), 26-34.

Wisplinghoff, H., Ebbers, J., Geurtz, L., Stefanik, D., Major, Y., Edmond, M. B., Wenzel, R. P., & Seifert, H. (2014). Nosocomial bloodstream infections due to Candida spp. in the USA: species distribution, clinical features and antifungal susceptibilities. *Int. J. Antimicrob. Agents*, *43*(1), 78-81. https://doi.org/10.1016/j.ijantimicag.2013.09.005

Xiao, Y., Guo, L., Jiang, X., & Wang, Y. (2013). Proteome-wide discovery and characterizations of nucleotide-binding proteins with affinity-labeled chemical probes. *Anal Chem*, *85*(6), 3198-3206. https://doi.org/10.1021/ac303383c

Xiao, Y., & Wang, Y. (2016). Global discovery of protein kinases and other nucleotide-binding proteins by mass spectrometry. *Mass Spectrom Rev*, *35*(5), 601-619. https://doi.org/10.1002/mas.21447

Xie, J. L., Qin, L., Miao, Z., Grys, B. T., Diaz, J. C., Ting, K., Krieger, J. R., Tong, J., Tan, K., Leach, M. D., Ketela, T., Moran, M. F., Krysan, D. J., Boone, C., Andrews, B. J., Selmecki, A., Ho Wong, K., Robbins, N., & Cowen, L. E. (2017). The Candida albicans transcription factor Cas5 couples stress responses, drug resistance and cell cycle regulation. *Nat Commun*, *8*(1), 499. https://doi.org/10.1038/s41467-017-00547-y

Zheng, X., & Wang, Y. (2004). Hgc1, a novel hypha-specific G1 cyclin-related protein regulates Candida albicans hyphal morphogenesis. *EMBO J*, *23*(8), 1845-1856. https://doi.org/10.1038/sj.emboj.7600195

Zheng, X. D., Lee, R. T., Wang, Y. M., Lin, Q. S., & Wang, Y. (2007). Phosphorylation of Rga2, a Cdc42 GAP, by CDK/Hgc1 is crucial for Candida albicans hyphal growth. *EMBO J*, *26*(16), 3760-3769. https://doi.org/10.1038/sj.emboj.7601814

Zhu, Y., Fang, H. M., Wang, Y. M., Zeng, G. S., Zheng, X. D., & Wang, Y. (2009). Ras1 and Ras2 play antagonistic roles in regulating cellular cAMP level, stationary-phase entry and stress response in Candida albicans. *Mol Microbiol*, *74*(4), 862-875. https://doi.org/10.1111/j.1365-2958.2009.06898.x

APPENDICES

APPENDIX A

Strains used in this study

Strains	Relevant characteristics or genotype	Reference
Candida albicans ATCC 90028	Reference strain	(CLSI, 2008)
C. albicans ATCC 90029	Reference strain	(CLSI, 2008)
C. albicans M1: SC5314	Wild-type *C. albicans* model strain	(Gillum et al., 1984)
C. glabrata ATCC 66032	Reference strain	(Institute, 2008)
C. tropicalis ATCC 750	Reference strain	(Institute, 2008)
C. albicans M4: Gu2	Clinical isolate from patient G, fluconazole-susceptible	(Franz et al., 1998)
C. albicans M6: F1	Clinical isolate from patient F, fluconazole-susceptible	(Franz et al., 1998)
C. albicans M5: Gu5	Clinical isolate from patient G, fluconazole-resistant, gain of function mutation in TF *TAC1*	(Franz et al., 1998)
C. albicans M7: F5	Clinical isolate from patient F, fluconazole-resistant, gain of function mutation in TF *MRR1*	(Franz et al., 1998)
C. albicans M2: ScTAC1R34A	$TAC1^{G980E}$ mutation, fluconazole-resistant	(Sasse et al., 2011)
C. albicans M3: ScMRR1R34A	$MRR1^{P683S}$ mutation, fluconazole-resistant	(Schubert et al., 2011)
C. albicans ATCC 64124	Multidrug resistant isolate, resistant to amphotericin B, caspofungin, fluconazole, and 5-fluorocytosine except and high concentrations	(Ryley et al., 1984)
Saccharomyces cerevisiae S288C	Grandparent strain to chemogenomic mutants	

APPENDIX B

Synthesis of SH1009 [(*Z*)-6,7-dihydroxy-2-(3-hydroxy-4-methoxybenzylidene)benzofuran-3(2*H*)-one]

To a solution of 6,7-dihydroxybenzofuranone (88 mg, 0.5 mmol) and 3-hydroxy-4-methoxybenzaldehyde (78 mg, 0.51 mmol) in glacial acetic acid (3 mL) was added 3 drops of concentrated hydrochloric acid. The mixture was stirred for 3 hours at room temperature. The mixture was diluted with deionized water (6 mL) to form the product as a tan precipitate (45 mg) that was separated by filtration and washed with an additional 2 mL of water. The aqueous layer retained significant amounts of product. Repeated extraction with ethyl acetate (3 x 10 mL), followed by evaporation of the solvent and extracted acetic acid, followed by trituration with diethyl ether (10 mL) afforded an additional 20 mg of the product. Total yield of product was 65 mg (44% yield), with spectral and physical properties consistent with those reported in the literature. Tan solid (MP = 275-280 °C). IR (neat, thin film): 3100-3500, 1700, 1400, 1200 cm^{-1}; ^{1}H NMR (DMSO, 300 MHz) 10.78 (s, 1H), 9.54 (s, 1H), 9.27 (s, 1H), 7.53 (d, J = 2.1 Hz, 1H), 7. 42 (dd, $J_{1,3}$ = 8.4 Hz, $J_{1,2}$ = 2.1 Hz, 1H), 7.09 (d, J = 8.1 Hz, 1H), 7.01 (d, J = 8.4 Hz, 1H), 6.75 (d, J = 8.4 Hz, 1H), 6.62 (s, 1H), 3.81 (s, 3H); ^{13}C NMR (DMSO, 75 MHz) 182.64, 155.59, 154.92, 150.00, 147.09, 146.84, 130.68, 125.42, 124.73, 118.28, 115.80, 114.91, 113.296, 112.62, 111.74.

APPENDIX C

A set of 24 forward indexed primers containing (Illumina-specific region, 10 bp index tag [highlighted], and 18 bp common priming site U1). The common reverse primer contains (Illumina-specific region and a common priming site from the resistant KanMX gene region).

Name of Primer	Sequence (5' - 3')
Non_Essentail_1009_1	AATGATACGGCGACCACCGAGATCTACACTCTTTCCCTACACGACGCTCTTCCGATCTAATAGGCGCTG ATGTCCACGAGGTCTCT
Non_Essentail_1009_2	AATGATACGGCGACCACCGAGATCTACACTCTTTCCCTACACGACGCTCTTCCGATCTTACAGTTGCGGA TGTCCACGAGGTCTCT
Non_Essentail_1009_3	AATGATACGGCGACCACCGAGATCTACACTCTTTCCCTACACGACGCTCTTCCGATCTATCCTAGCAGG ATGTCCACGAGGTCTCT
Non_Essentail_1009_4	AATGATACGGCGACCACCGAGATCTACACTCTTTCCCTACACGACGCTCTTCCGATCTGATTAGCCTCGA TGTCCACGAGGTCTCT
Non_Essentail_MMS_1	AATGATACGGCGACCACCGAGATCTACACTCTTTCCCTACACGACGCTCTTCCGATCTAATGAGCCGTG ATGTCCACGAGGTCTCT
Non_Essentail_MMS_2	AATGATACGGCGACCACCGAGATCTACACTCTTTCCCTACACGACGCTCTTCCGATCTACGCGGATTAG ATGTCCACGAGGTCTCT
Non_Essentail_MMS_3	AATGATACGGCGACCACCGAGATCTACACTCTTTCCCTACACGACGCTCTTCCGATCTGCTTACGGAAG ATGTCCACGAGGTCTCT
Non_Essentail_MMS_4	AATGATACGGCGACCACCGAGATCTACACTCTTTCCCTACACGACGCTCTTCCGATCTCGGTAGACTAG ATGTCCACGAGGTCTCT
Non_Essentail_DMSO_1	AATGATACGGCGACCACCGAGATCTACACTCTTTCCCTACACGACGCTCTTCCGATCTATTGCCGGAAG ATGTCCACGAGGTCTCT
Non_Essentail_DMSO_2	AATGATACGGCGACCACCGAGATCTACACTCTTTCCCTACACGACGCTCTTCCGATCTGACATGCTAGG ATGTCCACGAGGTCTCT
Non_Essentail_DMSO_3	AATGATACGGCGACCACCGAGATCTACACTCTTTCCCTACACGACGCTCTTCCGATCTTACGCTGCATGA TGTCCACGAGGTCTCT
Non_Essentail_DMSO_4	AATGATACGGCGACCACCGAGATCTACACTCTTTCCCTACACGACGCTCTTCCGATCTGTCAAGCACTG ATGTCCACGAGGTCTCT
Essentail_1009_1	AATGATACGGCGACCACCGAGATCTACACTCTTTCCCTACACGACGCTCTTCCGATCTAGCGTATGTCGA TGTCCACGAGGTCTCT
Essentail_1009_2	AATGATACGGCGACCACCGAGATCTACACTCTTTCCCTACACGACGCTCTTCCGATCTGCGGATTAACG ATGTCCACGAGGTCTCT
Essentail_1009_3	AATGATACGGCGACCACCGAGATCTACACTCTTTCCCTACACGACGCTCTTCCGATCTATACCTCGGAG ATGTCCACGAGGTCTCT
Essentail_1009_4	AATGATACGGCGACCACCGAGATCTACACTCTTTCCCTACACGACGCTCTTCCGATCTGGTAGACATCG ATGTCCACGAGGTCTCT
Essentail_MMS_1	AATGATACGGCGACCACCGAGATCTACACTCTTTCCCTACACGACGCTCTTCCGATCTAGGTACCTACG ATGTCCACGAGGTCTCT
Essentail_MMS_2	AATGATACGGCGACCACCGAGATCTACACTCTTTCCCTACACGACGCTCTTCCGATCTCGATAACGCTG ATGTCCACGAGGTCTCT
Essentail_MMS_3	AATGATACGGCGACCACCGAGATCTACACTCTTTCCCTACACGACGCTCTTCCGATCTTACCGGAATGG ATGTCCACGAGGTCTCT
Essentail_MMS_4	AATGATACGGCGACCACCGAGATCTACACTCTTTCCCTACACGACGCTCTTCCGATCTTAGGACCAGTG ATGTCCACGAGGTCTCT
Essentail_DMSO_1	AATGATACGGCGACCACCGAGATCTACACTCTTTCCCTACACGACGCTCTTCCGATCTCTGCAAGTTCGA TGTCCACGAGGTCTCT
Essentail_DMSO_2	AATGATACGGCGACCACCGAGATCTACACTCTTTCCCTACACGACGCTCTTCCGATCTTCGCGATTCAGA TGTCCACGAGGTCTCT
Essentail_DMSO_3	AATGATACGGCGACCACCGAGATCTACACTCTTTCCCTACACGACGCTCTTCCGATCTGGTAACGTACG ATGTCCACGAGGTCTCT
Essentail_DMSO_4	AATGATACGGCGACCACCGAGATCTACACTCTTTCCCTACACGACGCTCTTCCGATCTAAGACCTGTGG ATGTCCACGAGGTCTCT
Common reverse primer	CAAGCAGAAGACGGCATACGAGCTCTTCCGATCTGCACGTCAAGACTGTCAAGG

APPENDIX D

List of primers used for RT–PCR

Gene Name	*Oligonucleotide Primer Sequence (5'->3')*	*References*
CDC28	F:GTTATCTGATTATCAACGTCAAGAAAA	(Mitra et al., 2014)
	R: TCTAATGCTTTATAAACAACCCCATA	
HGC1	F: AATATGCAACCACCACCACC	(Greig et al., 2015)
	R: GAAACAGCACGAGAACCAGC	
CDC25	F: GGTGGTTGACGTTTGCTCAC	This study
	R: GGGCAGGAGGCTTGGTATTT	
RAS1	F: CAACTATTGAGGATTCTTATCG	(Zhu et al., 2009)
	R: CGGTTCTCATATATTGTTCTC	
RAS2	F: CAATCATTCACTGCATTAGAAG	(Zhu et al., 2009)
	R: CAAATTCTGCTCCTTCATAATAG	
CDC42	F: GGGTGAAAAATTGGCTAAGGAA	(Bassilana et al., 2005)
	R: CCTCTTTGAGTCAATGCAGAACA	
MCM2	F: CATCAAGAAGTTCACGTTAG	(Xie et al., 2017)
	R: CAGTATTCGAATCTTGAACG	
TCS11	F: ATCCCATCACGCAGCATTGA	This study
	R: TCGGCGGGCAAATAGTTGTT	
RPS4A	F:TGCTTACTTATTGTTAGTTCAAGGTGGTA	(Lu et al., 2015)
	R: CAACACCAACGGATTCCAATAAA	
RSP5	F: GGTTGGGAACAAAGATTTAC	(Leach & Cowen, 2014)
	R: GAGCAGTATTGGTTAATCTC	
CBK1	F: CCGCAAATGTCGGCATTCAT	This study
	R: TCGATGCTGGTGGTTGGAAA	
GAPDH	F: CGGTCCATCCCACAAGGA	(Nailis et al., 2006)
	R: AGTGGAAGATGGGATAATGTTACCA	

APPENDIX E

Enrichment analysis of KEGG pathway and gene ontology (biological process, molecular function, and cellular component) of 238 significantly responsive heterozygous (HIP-profile) and homozygous (HOP-profile) mutants to aurone SH1009. Hypergeometric testing through ClueGo app was used to find the significantly enriched KEGG/GO terms using GO categories in the *Saccharomyces cerevisiae*-S288C as a background with FRD < 0.05 as a cutoff significant value:

Ontology Source	GO-Term	*P*-value	No. of Genes	Associated Genes from HOP Profile	Associated Genes from HIP Profile
KEGG Pathway	Cell cycle	0.0000267	15	BUB1, CLB3, CLN2, FOB1, LTE1, SLK19, SWI4	APC1, APC4, CDC28, CDC5, MCM2, MCM7, MOB1, ORC4
	Meiosis	0.000536	13	BUB1, CLB3, CLN2, SLK19, SWI4, UME6	APC1, APC4, CDC28, CDC5, MCM2, MCM7, ORC4
	Ribosome	0.299472	9	RPL27A, RPL41A, RPL4A, RPS1B, RPS24B, RPS30B, RPS4A	RPL3, RPS31
	Endocytosis	0.01292	7	CHM7, EDE1, GLO3	ARC15, CDC42, RHO1, RSP5
	DNA replication	0.003922	5		MCM2, MCM7, POL3, RFC1, RFC3
	Nicotinate and nicotinamide metabolism	0.004427	4	HST2, HST4, ISN1, SDT1	
Biological Process	Cell division	0.0000726	25	BOI2, CLB3, CLN2, EDE1, ELM1, END3, LTE1, SLK19, TOF2, VPS51	APC1, APC4, CBK1, CDC13, CDC25, CDC28, CDC34, CDC42, CDC5, GNA1, MCM7, MOB1, RFC1, RHO1, SPC24
	Exit from mitosis	0.000155	8	GIC1, GIC2, LTE1, TOF2	APC1, CDC42, CDC5, MOB1
	cell budding	0.001004	8	BOI2, ELM1, END3, VPS51	CBK1, CDC28, CDC42, RHO1
	DNA replication	0.001418	14	CSM3, FOB1, TOF1	CDC28, CDC34, IPI1, MCM2, MCM7, ORC4, POL3, PSF3, RFC1, RFC3, SLD2
	Cytoskeleton organization	0.002668	19	ARC15, ARK1, CBK1, CDC28, CDC42, CDC5, CLB3, ELM1, END3, GIC1, GIC2, KIP3, MPS3, NIP100, RHO1, RSP5, SLK19, SPC24, TSC11	ARC15, CBK1, CDC28, CDC42, CDC5, MPS3, RHO1, RSP5, SPC24, TSC11

APPENDIX E: 2 of 4

Ontology Source	GO-Term	*P*-value	No. of Genes	Associated Genes from HOP Profile	Associated Genes from HIP Profile
	Regulation of endocytosis	0.002952	4	ARK1, LDB19	RHO1, RSP5
	Actin cortical patch organization	0.003639	4	ARK1, EDE1, END3	ARC15
	Establishment of cell polarity	0.003903	8	BOI2, END3, GIC1, GIC2, KIP3, NIP100	CDC42, TSC11
	Septin ring organization	0.003922	5	ELM1, GIC1, GIC2	CDC42, RHO1
	Regulation of cellular carbohydrate metabolic process	0.017427	5	FLO8, PCL6, UME6	CDC28, RHO1
	tRNA processing	0.005963	11	ELP2, IKI3, MSF1, POA1, PTC1, TGS1, TRM13	CEG1, CLP1, PTA1, RSP5
	Receptor-mediated endocytosis	0.00721	3	LDB19	RSP5, YPP1
	ncRNA transcription	0.017205	6	HHT1	NCB2, RPA135, RPC17, RRN3, RRN9
	DNA repair	0.021107	18	BLM10, CSM3, EAF5, HHT1, IES2, MLH3, RAD16, RAD18, TOF1	CDC28, MCM2, MCM7, POL3, PSF3, RFC1, RFC3, SLD2, SPP382
	Chromatin silencing	0.025447	11	FOB1, GIC1, HST2, HST4, SCS2, SPT21, TOF2, YAP5	MCM7, MPS3, ORC4
	Cell morphogenesis	0.026637	5	ELM1, GIC1, GIC2	CDC42, RSP5
	Phosphorylation	0.05002	22	ACK1, ARK1, BUB1, CLB3, CLN2, COX9, DAS2, ELM1, MOB1, PCL6, PKP1, PRR1, PTC1, RTK1, TOS3, YJL045W, YPK3	CBK1, CDC28, CDC5, CLP1, TSC11
	Vesicle-mediated transport	0.05002	22	APS1, ARK1, BOI2, EDE1, ELO3, EMP46, END3, FEN2, GGA2, GLO3, LDB19, LTE1, PEP12, VAM7, VPS51, YPP1	CDC28, CDC42, RHO1, RSP5, SEC12, SEC24, YPP1
Molecular Function	Nucleotide binding	0.000382	51	AIM10, ARK1, BUB1, CUS2, DAS2, ELM1, ELO3, ERV1, GSP2, GTF1, HST2, HST4,	CBK1, CDC28, CDC34, CDC42, CDC5, CEG1, CLP1, DED81, ERV1, GPN2, LSG1, MCM2,

APPENDIX E 3 of 4

Ontology Source	GO-Term	*P*-value	No. of Genes	Associated Genes from HOP Profile	Associated Genes from HIP Profile
				KIP3, MEF2, MLH3, MSD1, MSF1, PKP1, PRR1, RAD16, RSP5, RTK1, SRP101, TOS3, YJL045W, YPK3, ZIP2	MCM7, MGE1, MPS3, PGA3, POL3, RFC1, RFC3, RHO1, RPC17, RSP5, TFG2, YDR341C, YHR020W
	Aminoacyl-tRNA ligase activity	0.002047	6	AIM10, MSD1, MSF1	DED81, YDR341C, YHR020W
	Ribonucleoside binding	0.003384	40	AIM10, ARK1, BUB1, DAS2, ELM1, ELO3, GSP2, GTF1, KIP3, MEF2, MLH3, MSD1, MSF1, PKP1, PRR1, RAD16, RTK1, SRP101, TOS3, YPK3	CBK1, CDC28, CDC34, CDC42, CDC5, CEG1, CLP1, DED81, GPN2, LSG1, MCM2, MCM7, MPS3, RFC1, RFC3, RHO1, RPA135, TFG2, YDR341C, YHR020W
	DNA binding	0.003933	33	CRP1, CSM3, FLO8, FOB1, HHT1, IES2, IOC2, LRP1, MLH3, RAD16, RAD18, STP2, SWI4, TOF2, UME6, VID22, YAP5, ZIP2	CDC13, CDC5, MCM2, MCM7, NCB2, ORC4, POL3, RFC1, RFC3, RPA135, RRN3, RRP14, SLD2, TAF9, TFG2
	Protein kinase activity	0.015	14	ACK1, ARK1, BUB1, DAS2, ELM1, PKP1, PRR1, RTK1, TOS3, YPK3	CBK1, CDC28, CDC5, CLP1
	GTP binding	0.024937	10	CEG1, GSP2, MEF2, GIC1, GIC2	CDC42, GPN2, LSG1, RHO1, SRP101
	ATP binding	0.049726	31	AIM10, ARK1, BUB1, DAS2, ELM1, ELO3, KIP3, MPS3, MSD1, MSF1, PKP1, PRR1, RAD16, RTK1, TFG2, TOS3, YDR341C, YPK3	CBK1, CDC28, CDC34, CDC5, CLP1, DED81, MCM2, MCM7, MPS3, RFC1, RFC3, TFG2, YDR341C, YHR020W
Cellular Component	Nucleus	0.0000013	105	APS1, BLM10, BUB1, CLB3, CLN2, CMG1, CRP1, CSM3, CUS2, DAS2, EAF5, ELO3, ELP2, FLO8, FOB1, FYV7, GSP2, HHT1, HST2, HST4, ICP55, IES1, IES2, IKI3, IOC2, IPI1, KIP3, LIN1, LRP1, MLH3, PCL6, PTC1, RAD16, RAD18, RBD2, RPL4A, RPS31, RSF1, RTK1, SCS2, SHE2, SKI8, SLK19, STP2, SVF1, SWI4, TGS1, TOF1, TOF2, TOS3, TRM13, UBP2, UME6, VID22, YAP5, YOR131C, YPK3, ZIP2	APC1, APC4, CBK1, CDC13, CDC25, CDC28, CDC34, CDC42, CDC5, CEG1, CLP1, FAF1, FCF1, GNA1, IPI1, MCM2, MCM7, MED7, MOB1, MPS3, NCB2, NOC2, NOP14, NUT2, ORC4, POL3, PRE1, PSF3, PTA1, RDS3, RFC1, RFC3, RPA135, RPC17, RPF2, RPS31, RRN3, RRN9, RRP1, RRP14, RSP5, SLD2, SPC24, SPN1, SPP382,TAF5, TAF9, TFG2, YDR341C
	Replication fork	0.000224	9	CSM3, HHT1, TOF1	MCM2, MCM7, POL3, PSF3, RFC1, RFC3
	Cytoskeleton	0.000981	19	ARK1, BOI2, EDE1, ELM1, END3, GIC1, GIC2, KIP3, MOB1, NIP100, SLK19	APC1, ARC15, CDC28, CDC42, CDC5, MPS3, RSP5, YPP1

APPENDIX E 4 of 4

Ontology Source	GO-Term	*P*-value	No. of Genes	Associated Genes from HOP Profile	Associated Genes from HIP Profile
	Cellular bud	0.002811	16	BOI2, EDE1, ELM1, GIC1, GIC2, LTE1, MOB1, SCS2, SHE2, YNL058C	CBK1, CDC28, CDC42, CDC5, RHO1, RSP5
	Cellular bud tip	0.003287	9	EDE1, GIC1, GIC2, SCS2, SHE2	CBK1, CDC42, RHO1, RSP5
	Cellular bud neck	0.007523	13	BOI2, EDE1, ELM1, GIC1, GIC2, MOB1, SCS2, YNL058C	CBK1, CDC28, CDC42, CDC5, RHO1
	Cytoskeletal part	0.008832	16	EDE1, ELM1, END3, KIP3, MOB1, NIP100, SLK19	APC1, ARC15, ARK1, CDC28, CDC42, CDC5,MPS3, RSP5, YPP1
	Site of polarized growth	0.011329	15	BOI2, EDE1, ELM1, GIC1, GIC2, MOB1, SCS2, SHE2, YNL058C	CBK1, CDC28, CDC42, CDC5, RHO1, RSP5
	actin cortical patch	0.017205	6	ARK1, EDE1, END3	ARC15, RSP5, YPP1
	nuclear pre-replicative complex	0.019613	3		MCM2, MCM7, ORC4
	Actin cytoskeleton	0.026133	7	ARK1, EDE1, END3, NIP100	ARC15, RSP5, YPP1
	Golgi apparatus	0.046058	16	APS1, BOI2, EMP46, GGA2, GLO3, LDB19, MNN2, PEP12, RBD2, VPS51, YCR007C	RHO1, RSP5, PIS1, SEC12, SEC24

APPENDIX F

The growth curves of the heterozygous mutants (HIP), homozygous mutants (HOP), and the wild type *S. cerevisiae*-S288C in the presence of 0 µM, 16 µM, and 200 µM of aurone SH1009 using the Bioscreen C growth curve instrument, and reading the OD_{600} at 30 min intervals for 25 h during incubation at 30°C.

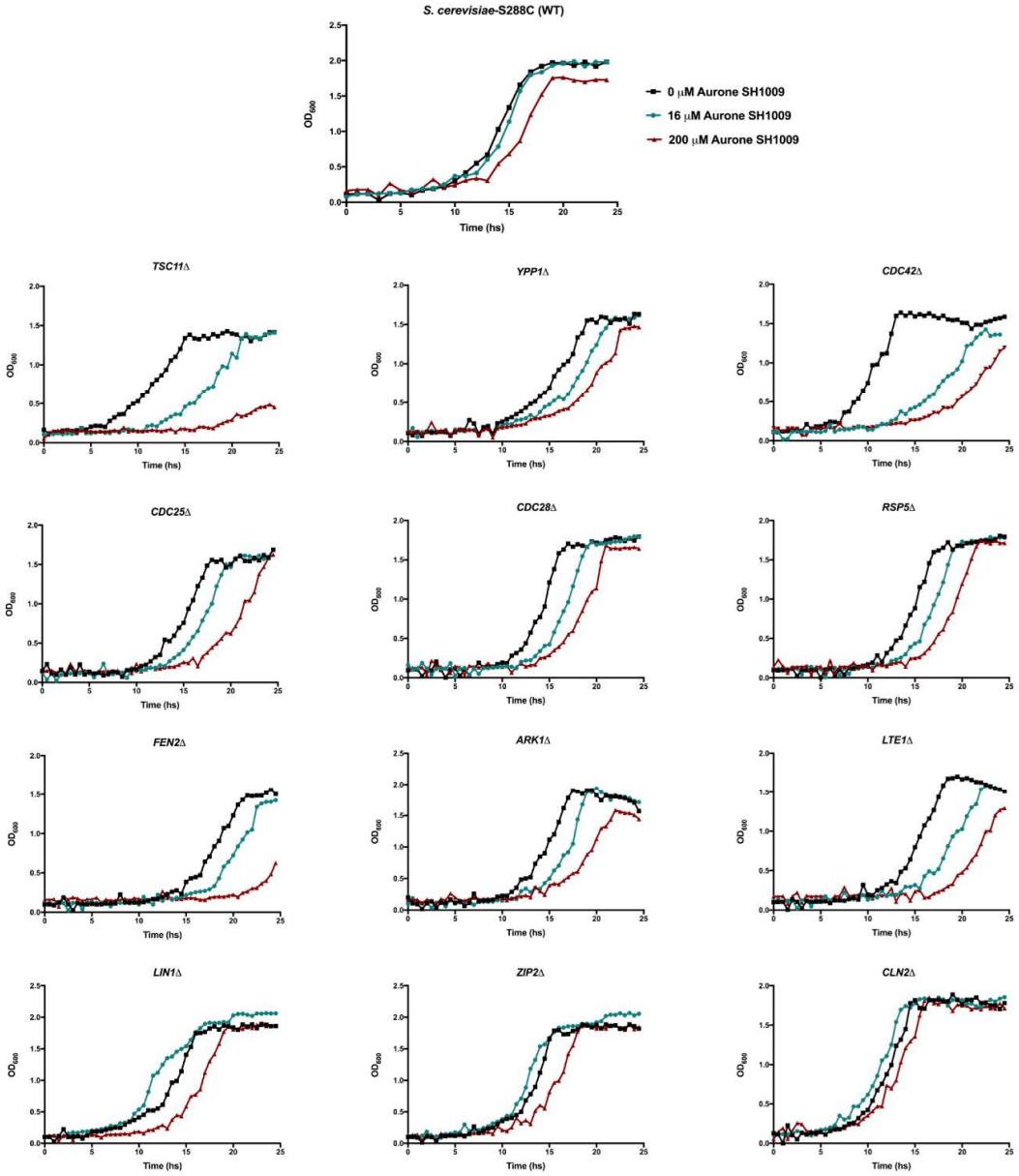

CHAPTER II

COMBINING GENOME-WIDE GENE EXPRESSION ANALYSIS (RNA-SEQ) AND GENE EDITING PLATFORM (CRISPR-CAS9) TO UNCOVER THE SELECTIVELY PRO-OXIDANT ACTIVITY OF AURONE COMPOUND AGAINST CANDIDA ALBICANS

Alqahtani FM, Handy ST, Sutton CL and Farone MB (2021) Combining Genome-Wide Gene Expression Analysis (RNA-seq) and a Gene Editing Platform (CRISPR-Cas9) to Uncover the Selectively Pro-oxidant Activity of Aurone Compounds Against *Candida albicans*. ***Front. Microbiol.*** **12:708267.**

ABSTRACT

Candida albicans is the major fungal cause of healthcare-associated bloodstream infections worldwide with a 40% mortality rate. The scarcity of antifungal treatments due to the eukaryotic origin of fungal cells has challenged the development of selectively antifungal drugs. In an attempt to identify novel antifungal agents, aurones SH1009 and SH9051, as synthetically bioactive compounds, have been recently documented as anti-*Candida* agents. Since the molecular mechanisms behind the inhibitory activities of these aurones in *C. albicans* are unclear, this study aimed to determine the comprehensive cellular processes affected by these aurones and their molecular targets. Genome-wide transcriptional analysis of SH1009- and SH9051-treated *C. albicans* revealed uniquely repressed expression in different metabolic pathways, particularly trehalose and sulfur amino acid metabolic processes for SH1009 and SH9051, respectively. In contrast, the most commonly enriched process for both aurones was the upregulation of RNA processing and ribosomal cleavages as an indicator of high oxidative stress, suggesting that a common aspect in the chemical structure of both aurones led to prooxidative properties. Additionally, uniquely induced

responses (iron ion homeostasis for SH1009 and arginine biosynthesis for SH9051) garnered attention on the key roles of the functional groups. The deletion of the transcriptional factor for the trehalose biosynthesis pathway, Tye7p, resulted in a SH1009-resistant mutant, which also exhibited low trehalose content, validating the primary molecular target of SH1009. Aurone SH9051 uniquely simulated an exogenous supply of methionine or cysteine, leading to sulfur amino acid catabolism as evidenced by quantifying an overproduction of sulfite. Phenyl aurone, the common structure of aurones, contributed proportionally in the prooxidative activity through the ferric ion reduction effects leading to high ROS levels. Our results determined selective and novel molecular mechanisms for aurone SH1009 and also elucidated the diverse cellular effects of different aurones based on functional groups.

INTRODUCTION

Candida albicans is a fungal-commensal microorganism that normally grows as a member of the skin and mucosal microbiota of healthy individuals. However, it can evolve in association with human hosts as an opportunistic pathogen. The resulting candidiasis can range from superficial (thrush) to life-threatening bloodstream infections. Systemic infections principally develop in immune-compromised patients with mortality rates of ~40% (Brown et al., 2012; Kullberg & Arendrup, 2015). The striking ability of *C. albicans* to cause persistent infections is attributed to the reversible transition from the planktonic-yeast form to a hyphal form in order to build multicellular structures known as biofilms on abiotic or biotic surfaces which enable this pathogenic fungi to resist the antifungals and overcome host defenses (Rajendra, 2017).

The biological similarities between fungal and human cells as eukaryotic cells obstruct the design and the development of antifungal drugs and limits their number to only five different chemical classes, including polyenes, echinocandins, azoles, pyrimidine analogues, and allylamines. The narrow range of targets for these available drugs and the resistances to them necessitate the need for new classes of antifungal agents (Prasad et al., 2019). Natural products that are derived from plants as secondary metabolites have been considered vital sources of potential antimicrobial compounds in the pharmaceutical industry in the last two decades. As plants evolved defenses against pathogenic fungi, the evolutionary pressure produced a high diversity of novel chemical skeletons by which to synthesize bioactive molecules with antifungal activity (Mishra & Tiwari, 2011). Aurones (2-benzylidene-1-benzofuran-3-one) are a subclass of flavonoids, widespread polyphenolic compounds in plants, with antifungal characteristics against *Candida* spp. (Sutton et al., 2017).

Our prior study showed that the bioactive aurone compound SH1009 exhibited selectively fungistatic-inhibitory activity against *Candida* spp. Additionally, mode-of-action screening using chemical genetic interaction in *Saccharomyces cerevisiae* indicated that SH1009 targets cell cycle-dependent organization of the actin cytoskeleton, providing informative clues about SH1009 antifungal activity but this cannot explain the selective toxicity of aurone SH1009 toward *Candida* spp. (Alqahtani et al., 2019). Despite the validation of chemical genetic interaction findings in the *C. albicans* SC5314 strain, the fundamental differences between *S. cerevisiae* and *C. albicans* physiology requires a target-identification approach in the major pathogenic yeast of our study *C. albicans*. These fundamental differences between *S. cerevisiae* and the pathogen include the ability of *C. albicans* to rapidly change its morphogenesis from yeast to true hyphae and differences in sensitivity and resistance

to antifungal agents. Moreover, a comparison between *C. albicans* and *S. cerevisiae* genome sequences has shown that only about two-thirds of *Candida* genes have obvious orthologs in *Saccharomyces* genes (Rajendra, 2017).

In this study, we further explore the antifungal activity of SH1009 in addition to another bioactive aurone compound, SH9051, which was previously documented for its inhibitory activity against *Candida spp*. and shares an identical core chemical structure with SH1009. However, instead of hydroxyl (-OH) and methoxy ($-OCH_3$) functional groups, SH9051 contains a nitrogen (-N) atom in its B ring (Sutton et al., 2017). Also, a whole-genome transcriptional analysis post aurone SH1009 and SH9051 treatments of the *C. albicans* SC5314 strain was performed using RNA-seq technique. Accordingly, a reverse genetic approach was also applied to generate *C. albicans* deletion strains in order to validate the repressed target pathway of each aurone. Quantitatively biochemical assays for specific cellular products were performed to precisely detect the cellular effects of the functional groups in the activity of each aurone. The results of this work improve the concept of structure-activity relationship for the aurones, providing a molecular and biochemical basis towards a comprehensive understanding of the mechanisms beyond the antifungal activity of aurones against *C. albicans*.

MATERIALS AND METHODS

Materials and Reagents

Candida albicans SC5314 strain was purchased from the American Type Culture Collection (Manassas, VA, USA). *Candida albicans MET4*Δ mutant (SFY39) was prepared by Aaron Mitchell and obtained from the FGSC (University of Missouri, Kansas City, MO). YPD agar and broth, 3-(N-morpholino) propanesulfonic acid

(MOPS) buffer, dimethyl sulfoxide (DMSO), BeadBug™ prefilled tubes, dithiothreitol (DTT), nourseothricin sulfate (NAT), and ampicillin (AMP) were all purchased form MilliporeSigma (St. Louis, MO, USA). RPMI-1640 medium was purchased from Corning Incorporated (Corning, NY, USA). PrestoBlue, TRIzol™ Reagent, phosphate buffered saline (PBS), salmon sperm DNA, lithium acetate (LiAc), polyethylene glycol (PEG) 3350, RiboPure™- DNase I Treatment, CM-H2DCFDA (Oxidative Stress Indicator), and Amplex™ Red Glucose/Glucose Oxidase Assay Kit were purchased from Life Technologies Corporation (Carlsbad, CA, USA). CutSmart Buffer, NgoMIV, PacI, Xho1 restriction enzymes, Phusion high-fidelity (HF) DNA polymerase, 2× Gibson assembly mix, and Chemically competent DH5α *Escherichia coli* cells were purchased from New England BioLabs (Ipswich, MA, USA). The RNase-Free DNase Kit, Miniprep plasmid extraction kit, Gel extraction kit, and PCR purification kit were purchased from QIAGEN (Germantown, MD, USA). The *E. coli* bacterial culture containing the CaCAS9 plasmid (reference number 89576) was purchased from Addgene Headquarters (Watertown, MA, USA). The trehalose assay kit and total sulfite assay kit were purchased from Megazyme Inc. (Chicago, IL, USA). The iron assay kit (colorimetric) was purchased from Abcam (Cambridge, MA, USA). Drop-out mix synthetic growth meduium, minus methionine and cysteine was purchased from USBiological Life Sciences (Salem, MA, USA).

Checkerboard assays

Stock solutions of aurone SH9051 and SH1009 were prepared in dimethyl sulfoxide (DMSO) at a high concentration of 40 mM. Aurone interactions were carried out in RPMI 1640 medium (adjusted to pH 7.0 with 0.165 M of MOPS buffer) in 96-well flat-bottomed microtitration plates using broth microdilution checkerboard assays as described previously (Shrestha et al., 2015). Two-fold serial dilutions were initially

prepared at four times the desired final concentrations (3.125 μM - 200 μM) of aurones. Aliquots of 50 μL of each concentration of SH9051 were added to columns 1 to 7, and then 50 μL of SH1009 was added to rows A to G. Row H and column 8 contained the 2-fold serial dilutions of SH9051 and SH1009 alone, respectively. Column 9 was the drug-free well that served as negative control. The inoculum culture of *C. albicans* SC5314 strain was prepared as described previously (Alqahtani et al., 2019). The final concentrations of SH9051 and SH1009 after adding 100 μL of the prepared inoculum ($0.5\text{-}2.5 \times 10^3$ CFU /mL) ranged from 200 μM to 3.125 μM. The microtiter plates were incubated at 35°C for 24 h. PrestoBlue reagent was used to detect the percentage of fluorescent-viable cells in each well using a SpectraMax M5e spectrophotometer (Molecular Devices, LLC, USA). The minimum inhibitory concentration (MIC) was defined as the concentration that reduced the growth by 90%. The assay was performed in triplicate and the IC_{50} values were calculated using GraphPad Prism (GraphPad Software, USA). Drug interaction was estimated by fraction inhibitory concentration index (FICI) model. This model was determined according to the formula: FIC SH1009 = MIC SH1009 in combination / MIC SH1009 alone. FIC SH9051 = MIC SH9051 in combination / MIC SH9051 alone. FIC index = FIC SH1009 + FIC SH9051. FICI value was interpreted to characterize aurone compounds interactions as; FIC index ≤ 0.5 = synergy, FIC index 0.5 - <1.0 = additivity, FIC index 1.0 - < 4.0 = indifference, FIC index > 4.0 = antagonism.

Cytotoxicity assay.

Three human cell lines (A549 human lung carcinoma epithelial, human monocytic THP-1, and HepG2 human liver carcinoma epithelial cells) were used to assay the toxicity of aurone SH9051. Human cell lines were grown, maintained and seeded into 96-well microtiter plates at a density of 10,000 viable cells/well as described previously

(Alqahtani et al., 2019). After seeding, the cells were treated with two-fold serial dilutions (3.125 μM– 200 μM) of aurone SH9051. After incubation for 24h at 37℃ with 5% CO_2 in a humidified incubator, the cell viability was evaluated using 20 μL of PrestoBlue. The assay for each cell line was performed in triplicate. The 50% cytotoxicity concentration values were calculated using GraphPad Prism (GraphPad Software, USA).

Genome-wide transcriptional analysis

RNA extraction, processing and sequencing. After growing *C. albicans* SC5314 cells at 30°C in YPD broth for 12 h, the culture was diluted 1:200 and allowed to grow with agitation at 30°C until reaching early exponential phase (OD_{530} = 0.15). The cell cultures (~1.5-1×10^7 CFU/mL) were treated with aurone SH1009 or SH9051 at the concentration that caused ~30% inhibition (400 μM and 200 μM, respectively) followed by incubation for an additional 1 h. Solvent (DMSO) was added to the negative control culture to reach the concentration of 1%. After harvesting the cells by centrifugation, yeast cells were disrupted mechanically with BeadBug™ prefilled tubes, containing glass beads. Afterward, the total RNA were extracted according to TRIzol™ reagent protocol (Rio et al., 2010) and treated with RiboPure™- DNase I reagent to remove any residue of chromosomal DNA. Total RNA from nine biological-independent replicates of SH1009-treated samples (3 replicates), SH9051-treated samples (3 replicates) and untreated samples (3 replicates) were checked for their quantities, qualities, and integrities using NanoDrop™ Lite Spectrophotometer (ThermoFisher Scientific, MA, USA), agarose gel electrophoresis, and Bioanalyzer 2100 system (Agilent Technologies, CA, USA). Volumes of ~20 μL of high-quality total RNA of all samples were sent to Novogene Corporation Inc. (Sacramento, CA. USA) for library preparation and RNA sequencing.

RNA-seq data analysis. An average of ~26873797 paired-end reads per sample (150 bp length) were received in Fastq files. Pre-processing quality control, mapping, quantification, and statistical summarizing of sequence reads were accomplished using web-based tools through the stand-alone platform, Galaxy server (Goecks et al., 2010). To enhance mappability, raw sequence reads were filtered by trimming low quality reads (Qscore < 20), adaptor sequences, and sequences containing N using FastQC (Leggett et al., 2013) and Trimmomatic (Bolger et al., 2014). Clean reads (~98.55 % of raw reads) were deposited at the Gene Expression Omnibus (GEO) database under the accession numbers GSE158472. The processed sequence reads were aligned to reference *C. albicans* genome SC5314_A21 using HISAT2 (Kim et al., 2015). The alignments for each sample was assembled using the *C_albicans*SC5314__A21_features.gff annotation file with StringTie (Pertea et al., 2015). The alignments with mapping quality < 20 scores were excluded. After assembling all samples, assembled transcripts were merged together by StringTie-merge in order to create a uniformly new set of transcripts for all the samples and restore any missing exon in any transcript in one sample due to the possibility of lacking sufficient coverage (Pertea et al., 2016). The merged transcripts were used as an input file to quantify the transcripts in each sample using featureCounts (Liao et al., 2014). Then, the Limma-voom tool compared the transcripts level of SH1009-treated and SH9051-treated samples to the transcripts level in untreated samples (Law et al., 2014). The count data were normalized with trimmed mean of M value (TMM) method after filtering out the genes (unexpressed genes) with < 1 count per million reads. Differentially expressed genes were determined for each treatment as ≥ 1.5 fold change with corrected *P* values that control the false discovery rate at 5%. The GO enrichment

analysis was conducted with the Candida Genome Database GO TermFinder (Boyle et al., 2004) and FungiDB data base (Basenko et al., 2018).

CRISPR/Cas9 mediated gene deletion strain construction

The CRISPR/Cas9 gene editing was used to delete the *TYE7* (C2_04060C) allele based on the gene drive platform as described previously with minor modifications (Halder et al., 2019). Briefly, sequences of gene drive constructs, that contain synthetic guide RNAs (sgRNAs), repair templates, and SNR52 RNA polymerase III promoter, and their verification primers are listed in (**Appendix A**). The CaCAS9 plasmid contains a cassette of the *Candida* codon-optimized CAS9 endonuclease gene, Nourseothricin sulfate (NAT), and ampicillin (AMP) cassettes (selective markers), gene drive cloning site, and NEUT5 locus sequences for genomic integration. After digesting the CaCas9 plasmid with NgoMIV, ~1000 bp Oligo pairs of *TYE7*-gene drive were cloned separately to CaCas9-digested plasmid using Gibson assembly master mix. Then, 1 µL of ligation reactions were introduced into chemically competent DH5α *E. coli* cells according to the manufacturer's transformation protocol. Transformants were selected on LB agar + ampicillin. Plasmids with corrected-orientation inserts were verified by amplifying the insert region with universal primers (PAC6725_F and PAC6389_R) and with plasmid fingerprinting using Xho1. After digesting with PacI to linearize the plasmids, ~1.5 µg were transformed into *C. albicans* cells (SC5314 background) with the LiAc/ssDNA/PEG/DTT method. Fungal cells were recovered in YPD broth for 4 h and then plated on YPD agar supplemented with 250 µg/mL of NAT. After incubation for 4 days at 30℃, NAT^R transformants were plated again onto fresh YPD agar+NAT plates. NAT^R mutants were validated for their desired gene deletions using colony PCR and gel electrophoresis.

Growth rate assay

The inocula of *C. albicans* SC5314 wild type, *TYE7*Δ, and *MET4*Δ cells were prepared in YPD broth media at working concentrations of 1-5 × 10^3 CFU /mL, and 100 µL were added into the wells of 100-well Bioscreen honeycomb plate. Then, 100 µL of SH1009 or SH9051 were added to respective wells to reach the final concentrations of the IC_{50}, 16 µM and 90 µM, respectively, with or without the supplements of methionine, cysteine, and iron(II) chloride. Plates were placed into the Bioscreen C instrument with Bioscreen software (Growth Curves USA, Piscataway, NJ, USA) at a temperature of 30℃ with continuous shaking for 24h. The optical density reads (OD_{530}) were measured every 30 min interval to monitor the growth curves.

Measurement of ROS levels

C. albicans, *TYE7*Δ, and *MET4*Δ cells from an overnight culture were diluted in fresh YPD to an OD_{530} of 0.12 and allowed to grow to the early exponential phase (OD_{530} = 0.15). Cells were pelleted in 96-wells plate at concentration of (2.5-5 × 10^5 CFU /mL) and treated with 200 µM of SH1009, SH9051, and phenyl aurone and incubated for one hour at 30°C. ROS levels were assessed using the fluorescent dye chloromethyl-dichlorodihydrofluorescein diacetate (CM-H2DCFDA) at final concentration of 20 µM. Cells were incubated at 37 °C for 1 h. The fluorescence intensity was measured with a 485 nm excitation and 535 nm emission using SpectraMax M5e spectrophotometer (Molecular Devices, LLC, USA). ROS accumulation was calculated with respect to background fluorescence.

Intracellular iron content and trehalose determination

Cultures of strains SC5314 and *TYE7*Δ were (*MET4*Δ mutant was excluded because of the limited resources) grown until reaching the exponential phase (as descried in measurement of ROS levels experiment) and plated in 12-wells plate at concentration of (1×10^7 CFU /mL) and treated with 200 µM of SH1009, SH9051, and phenyl aurone, and incubated for one hour at 30°C. After treatment, cells were washed once with water, and resuspended in water. Afterward, cells were lysed mechanically with BeadBug™ prefilled tubes, containing glass beads. 50 µL of each sample was plated in 96-wells plate for intracellular ferrous iron (Fe^{2+}) and ferric iron (Fe^{3+}) ions determination according to the instructions of Abcam iron assay kit (colorimetric).

For trehalose determination, yeast cell lysates were prepared by incubation at 95°C for 30 min after which 200 µL supernatants were used for enzymatic analysis (Megazyme Trehalose Assay Kit) following the manufacturer's procedure with modifications. Briefly, 10 µL of solution 2 (NADP+ and adenosine 5′- triphosphate), 20 µL of solution 1 (buffer), and 2 µL of suspension 3 (hexokinase and glucose-6-phosphate dehydrogenase enzymes) were added to the wells to convert the glucose to gluconate-6-phosphate. After incubation with constant shaking for 60 min at 30°C to remove glucose, the reaction was sealed and heated at 90°C for 15 min to inactivate the enzymes. After cooling, 2 µL of suspension 4 (trehalase enzyme) was added, and incubated at room temperature for 8 min. The released glucose monomers were assayed fluorometrically using Amplex™ Red Glucose/Glucose Oxidase Assay Kit. Fluorescence readings were converted to absolute concentrations of trehalose based on an internal calibration curve of nmol trehalose standards and normalized for the cell protein concentration (mg) using the BCA protein assay.

Detection of sulfite

A commercially available total sulfite detection kit (Megazyme) was used for sulfite identification in *C. albicans* and *MET4*Δ cultures. In brief, cultures of strains SC5314 and *MET4*Δ were grown in YPD media (as descried in the measurement of ROS levels). After reaching exponential phase, cells were treated with 200 μM of each aurone, 20 mM methionine, and 10 mM cysteine for one hour at 30°C. Afterward, sulfite concentrations were measured according to the instructions of the manufacturer. All sample measurements were normalized to its respective background blank media.

RESULTS

Antifungal assessments of aurones SH1009 and SH9051.

Aurones SH1009 and SH9051 possess an identical core of their chemical structure with different functional groups, but they exhibited different half maximal inhibitory concentration (IC_{50}) values against *C. albicans* (**Fig. 1A and 1B**). Therefore, the potential of any synergistic interaction of their combination was investigated using a classical checkerboard microdilution assay. The fractional inhibitory concentration index (FICI) value between SH1009 and SH9051 was observed to be an indifferent effect (FICI = 1.25) against *C. albicans* SC5314 (**Fig. 1C**). The growth inhibition by both compounds in combination was more than 90% at the concentrations of 25 μM for SH009 and 100 μM for SH9051, which is in the zone of indifference, suggesting different modes of toxicity (**Fig. 1D**).

Cytotoxic effects of aurone SH1009 in mammalian cells was reported previously, indicating a selective antifungal toxicity toward pathogenic *C. albicans* SC5314 strain (Alqahtani et al., 2019). The cytotoxic effects of aurone SH9051 on the same human cell lines (THP-1, HepG2, and A549) was carried out to examine the selectivity toward fungal cells. **Appendix B** shows the cytotoxic concentrations of SH9051 that caused 50% loss of cell viability for each cell line, with SH9051 showing

high CC_{50} values for each cell line. Since the IC_{50} of aurone SH9051 against C. *albicans* was 91.05 μM, low selective index values were obtained for THP-1 and HepG2 cells, but the difference between the CC_{50} of A549 cells and IC_{50} of fungal cells was 2-fold. Conversely, aurone SH1009 demonstrated highly selective toxicity toward *C. albicans* cells. The concentration of 25 μM of SH1009 caused significant inhibition on *C. albicans* growth (> 90% inhibition) while the cell viabilities for the human cells remained high at this concentration (Alqahtani et al., 2019). Here, a concentration of 100 μM of SH9051 showed the same inhibitory effects on *C. albicans* as 25 μM of SH1009, although this concentration of SH9051 decreased cell viabilities for the human cell lines (**Appendix C**). These disparities in inhibitory concentrations and the indifference in the checkerboard results suggest that aurones SH1009 and SH9051 could target different biological pathways. Therefore, genome-wide gene expression analyses of *C. albicans* cells in response to aurone treatments were performed.

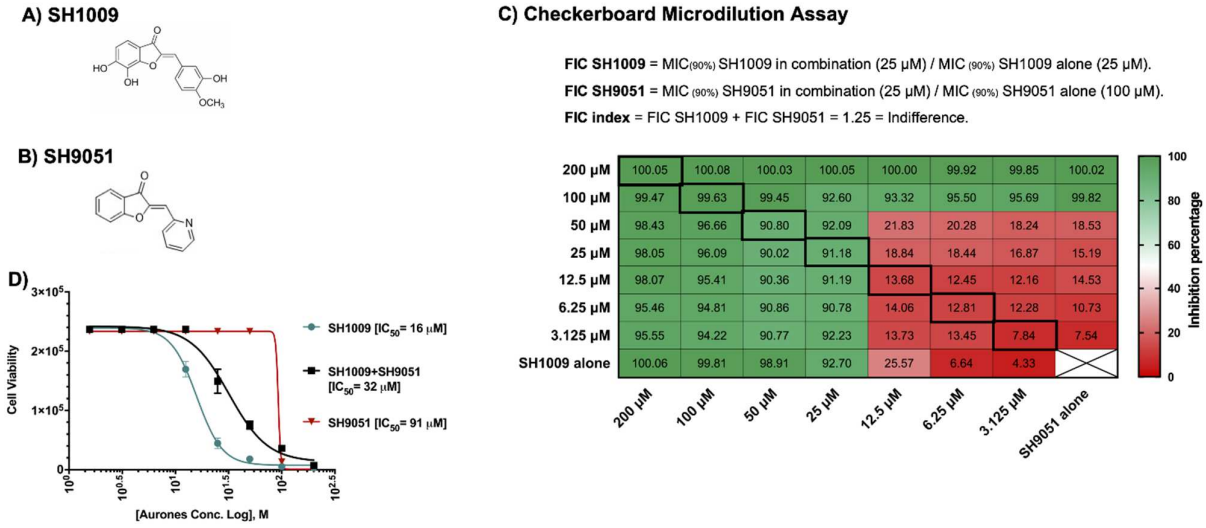

Figure 1: Antifungal assessments of aurones SH1009 and SH9051 against *C. albicans* SC5314 strain. A) The chemical structure of aurones SH1009 and **B)** SH9051. **C)** The checkerboard microdilution assay in 96-well plate format. Each cell represents the inhibition percentage of *C. albicans* (2.5-0.5 × 10^3 CFU/mL) growth during aurone SH9051 and SH1009 treatments (3.125 µM – 200 µM) in RPMI-1640 medium for 24 hours at 35°C either in combination or alone. **D)** Graphing the nonlinear regression of the cell viability readings based on the fluorescence intensity of PrestoBlue reagent using GraphPad Software to calculate the IC_{50} (concentration causing 50% growth inhibition) values of SH1009, SH9051, and SH1009+SH9051 combination after transforming the molar concentrations of the aurones into the logarithmic form. The cell viability readings of SH1009+SH9051 combination were obtained from the bold squares in the checkerboard plate.

Transcriptional analysis of SH1009- and SH9051-treated *C. albicans* cells.

The effect of aurone treatments on *C. albicans* SC5314 transcriptional responses was investigated after 1 h incubation with sub-inhibitory concentrations. A high quality of total RNAs (≥ 1.5 μg and an A260/A280 ratio ≥ 2.0) with high RNA integrity number (RIN ≥ 9.7) (**Appendix D)** were recovered for SH1009-treated, SH9051-treated and untreated cells. Genome-wide transcriptional analysis was performed using transcriptome sequencing (RNA-seq). The pre-analysis of RNA-seq computational analyses is a major step to detect any technical biases that may alter the biological differences. Therefore, diagnostic plots showed high-quality RNA-seq data regarding the alignment accuracy, sequencing depth, and filtered and normalized counts distribution (**Appendix E**). The reproducibility among the conditional groups and the within technical replicates demonstrated different gene expression profiles with no impact of batch effects. Notably, the two-dimensional plot of principal component analysis showed a distinct separation with greater variability between experimental groups by the first component, indicating that the treatment with aurones was the major source of differences (**Fig. 2A**). In addition, the variability of gene expression profiles of SH1009-treated and SH9051-treated cells was increased to 86% variance when comparing these profiles to each other only, suggesting different modes of action of different aurones and supporting the checkerboard assay results (**Fig. 2B**). The hierarchical clustering with pairwise correlations showed similar clustering that identified three groups of samples based on the treatment with dramatically different patterns of transcriptional profiles (**Fig. 2C**). Treatment with SH1009 and SH9051 resulted in 1249 and 1085 differentially expressed genes between treated and untreated samples (P (FDR) ≤ 0.05 and fold change ≥ 1.5), respectively. A total of 585 genes were upregulated, and 664 genes were downregulated upon SH1009 treatment, whereas

689 genes were upregulated, and 396 genes were downregulated upon SH9051 treatment compared to their regulation in *C. albicans* under untreated conditions (**Fig. 2C** and **E**).

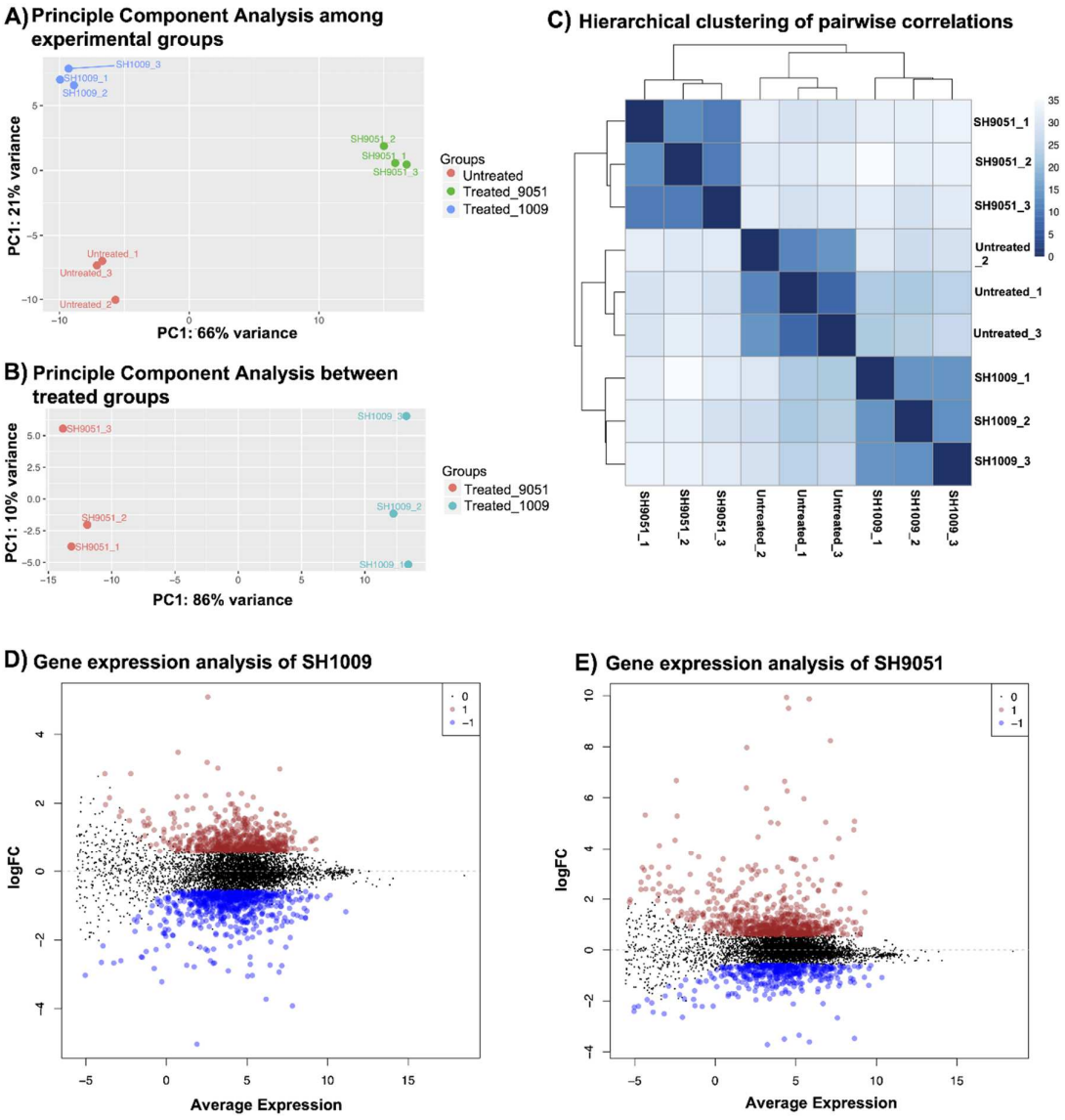

Figure 2: The reproducibility and the differential expression analyses of SH1009-treated, SH9051-treated and untreated *C. albicans* samples. A) and **B)** The principal component analysis plots of log-transformed counts where the x-axis represents the first dominant principal component (PC1) to measure the variance between experimental conditions and the y-axis represents the second dominant principal component (PC2) to measure the variance among the replicates within each sample. **C)** The Hierarchical clustering with heatmap to measure sample-to-sample distances where the depth of the blue color indicates the correlation values. **D)** and **E)** The mean dot (MD) plots of the log (fold change $\geq$ 1.5) for statistically significant genes (FDR $\leq$ 0.05) that are upregulated (red dots) and downregulated (blue dots) after 1h exposure to aurones SH1009 and SH9051, respectively.

To elucidate the transcriptional response of *C. albicans* SC5314 during aurone treatment, the induced and repressed genes were examined for clustered analysis of over-represented functionally annotated KEGG pathways and gene ontology (GO) terms in SH1009 and SH9051 transcriptomes. GO enrichment analyses showed that a large subset of down-regulated genes were significantly (*P* (FDR) values < 0.0001) enriched in response to the transporters and cell regulations that are associated with metabolic processes (carbon metabolism for SH1009 and sulfur metabolism for SH9051), suggesting that the exposure to chemically different structure of aurones robustly alters the nutrient availability in which the expression of genes that are involved in cellular metabolism and nutrient uptake are distinctively repressed. However, for up-regulated genes that were responsive to aurone treatment, GO enrichment analysis showed (*P* (FDR) < 0.0001) genes that are associated with RNA processing and ribosomal biogenesis in both aurone profiles in addition to uniquely induced responses for each aurone profile (iron ion homeostasis for SH1009 and arginine biosynthesis for SH9051), suggesting common aspects of detoxification mechanisms for *C. albicans* with specifically induced routes of adaptations in order to buffer the effects of particular nutrient deprivations (**Fig. 3**).

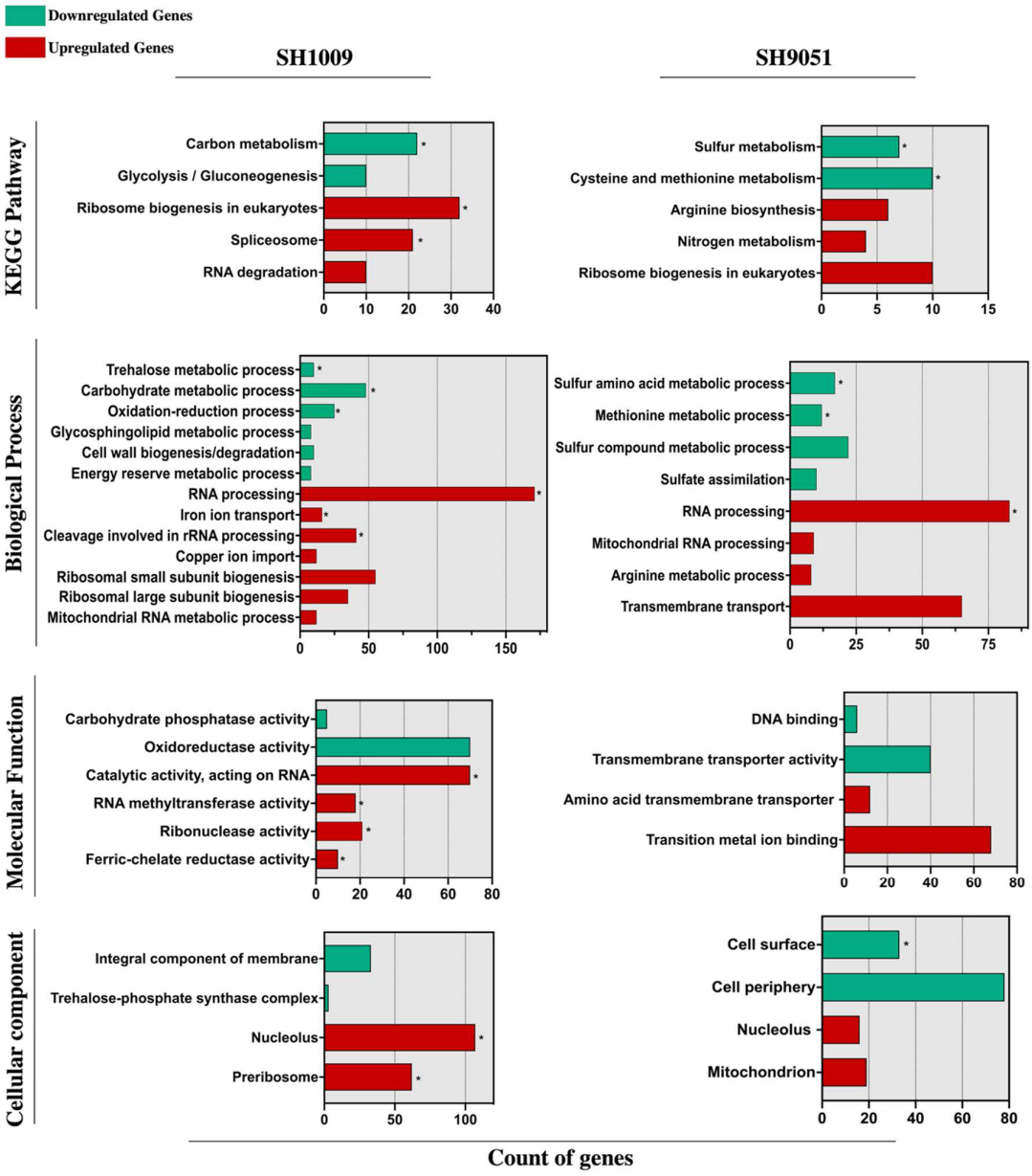

Figure 3: Functional enrichment analysis of KEGG pathway and gene ontology (biological process, molecular function, and cellular component) categories of significantly differential genes (FDR ≤ 0.05 and fold change ≥ 1.5) down- and up-regulated in response to aurone SH1009 and SH9051 treatment. TermFinder and FungiDB were used to find the significantly enriched KEGG/GO terms using GO categories based on a hypergeometric testing in the *C. albicans* SC5314 annotation with FRD ≤ 0.05 as a cutoff significant value. Green and red bars represent the number of down- and up-regulated genes that are clustered in each KEGG/GO term. GO terms within each group are listed according to increasing *P* values. Asterisks depict the highly significant KEGG/GO categories with $P \leq 0.0001$.

Different metabolic pathways are significantly enriched by growth with different aurones.

To obtain a clearer view of the sequential changes in gene expression patterns of *C. albicans* cells after SH1009 or SH9051 treatment, a gene regulatory network for the targeted pathway of each transcriptome profile is summarized in **Fig. 4A** for SH1009 and **4B** for SH9051. As aforementioned, SH1009 caused a repression in the carbon metabolism pathway which is tightly regulated by the Ras1/cAMP/protein kinase A (PKA) pathway (Sabina & Brown, 2009). The glucose G-protein receptor gene *GPR1*, for which expression was down-regulated by -1.5-fold, controls the production of cAMP from ATP by activating the downregulated GTPase gene *RAS1* (by -1.48-fold). In addition to Ras1, other key components of the Ras1/cAMP/PKA pathway were differentially expressed by the treatment. The up-regulated genes GTPase *RAS2* (by 2.2-fold) and phosphodiesterase *PDE2* (by 2.6-fold) primarily reduce the cellular level of cAMP, which is required for inactivation of the inhibitory subunit Bcy1 of PKA. The *PDE1* gene, which was down-regulated (by -1.49-fold), acts as the substrate for the PKA complex and provides negative feedback in carbohydrate signaling and regulation. When cAMP binds to the inhibitory subunit of the PKA complex, it releases its catalytic subunits, *TPK1,* which was up-regulated by 1.6-fold and is involved in stress response, and *TPK2,* which was down-regulated by -1.56-fold and involved in trehalose synthesis and iron uptake (Lin & Chen, 2018; Robertson et al., 2000). Activated PKA phosphorylates a series of transcription factors that control carbon metabolism, stress adaptation, cell cycle, and other functions, but the terminal point of the Ras1/cAMP-PKA pathway in *C. albicans* activation is the master transcription factor Efg1p. This transcription factor, for which expression was downregulated by -2.4-fold, promotes yeast-to-hyphal transition through controlling

carbon metabolism by directly regulating expression of the major glycolytic activator Tye7p that was downregulated by -2.2-fold as well (Robertson et al., 2000).

The transcriptional factors in the downregulated genes set for the SH1009-treated transcriptome were ranked based on the percentage of transcriptome regulation using the PathoYeastract database (Monteiro et al., 2017). The transcriptional regulator Tye7p was the top transcriptional factor that plays a key role in cellular response to SH1009 by regulating 44% of downregulated genes. Tye7p regulates the downregulated genes *TPS1* (by -2.3-fold), *TPS2* (by -2.5-fold), *TSP3* (by -2.4-fold), *ATC1* (by -1.5-fold), and *NTH1* (by -1.5-fold), involved in the most significantly enriched biological process in the SH1009 repressed transcriptome, the trehalose metabolic process (Askew et al., 2009). Moreover, genes that are associated with glucose, glycogen, and galactose biosynthesis were found dysregulated by SH1009 treatment, consequently resulting in a poor supply of carbohydrate, which is the preferred source of energy in *C. albicans,* for glycolysis and the tricarboxylic acid (TCA) cycle. The dysregulation of the TCA cycle attenuates the production of ATP, leading to a low intracellular level of cAMP, which dramatically affects the activation of Ras1/cAMP-PKA pathway (Tao et al., 2017), supporting our previous results that suggested the modulatory effect of SH1009 on the ATP-binding cassette (ABC) efflux pumps which drive the fluconazole resistance mechanism (Alqahtani et al., 2019). Significantly, the top downregulated gene in the SH1009 transcriptomic profile (by -32-fold), *HSP21,* lies downstream of the Ras1/cAMP-PKA pathway (Gong et al., 2017). The deletion of this small-heat shock protein, Hsp21, weakens *C. albicans* resistance to oxidative and thermal stresses by accumulating significantly lower intracellular levels of trehalose sugar which is considered an oxidative stress protectant (Mayer et al., 2012). The involvement of Hsp21 in the regulation of trehalose

homeostasis and the tight control of trehalose level by G protein receptor (Gpr1) suggest that Hsp21 is a possible link between the Ras1/cAMP-PKA pathway and trehalose biosynthesis (Serneels et al., 2012). Additionally, SH1009 downregulates the basic carbon metabolism that controls trehalose biosynthesis, the key nutritional and protectant cue for carbohydrate regulation and oxidative resistance in *C. albicans*.

C. albicans cells exhibited a different repressed transcriptomic profile in response to SH9051 (**Fig. 4B**). Organic sulfate compounds may be transported into the cells by the putative sulfate transporter (Seo1) for which expression was downregulated by -2.06-fold. Sulfate, then, should be reduced through the sulfate assimilation pathway genes, *MET3*, *MET14*, *MET16*, *ECM17* (or *MET10*) that were among the top downregulated genes (by -10, -11, -12, and -1.7-fold, respectively), to sulfide which would afterward be incorporated into the formation of homocysteine by downregulated gene *MET15* (by -1.9-fold) along with O-acetylhomoserine derived from homoserine by the *MET2* gene (downregulated by -1.7-fold). In addition, expression of genes involved in sulfur amino acid (methionine and cysteine) biosynthesis pathways were downregulated. Homocysteine is converted to methionine by *MET6* (downregulated by -2 fold) and to *S*-adenosylmethionine (SAM) in the methyl cycle by *SAM2*, *SAM4*, and *SAH1* (downregulated by -1.5, -2, and -1.6-fold, respectively). *CYS1* and *CYS4*, which convert homocysteine to cysteine in the two steps of the transsulfuration process, were downregulated by -2 and -1.9-fold, respectively. In *S. cerevisiae*, the levels of methionine, cysteine, and SAM negatively control the activity of transcription factor Met4p (expression downregulated by -3-fold) that controls the activity of sulfur metabolism pathway by positively regulating the activity of *MET* genes (Ljungdahl & Daignan-Fornier, 2012). These findings indicate that SH9051 downregulates the sulfur metabolism pathway which dysregulates the methionine and cysteine biosynthesis

processes. Taken together, both repressed transcriptomic profiles of SH1009 and SH9051 demonstrated significantly and distinctively major perturbations of different metabolic pathways in *C. albicans* cells, suggesting different molecular targets.

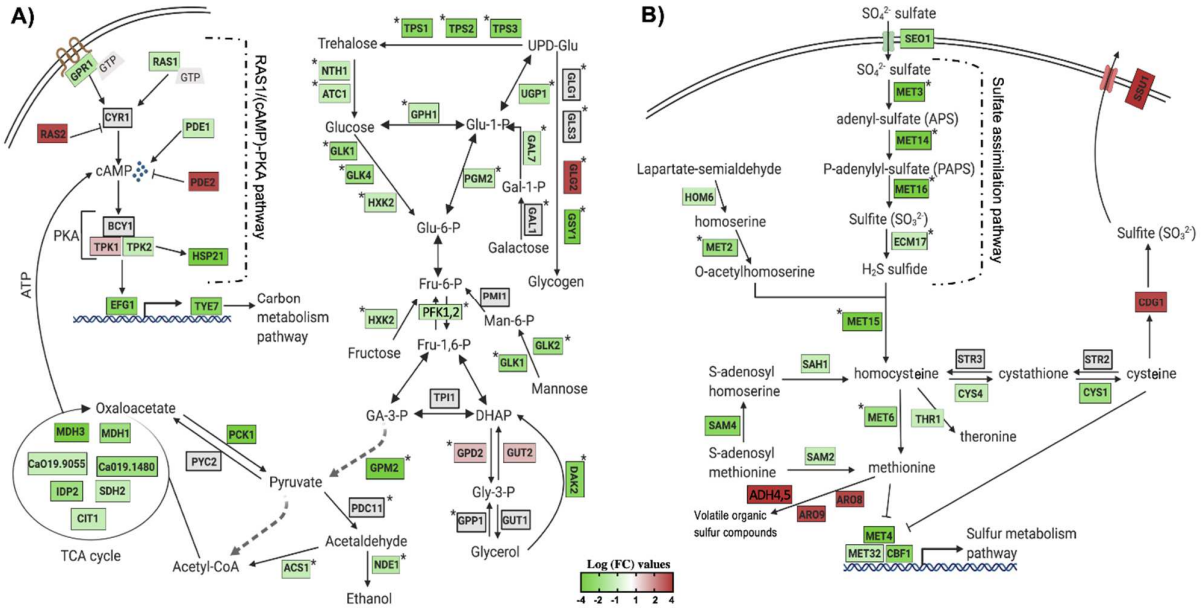

Figure 4: Visualization of the impact of aurone treatment on the central metabolism of significantly enriched KEGG pathways. The changes in gene expression in central carbon and sulfur metabolic pathways in response to SH1009 (**A**) and SH9051 (**B**) treatments, respectively. Detected genes are colored based on their values of log fold change, green and red colors indicate downregulated and upregulated genes, respectively, while a gray color indicates undetected genes. Pathway annotations and gene names are customized from different studies on *C. albicans* or based on their homology in *S. cerevisiae* and created with BioRender.com. Stars indicate genes that are directly activated by the major transcriptional activators Tye7p for carbon metabolism and Met4p for sulfur metabolism.

Cross-transcriptome profiling reveals overlapping biological processes.

To detect any potentially synergistic or antagonistic interaction between SH1009 and SH9051 at the molecular level, a Venn intersections diagram was constructed to compare the repressed and induced transcriptomic profiles (**Fig. 5**). Although ~197 genes were commonly downregulated in both repressed datasets of SH1009 and SH9051, 44% of these genes were enriched for unknown biological process while only 11 genes were enriched insignificantly (*P* (FDR) value < 0.07) for carbohydrate metabolic processes, especially genes that are involved in drug stress response, indicating no synergistic interaction for repressed transcriptomic responses. Comparing the upregulated genes for SH9051 and the downregulated genes for SH1009 detected 53 commonly dysregulated genes that are not enriched for any GO term. By way of contrast, a low number of overlapped genes (only 14) for iron ion transport and sulfur amino acid metabolic processes are significantly enriched between the upregulated genes for SH1009 and the downregulated genes for SH9051. The upregulated genes for sulfur amino acid metabolic processes (*MET4*, *MET3*, *MET15*, and *CYS1*) in the induced transcriptome of SH1009 could be attributed to carbohydrate starvation, which subsequently causes the cells to utilize amino acids as alternative sources of carbon (Miramón & Lorenz, 2017). The downregulation of genes for iron ion transport (*RBT5*, *FET34*, *FTR1*, and *CFL4*) in the repressed transcriptome of SH9051-treated cells could be attributed to elevated levels of organic sulfur compounds as a consequence of sulfur amino acid catabolism. This might be concomitant with repression in iron ion import in order to hinder the synthesis of iron–sulfur (Fe-S) proteins (Petti et al., 2012). Nevertheless, this low level of antagonistically differential expression of a small number of genes cannot be interpreted as a fundamentally

antagonistic interaction between the aurone modes of action because these antagonistic processes seemed to be secondary effects of the essentially targeted pathways.

However, the induced transcriptome in both SH1009 and SH9051 profiles was remarkably comparable. A large set of genes (~299) were commonly upregulated upon SH1009 and SH9051 treatments. These genes were significantly enriched (*P* (FDR) values < 0.0001) for RNA processing, ribosomal biogenesis, mitochondrial RNA processing, and cleavages involved in rRNA processing. High transcript levels for rRNA processing and ribosomal biogenesis in *S. cerevisiae* after exposure to high lethal concentration of H_2O_2 has been observed previously, suggesting an urgent need to accelerate the rRNA processing and ribosomal biogenesis that are required for synthesizing oxidative stress response proteins or to replace the rRNA that was damaged by oxidative stress (Shenton et al., 2006). Additionally, nutrient depletion has been associated with ribosomal stress by inducing ribosomal degradation and formation of free ribosomal proteins that can eventually accumulate in the nucleoplasm (Zhou et al., 2015).

In addition to commonly induced genes in response to either SH1009 or SH9051 treatments, uniquely upregulated genes in response to each aurone have been significantly enriched for prominent biological processes. For SH1009, a set of genes was uniquely induced and enriched for iron ion transport. Most of these genes (C4_03340C_A, 11-fold; *CFL2*, 9-fold; *RBT5*, 7.9-fold; *CFL4*, 7.2-fold; *FRE9*, 4.5-fold; *FTR1*, 4.5-fold; *FTH1*, 3.6-fold; *CFL5*, 3.4-fold; *SIT1*, 3-fold; *FRE10*, 3-fold; *FRP1*, 2.8-fold; *FRE30*, 2.7-fold; C7_00430_A, 2.6-fold; *FRE7*, 2.4-fold; *FET34*, 1.9-fold; *CTR1*, 1.67-fold; and *CFL1*, 1.5-fold) were among the top upregulated genes. The expression of iron ion acquisition genes in *C. albicans* is regulated by the induced transcriptional repressor (Hap43p, 2fold), which responds to low intracellular levels of

iron by inhibiting the transcriptional activator of iron utilization, Sfu1p which was downregulated by -1.86 fold. The Sfu1p transcription factor represses genes encoding iron uptake through direct inhibition of a third transcription factor Sef1p, for which expression was upregulated 3-fold, and indirect inhibition of Hap43p expression, since Sef1p regulates the activity of Hap43p (Chen et al., 2011). This strict regulation of iron acquisition and utilization reflects the significance of maintaining ordinary intracellular iron homeostasis to thereby prevent the iron toxicity that leads to severe oxidative stress. Overabundance of iron catalyzes the production of reactive oxygen species (ROS) by the Fenton reaction, resulting in oxidative damage in biomolecules (Missall et al., 2004). A recent study has reported that iron overload is the major determinant of the oxidative stress associated with rRNA cleavage and degradation through promoting stress-strand breaks in rRNA by ribosome-bound iron (Zinskie et al., 2018).

For SH9051, a set of genes that are involved in the arginine biosynthetic process was uniquely induced (*DUR1,2*, 8.4-fold; *GDH1*, 5.9-fold; *AFP99*, 3.6-fold; *ARG11*, 2-fold; *ARG8*, 2-fold; *ARG1*, 1.89-fold; *ECM42*, 1.9-fold; *CAR1*, 1.75-fold; *CAP2*, 1.65-fold; *ARG5*, 1.6-fold; and *CAP1*, 1.56-fold) in response to the aurone. The induction of the arginine biosynthetic pathway has been reported previously as transcriptional responses in *C. albicans* to oxidative stress resistance (Issi et al., 2017). Additionally, as a defense mechanism against host-phagocytosed cells, *C. albicans* induces the arginine biosynthetic pathway to resist macrophage-derived antimicrobial ROS (Jiménez-López et al., 2013). These findings indicate that both aurones could induce cellular oxidative stress; however, uniquely upregulated mechanisms also suggest key roles for the functional groups in the chemical structure of each aurone.

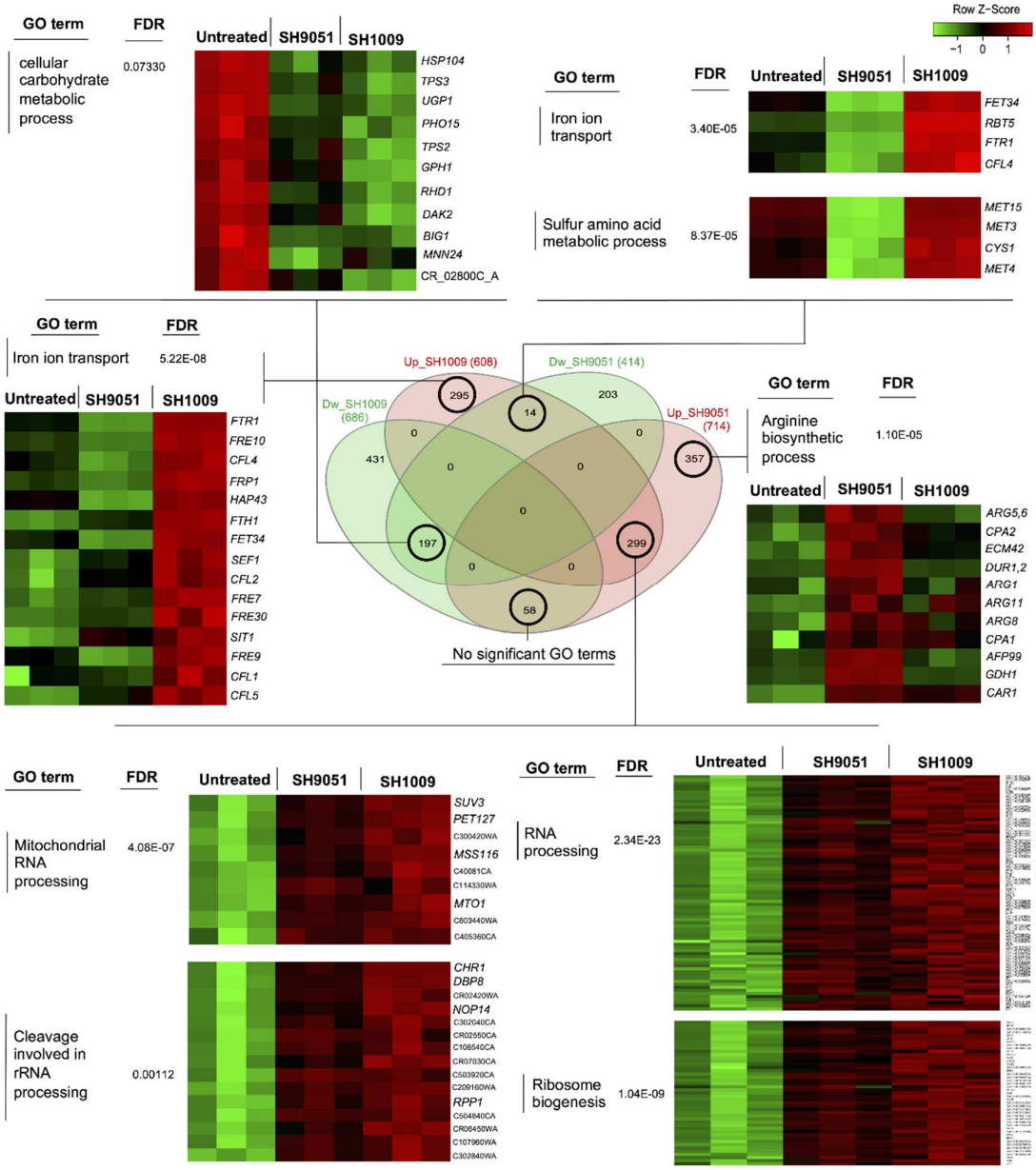

Figure 5: Comparisons between induced and repressed transcriptomic profiles of aurones SH1009 and SH9051. The Venn diagram shows the number of commonly or uniquely dysregulated genes between four datasets: downregulated-SH1009, downregulated-SH9051, upregulated-SH1009, and upregulated-SH9051 dataset. Heatmaps demonstrate the differential gene expression of sets of genes that are clustered and enriched for significant GO terms in each overlap. The corrected *P* values (FDR) are indicated for each GO term. The heatmaps were generated to visualize the comparisons of differential gene expression across the SH1009- and SH9051-treated and untreated samples using the shinyheatmap tool by which the expression of genes were scaled per row based on the Z-score of standard deviations (positive or negative) and plotted on a red-green color scale where the high level of expression is colored red and the low level of expression is colored green.

By linking the transcriptional responses of aurones SH1009 and SH9051 to their core chemical structures and functional groups, three critical hypotheses can be proposed. First, the hydroxyl groups and/or methoxy group in aurone SH1009 can react with transition metal ions (iron), which produces high levels of toxic ROS that would result in rRNA cleavage and degradation along with ribosome stress, resulting in a potent prooxidant activity. Additionally, these functional groups could uniquely affect the accumulation level of the oxidative protectant, trehalose (Gencer et al., 2018), which in turn downregulates the Ras1/cAMP-PKA pathway and negatively impacts carbon metabolism and its regulation (Perfect et al., 2017) (**Fig. 4A**). Second, since *C. albicans* utilizes amino acids as a nitrogen source, the nitrogen atom in aurone SH9051 could interfere with the negative regulation of transcriptional factor Met4p, simulating a high level of methionine and cysteine supply resulting in inactivation of MET genes, thus suppressing the sulfate assimilation pathway (Hébert et al., 2013) and inducing sulfur amino acid catabolism (**Fig. 4B**). Third, the C ring structure of both aurones could contribute to generating more ROS, which results in the common upregulation processes (rRNA processing and ribosomal biogenesis). This would provide SH9051 a mild prooxidant activity, but it is lower than that of SH1009 which can be observed from the depth of the red color of the heatmap in the SH1009 gene expression profile compared to that for SH9051 (**Fig. 5**). Therefore, a reverse genetics approach and quantitative biochemical assays were applied to validate the transcriptional signatures of aurones SH1009 and SH9051 and to establish the structure-activity relationship.

Aurones SH1009 and SH9051 inhibit distinctive carbon and sulfur amino acid metabolic pathways.

The enrichment analysis of differentially regulated genes upon aurone treatment indicated carbon and sulfur metabolism as the most significantly downregulated pathways. Accordingly, engineering of *C. albicans* deletion strains was attempted using the CRISPR-Cas9 gene editing technique in order to validate that the trehalose and sulfur amino acid biosynthetic metabolic pathways are the primary targets of aurones SH1009 and SH9051, respectively (**Fig. 6A** and **B**). We reasoned that if the transcriptional factors of carbon metabolism, Tye7p, and sulfur metabolism, Met4p, are absent, then the aurones would not be active against the mutants. **Appendix F** depicts the genetic modification of a *TYE7*Δ mutant from *C. albicans* SC5314 strain background by introducing double-strand breaks in which two gRNAs guide Cas9 nuclease to catalyze the cleavages at the 5′ and 3′ ends of the open reading frame (ORF) of the targeted gene *TYE7* and replace the gene sequence with the gene drive cassette (Halder et al., 2019). Although the gene drive system harbors two single gRNAs sequences and SNR52 RNA polymerase III promoter, allowing the gene drive to transcript and propagate to any wild-type locus for deletion, the platform failed to generate a *MET4*Δ mutant even with multiple rounds of transformations using three different gene drive systems containing three different dual gRNAs which target different sites on the *MET4* gene sequence. Therefore, a *MET4*Δ deletion mutant was obtained from the Fungal Genetics Stock Center (FGSC, University of Missouri, Kansas, USA), and the absence of the *MET4* gene sequence was verified by colony PCR (**Appendix F**).

The *TYE7*Δ mutant was documented previously for higher storage carbohydrate levels (trehalose and glycogen) as a result of severely reduced glycolytic flux due to the

repressed expression of the genes encoding the glycolytic-committing enzyme phosphofructokinase (*PFK1* and *PFK2*). This gives Tye7p the role to regulate the flux between carbohydrate storage and production at the glucose-6-phosphate branch point in order to avoid futile glycolysis cycling (**Fig. 4**) (Askew et al., 2009). Consequently, while the growth of *C. albicans* SC5314 was inhibited by ~4-fold during the exponential phase of the growth curve under the IC_{50} concentration of SH1009 (16 μM), the *TYE7*Δ mutant showed evident SH1009-resistant growth (**Fig. 6C**), suggesting that the greater storage of oxidative stress protectant (trehalose) could rescue *TYE7*Δ from the proposed prooxidant activity of SH1009. Additionally, it has been reported that exposing *C. albicans* to extracellular ~30 μM iron led to accumulation of more ROS, which could cause a synergistically inhibitory activity with SH1009 (Kaba et al., 2013). However, supplying growth media with different concentrations of extracellular iron did not increase the inhibitory activity of SH1009 (**Appendix G**). In fact, it marginally reversed the inhibitory activity which could support the claim that the uniquely upregulated genes for iron ion uptake signifies the low intracellular level of iron ions upon SH1009 treatment. Because *C. albicans* possess a sophisticated system of regulation of iron ion transport due to the potential toxicity of iron by generating ROS, it could be speculated that the impact of SH1009 on the level of iron ions was endogenous and it cannot be affected exogenously.

Treatment of the *MET4*Δ mutant with SH9051 resulted in significantly more susceptible response compared to the wild type indicating a potential secondary effect or pleiotropic effects of the mutation (**Fig. 6D**). Interestingly, unlike the strict methionine auxotrophic phenotype of the *S. cerevisiae MET4*Δ mutant, but like the *Schizosaccharomyces pombe ZIP1*Δ transcription factor mutant (Harrison et al., 2005), *C. albicans MET4*Δ is not auxotrophic for sulfur amino acids (methionine or cysteine)

(**Appendix F**). Also, the additional supplements of cysteine or methionine were not able to restore the fitness of *MET4*Δ without any stress. In addition to the SH9051 stress, addition of sulfur amino acids further inhibited the growth of *MET4*Δ (**Fig. 6E and F)**. This could support the hypothesis from RNA-seq data where SH9051 treatment stimulated a toxic supply of sulfur amino acids, suggesting a synergistically toxic effect between the SH9051 and these amino acids through sulfur amino acid catabolism. For this reason, most of methionine and cysteine that was taken up by *MET4*Δ cells might be degraded thus reducing SH9051 toxicity even in the lack of de novo biosynthesis of these amino acids. Therefore, in order to further investigate the cellular responses of the wild type and relevant mutants during aurone SH1009 and SH9051 treatments, quantitative biochemical assays were conducted.

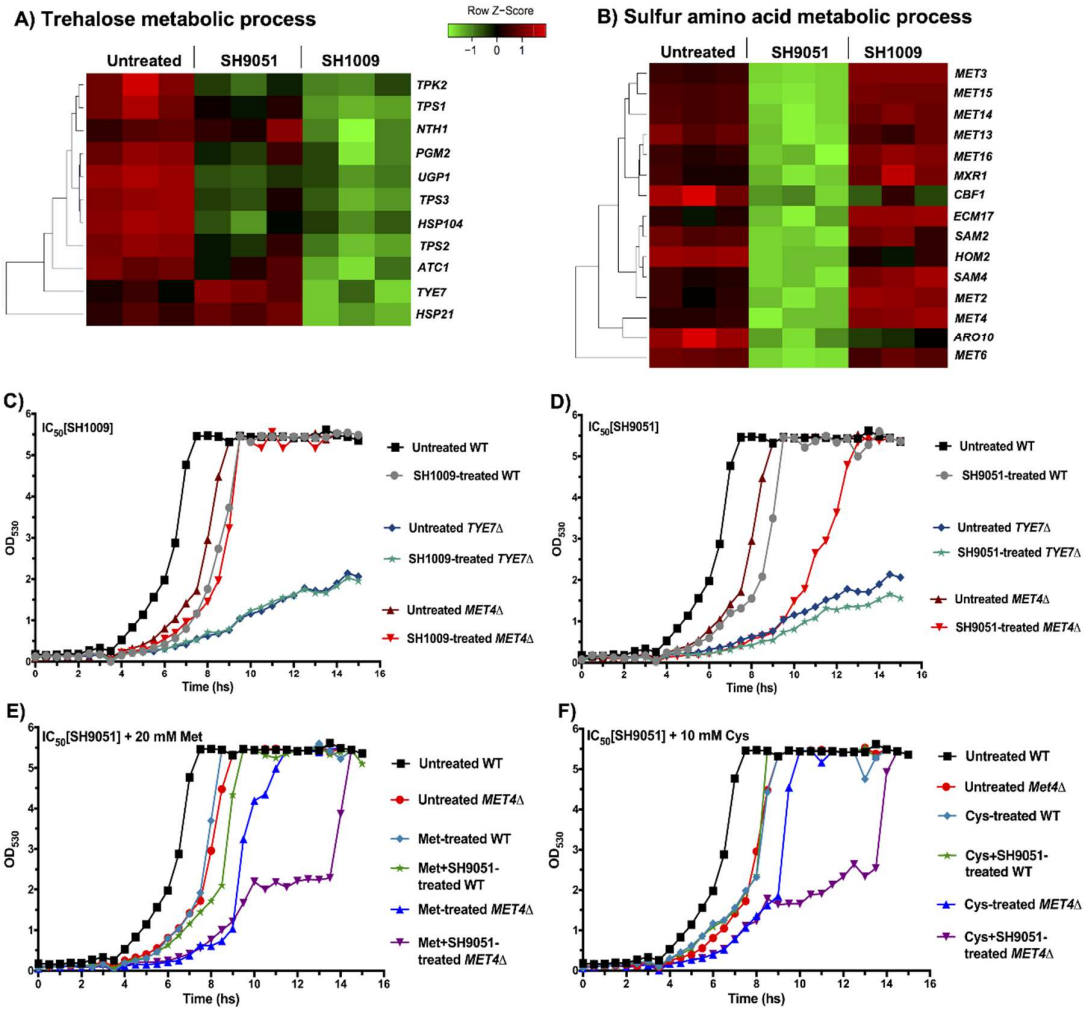

Figure 6: The most repressed transcriptional responses of aurones SH1009 and SH9051 treatments. (**A** and **B**) Aurone SH1009 and SH9051 treatments resulted in downregulation of trehalose and sulfur amino acid metabolic processes. The relative expression of the genes of these processes was illustrated by green-red color scale in heatmap. (**C** and **D**) The growth curves of *C. albicans* SC5314 wild-type strain, *TYE7*Δ, and *MET4*Δ mutants under the IC_{50} concentrations of aurone SH1009 (16 μM) and SH9051 (90 μM), respectively. (**E** and **F**) The growth curves of *C. albicans* SC5314 wild-type strain and the *MET4*Δ mutant under the IC_{50} concentration of aurone SH9051 (90 μM) with supplements of 20 mM methionine and 10 mM cysteine, respectively. The growth conditions were carried out in YPD broth media using the Bioscreen C growth curve instrument and the OD_{530} reads were recorded at 30 min intervals for 24 h incubation at 30℃.

Biochemical assays specify the structure-activity relationship of each aurone.

Comparisons between the repressed and induced transcriptomic profiles of *C. albicans* cells treated with aurones SH1009 and SH9051 indicated a common feature in the aurone chemical structures could contribute to elevate the intracellular ROS levels. Additionally, distinct functional groups in each aurone indicated uniquely upregulated and downregulated pathways (**Fig. 5**). Accordingly, the core chemical structure of an aurone without any functional group (phenyl aurone, **Fig. 7A**) was included in cellular metabolism assays to quantitively measure the structure-activity relationships of the aurone core and functional groups. The cell viability assay for the phenyl aurone showed that inhibition of *C. albicans* SC5314 at the highest concentration of 200 μM was approximately 28%, predicting that approximately one third of any aurone inhibitory activity was proportionally derived from this basic chemical structure (**Fig. 7A)**.

Since the core chemical structure was the only common feature between aurones SH1009 and SH9051, we hypothesized that the C ring structures, comprised of the oxygen double bound, oxygen atom, and/or the extended conjugation that connects the benzofuranone heterocyclic ring with the phenyl group (**Fig. 7A)**, could contribute in generating ROS. Therefore, the exponential growth of *C. albicans* SC5314 wild-type, *TYE7*Δ, and *MET4*Δ cells was perturbed by 200 μM of each aurone for one hour, after which yeast cells were stained with the oxidative stress indicator, CM-H_2DCFDA, that is oxidized by ROS to a fluorescent molecule (Hassani & Dupuy). Intracellular ROS accumulation relative to fluorescence intensity illustrated that the highest oxidative stress was caused by SH1009 with a 77.4% significant increase (P value < 0.001) in ROS levels compared to the untreated sample, confirming the prooxidant

activity of this aurone against *C. albicans* cells. In comparison, the prooxidant activity of the phenyl aurone raised the ROS level significantly by 45.4% (P value < 0.01) relative to the untreated sample. It was statistically significant that the basic structure was responsible for 24.2% and 48.1% of (ROS) generation in SH1009 and SH9051, respectively, relative to untreated sample (**Fig. 7B)**.

Because aurone SH1009 uniquely induced expression of iron ion transport pathways, it was speculated that treated cells would have low intracellular iron ion levels due to the catalyzing of these stress ions by the SH1009 structure, promoting the prooxidant activity. There are two intracellular states of transition metal iron, the oxidized form of iron, ferric (Fe^{3+}) ions, which react with oxygen to form oxides with relatively low solubility, and the reduced form of iron, ferrous (Fe^{2+}) ions, which react with oxygen to form ROS through Fenton reactions (Fourie et al., 2018a). Typically, the reduction of ferric iron(III) to ferrous iron(II) by reductases increases the availability and solubility of iron. However, compromising the efficiency of the network controlling iron homeostasis or changing the availability of ferrous ions are highly related to toxic ROS production (Gammella et al., 2016). Therefore, the levels of Fe^{3+} and Fe^{2+} iron ions were determined using an iron probe assay (iron chromogen) after treating *C. albicans* wild type and *TYE7*Δ cells with aurones.

Fig. 7C demonstrates the concentrations of Fe^{3+} and Fe^{2+} where the ratio of Fe^{2+}/ Fe^{3+} in *C. albicans* SC5314 wild type cells treated with SH1009 was the highest (3.7) compared to treatments with SH9051 (2.2) and phenyl aurone (2.03) in wild type cells. This validates the transcriptional signature of SH1009 and support the proposed prooxidant activity and the results of the ROS generation assay. Although the Fe^{2+}/ Fe^{3+} ratio of SH1009 in *TYE7*Δ mutant was 6.0, this strongly underscores the role of trehalose in protecting the cells since the *TYE7*Δ mutant showed an intrinsically

resistant phenotype against SH1009 (**Fig. 6C**). SH9051 treatment resulted in a 2.2 higher Fe^{2+}/ Fe^{3+} ratio in the wild type compared with a ratio of 2.03 in response to the phenyl aurone, suggesting that most of the ferric ion reduction trait in SH9051 (~89.3%) could be the impact of the C ring structure. This impact contributes to (~54%) the ability of SH1009 in catalyzing the reaction with metal ion stress (iron) which poses a question about the role of the hydroxyl groups and/or methoxy group in the trehalose level.

Intracellular trehalose levels were determined enzymatically based on hydrolysis of trehalose by trehalase into two glucose monomers after eliminating the original glucose from the samples. The glucose concentration, which is directly proportional to the trehalose concentration, was detected fluorometrically by coupling the oxidation of glucose to peroxidation of the fluorogenic substrate, Amplex Red (Carillo et al., 2013). This method overcomes the previous limitation of colorimetric detection which did not have the sensitivity to detect the low trehalose levels in exponentially growing yeast cells (Askew et al., 2009). We observed significantly increased levels of trehalose in the wild type and *TYE7*Δ cells under all treatments except the SH1009-treated wild type sample (**Fig. 7D**). As expected and documented before (Askew et al., 2009), trehalose level was two times higher ($P < 0.001$) in untreated *TYE7*Δ mutant compared to untreated wild type cells which provides the *TYE7*Δ cells protection from the SH1009-prooxidant effect. SH1009 treatment considerably decreased the trehalose level in wild type cells 7.7 times ($P < 0.001$) relative to untreated-wild type sample and 10.6 times ($P < 0.0005$) relative to SH1009 treated-*TYE7*Δ sample, demonstrating SH1009 resistance via higher trehalose storage in the *TYE7*Δ mutant. Additionally, a significant observation was the failure of phenyl aurone to suppress trehalose synthesis with insignificant differences in trehalose concentrations compared with untreated samples either in wild type or mutant cells.

This suggests that suppression of trehalose synthesis could be almost entirely attributed to the functional groups in SH1009 aurone, hydroxyl groups and/or methoxy group.

The impact of the nitrogen functional group of aurone SH9051 was not only inactivation of sulfur amino acid biosynthesis, but also activation of degradation of these amino acids, simulating a high exogenous supply of methionine or cysteine (Hennicke et al., 2013; Xu et al., 2018) (**Fig. 4B**). According to previous studies, the end products of methionine catabolism are volatile organic sulfur-containing compounds (VOSCs) such as thioesters, thioethers, dimethyl trisulfide (DMTS), and dimethyl disulfide (DMDS) (Landaud et al., 2008). In *C. albicans*, large quantities of sulfite have been reported as a consequence of cysteine catabolism (Hennicke et al., 2013). To determine the role of the aurones in sulfur amino acid catabolism, total sulfite was measured based on the sulfite-triggered cleavage of the disulfide bond in Ellman's reagent, which also reacts with compounds containing free thiols, such as VOSCs (Coulomb et al., 2017). SH9051 was the only aurone treatment that significantly ($P < 0.0001$) elevated the sulfite levels (**Fig. 7E**) while the values produced by SH1009 and phenyl aurone treatment of cells were nearly zero, similar to untreated cells. The overproduction of sulfite associated with SH9051 treatment demonstrated the impact of nitrogen atom on the uniquely transcriptional responses to SH9051. In addition, combining SH9051 with methionine or cysteine indicated their synergistic effects on *C. albicans* growth (**Fig. 6E and F**) by considerable overproduction of sulfite and VOSCs which were more significantly produced ($P < 0.0001$) in *MET4*Δ mutant than wild type cells, demonstrating the hypersensitivity of *MET4*Δ toward SH9051 (**Fig. 6D**). These observations indicate that Met4p activity in *C. albicans* might not only be involved in sulfur metabolism but also participate in defense against several stresses, including oxidative stresses.

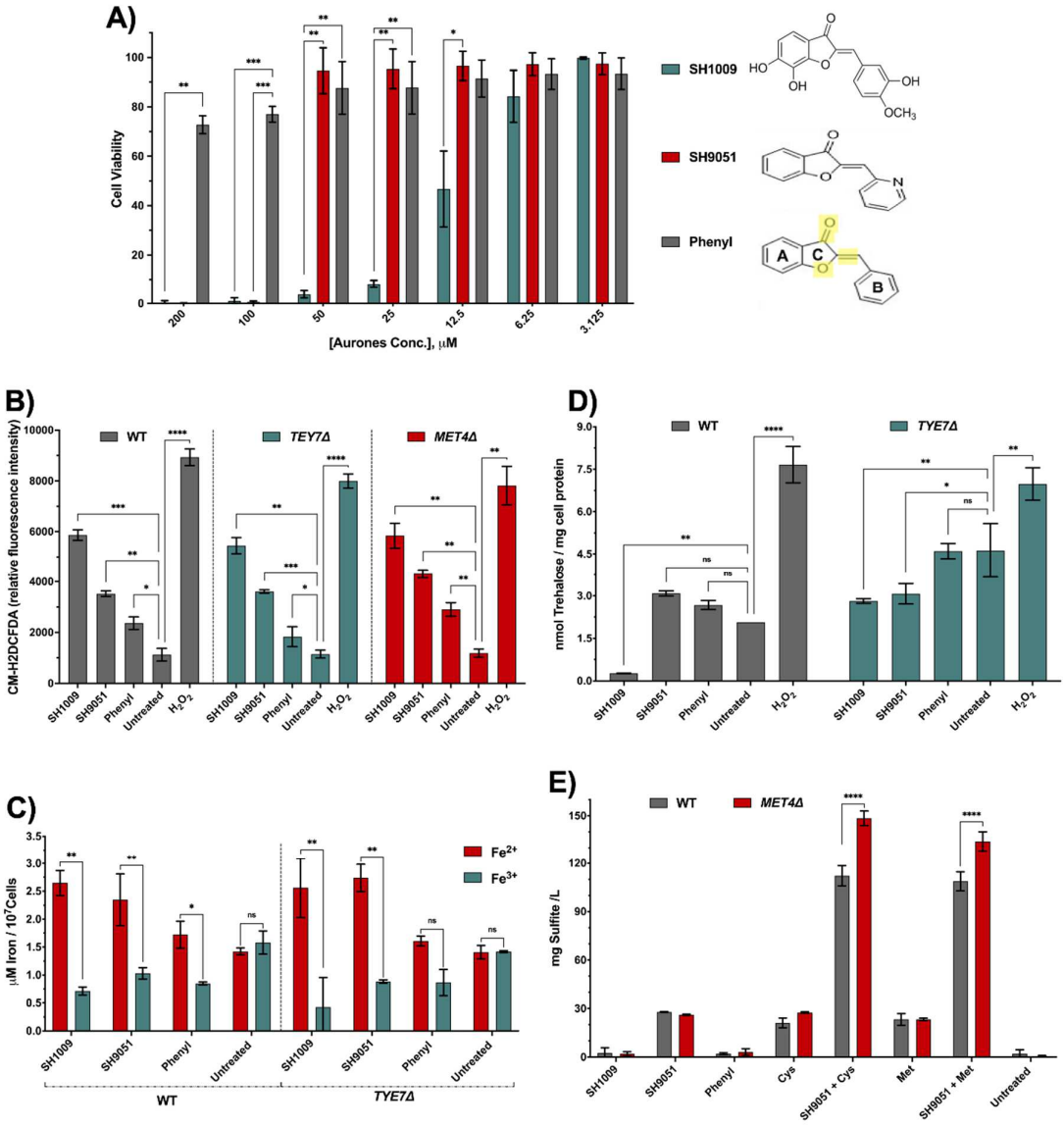

Figure 7: *C. albicans* cellular growth and metabolism responses to SH1009, SH9051, and phenyl aurones. A) The inhibitory activity of SH1009, SH9051, and phenyl aurones on *C. albicans* SC5314 cell suspensions (0.5 – 2.5 ×10^3 CFU/mL) with treatments of 2-fold serial dilutions of each aurone (3.125μM – 200μM) in RPMI-1640 medium for 24 hours at 35℃. PrestoBlue reagent was used to assay the cell viability. C ring structure is highlighted in yellow color in the phenyl aurone where the benzofuranone heterocyclic A and C rings are connected to the phenyl B ring by extended conjugation. **B)** Changes in ROS production after one hour treatment of 200 μM of each aurone (H_2O_2 was used as positive control) on exponentially growing *C. albicans* SC5314, *TYE7*Δ, and *MET4*Δ cells in YPD media using the fluorescent dye CM-H_2DCFDA. **C)** Determination of intracellular ferrous (Fe^{2+}) ions in *C. albicans* SC5314 and *TYE7*Δ mutant cells based on the formation of a complex between Fe^{2+} and an iron chromogenic substrate; ferric (Fe^{3+}) ions were determined using an iron

reducer on separate samples to determine the total iron content and then subtracting the Fe^{2+} ions from total iron to determine the Fe^{3+} ion concentration. **D)** The intracellular trehalose content of wild type *C. albicans* SC5314 and *TYE7*Δ at logarithmic phases were measured enzymatically following aurone treatment using trehalase coupled with Amplex red reagent as described in the Materials and Methods section. **E)** Total sulfite production was measured in wild type *C. albicans* SC5314 and *MET4*Δ based on the reaction with Ellman's reagent after treating cells with aurones and amino acids, 20 mM methionine or 10 mM cysteine. All data points are mean ± *SD* (n = 3). Significances were calculated using two-way ANOVA for multiple comparisons. The asterisks indicate the difference was significant. *P* values: (**** $P \leq 0.0001$), (** $P \leq 0.001$), (* $P \leq 0.01$).

DISCUSSION

The aim of our study was to comprehensively understand the modes of action for aurones SH1009 and SH9051 treatment in *C. albicans* SC5314 using the global transcriptional signature and leveraging the power of the RNA-seq technique. Our gene expression analysis showed that aurone SH1009 and SH9051 led to the dysregulation of a staggering number of diverse genes (1249 and 1085 genes, ~21% and 19% of the genome, respectively for SH1009 and SH9051). These genes are primarily enriched for different metabolic pathways, carbohydrate and sulfur metabolisms in response to SH1009 and SH9051, respectively. The pathogenicity of *C. albicans* is strictly linked to metabolic processes to support the bioenergetic requirements of infectious growth. Thereby, one of the most important metabolic contributors to the pathogenicity of this opportunistic fungus is stress adaptation by synthesizing the disaccharide, trehalose (Brown et al., 2014).

The transcriptional response of aurone SH1009 treatment showed that the trehalose metabolism was the most significantly repressed biological process. This non-reducing sugar is not only carbohydrate storage in fungal cells, but also accumulates in response to thermal and oxidative stresses. Due to its physical interaction with proteins and phospholipids as a highly hydrophilic molecule, trehalose plays a critical role in stabilizing enzyme activities and protecting cellular membranes during stress. Trehalose acts as a free radical scavenger under ROS-induced conditions, supporting the fungal pathogenicity against the human immune system defense by accumulating this stress protectant by upregulating the trehalose biosynthesis genes (Missall et al., 2004). Trehalose biosynthesis and storage are tightly linked to the glycolytic pathway and controlled by transcriptional regulator Tye7p (Askew et al., 2009). The uniquely repressed effect of aurone SH1009 on the transcription regulator Tye7p as evidenced

by RNA-seq data showed by far the greatest impact as a regulator of 44% of downregulated genes. The result of deleting this transcription factor (*TYE7*Δ) was an SH1009 resistant mutant (**Fig. 6C**) that uses the higher storage of oxidative stress protectant (trehalose) as an intrinsic line of defense (**Fig. 7D**). Previous studies have been shown that the disruption of the trehalose biosynthesis pathway results in dysregulation of the central carbon metabolism and alteration in stress response and virulence. In *C. albicans,* disruption of Tps1 or Tps2 increased the susceptibility to oxidative stress and attenuation of virulence in a systemic mouse model (Perfect et al., 2017; Thammahong et al., 2017). Furthermore, in trehalose-deficient mutants, the enzymatic antioxidant activities were synergistically induced during exposure to oxidative stress inducer H_2O_2 (González-Párraga et al., 2003).

Typically, treating *C. albicans* with H_2O_2 leads to increased trehalose content and up-regulation of enzymatic antioxidant activities that are considered oxidative stress defenses (Pedreño et al., 2006). These defenses include a single catalase gene for conversion of H_2O_2 to water and oxygen (Wysong et al., 1998), six superoxide dismutase SOD genes that convert superoxide anions to hydrogen peroxide subsequently processed by catalase (Hwang et al., 2003), four glutaredoxins GRX genes (Chaves et al., 2007), and two thioredoxin TRX genes, all of which are involved in the oxidative stress response (Dantas et al., 2010). However, none of these antioxidant enzymes were differentially expressed upon SH1009 treatment. Nonetheless, these antioxidant enzymes were modulated by the prooxidant activity of SH1009 because, in *C. albicans,* these enzymes are regulated by iron availability (Chakravarti et al., 2017). SH1009 uniquely upregulated Hap43p, which has been recorded as the sole transcriptional regulator responsible for iron-dependent oxidative stress response. Under iron deprivation conditions, it acts as a transcriptional activator

for iron ion uptake genes (Hsu et al., 2011) and as a repressor of numerous genes encoding enzymes that utilize iron as a cofactor, including antioxidant enzymes (Cat1, Sod4, Grx5, and Trx1), possibly to permit the utilization of iron in more essential processes (Chakravarti et al., 2017).

The prooxidant activity has been identified as the ability to reduce transition metal ions ferric(III) to lower oxidation states ferrous(II), which increase the production of ROS (Truong et al., 2020), which can be used in cell signaling depending on context and concentration. However, ROS are highly reactive molecules and can inflict damage to cellular macromolecules (Shcherbik & Pestov, 2019) like cleavages involved in rRNA and ribosomes by stress-strand breaks via ribosome-bound iron (Zinskie et al., 2018) which was the commonly upregulated process for both SH1009 and SH9051 treatments. The structure-activity relationship metabolic assays evidenced the role of the C ring structure in generating ROS through disruption of iron homeostasis. Based on the phenyl aurone treatments, the core chemical structure contributes to 24.2% of SH1009 activity for generation of ROS and 51.3% for catalyzing iron ions. Our results support prior studies that suggested the role of oxygen atoms and the double bond of the C ring structure in increasing prooxidant potential in flavonoids. Also, the number of hydroxyl groups, their positions, and methoxylated B ring were important factors for the structure-prooxidant activity (Baldim et al., 2017; Eghbaliferiz & Iranshahi, 2016). These functional groups complete the residual prooxidant potency of SH1009 by contributing 75.8% to ROS generation, 48.7% to catalyzing iron ions, and most significantly, 100% of the impact on trehalose protection in *C. albicans*.

Although flavonoid compounds are naturally synthesized as antioxidant metabolites in plants, the prooxidative properties of these compounds can be enhanced in the presence of iron (III) or copper (II) ions mainly because of their ability to reduce

metal ions based on Fenton-type reaction and generate ROS (Eghbaliferiz & Iranshahi, 2016). This property allows flavonoids to selectively target particular cells with characteristics such as extra quantities of redox metal ions. For example, it has been observed that flavonoids can boost cellular levels of ROS to cytotoxic ranges in cancer cells but not in normal cells due to the higher concentration of copper(II) ions in the metabolically active cancer cells (Eghbaliferiz & Iranshahi, 2016; Jomová et al., 2019). In this regard and supporting our previous work showing the selective toxicity of SH1009 for *C. albicans* over human cells (Alqahtani et al., 2019), the selectively prooxidant potency of SH1009 could be attributed to the naturally high redox metal iron ions inside *C. albicans* cells. Whereas the iron ions in the host are largely unavailable as it is constantly sequestered by iron-binding protein like heme and ferritin, *C. albicans*, as a commensal opportunistic pathogen, has evolved sophisticated iron acquisition and storge systems which enable this fungus to scavenge iron from the host and store it in compartments such as vacuoles and mitochondria (Fourie et al., 2018b). The pathway that controls the intracellular iron mobilization and storage has been identified in *C. albicans*. The two vacuolar transporters Ccc1 and Smf3 were dysregulated upon SH1009 exposure where Ccc1 (expression upregulated by 2.14 fold) increases vacuolar storage of iron and Smf3 (expression downregulated by -1.8 fold) appears to play a role in vacuolar export (Xu et al., 2014). Seemingly, *C. albicans,* under SH1009 exposure, conceals free iron ions from the cytoplasm by storage in vacuoles as a detoxification mechanism to avoid the iron(III)-SH1009 reduction effect. Furthermore, the genes, *CCC1* and *SMF3*, controlled by the upregulated Hap43p, indicating that regulation of iron ion uptake was not only for acquiring iron from external sources but also to control intracellular iron homeostasis (Monteiro et al., 2020; Singh et al., 2011).

The structure-activity relationship also indicated that aurone SH9051 induces a mild prooxidant activity by generating ROS through catalyzing iron ions. Even though SH9051 reduction of metal ions was primarily (86.3%) derived from the C ring structure, SH9051 generation of ROS was much higher than the phenyl aurone (51.4%), indicating that another factor increases ROS generation with SH9051 treatment. It has been shown that growth inhibition of *C. albicans* occurs after addition of sulfite as reactive sulfur species (RSS), suggesting an increase in the intracellular oxidative stress (Ogasawara et al., 2008). Previous work on *S. cerevisiae* also documented induction of ROS levels in volatile sulfur compound (SO_2)-challenged cells (Lage et al., 2019). This leads us to conclude that the increased effects of ROS generation in SH9051 compared to the phenyl aurone was due to higher accumulation of sulfite and VOSCs as byproducts of sulfur amino acid catabolism, which is essentially the unique impact of the nitrogen atom in SH9051.

Although methionine catabolism has not yet been intensively studied in *C. albicans*, based on previous studies in the industrial yeasts *Kluyveromyces lactis* (Kagkli et al., 2006), *Yarrowia lipolytica* (Hébert et al., 2013), and the myco-parasitic fungus *Clonostachys rosea* (Xu et al., 2018), methionine can be degraded cellularly through Ehrlich and demethiolation pathways into VOSCs by different steps (Kagkli et al., 2006). Even with poor enrichment of the genes that encode the enzymes of the Ehrlich pathway in *C. albicans*, essential genes in this pathway were detected in the RNA-seq data, including the upregulated aminotransferases (ARO8, 3-fold and ARO9, 2.4-fold) and oxidoreductases (ADH5, 2-fold and ADH4, 102.3-fold) (**Fig. 4B**). Cysteine catabolism was investigated previously in *C. albicans* in which the cells responded to high levels of cysteine by activation of the transcription factor Zcf2p (expression upregulated 3.46-fold) which regulates the cysteine dioxygenase Cdg1

(expression upregulated 3.5-fold) to convert cysteine to sulfite. As a result, the toxic accumulation of sulfite is exported via the highly upregulated sulfite flux pump, Ssu1 (expression upregulated 32-fold) (**Fig. 4B**) (Hennicke et al., 2013).

Sulfur amino acid biosynthesis and catabolism are regulated by Met4p, which is naturally inactivated by excess levels of methionine and cysteine. The *MET4*Δ mutant was inhibited by SH9051 treatment even with methionine and cysteine additions (**Fig 6D-F**), indicating that the SH9051 caused the same effects of excess levels of these amino acids. Because methionine intracellularly shuttles organic nitrogen and the amino acids play a key role in intracellular nitrogen availability in eukaryotic cells (Pratelli & Pilot, 2014), SH9051, as a nitrogenous compound, could increase intracellular nitrogen overabundance. The upregulation of nitrogen catabolite repression pathway genes, which control the detoxification of poor nitrogen supply, *GAT1, GZF3,* and *UGA3* (upregulated by 1.77-, 2.02-, and 1.52-fold, respectively) was detected. The activation of this pathway has also been reported as a response to high-toxic level of ammonium in *S. cerevisiae* by increasing amino acid excretion (Hess et al., 2006). In *C. rosea,* the activation of the Ehrlich pathway and demethiolation in response to highly exogenous methionine was regulated by nitrogen catabolite repression (Xu et al., 2018). For *C. albicans*, in addition to upregulation of the nitrogen catabolite repression pathway that is associated with sulfur amino acid catabolism (Chebaro et al., 2017), the arginine biosynthesis pathway has been linked to the urea cycle (Jastrzębowska & Gabriel, 2015). Under poor nitrogen supply, the arginine biosynthesis pathway is induced in order to regulate the urea amidolyase, Dur1,2 (expression upregulated by 9-fold), which converts the excess nitrogen to CO_2 and ammonia in order to export the later out of the cell through the upregulated ammonia

transport pumps (*DUR3* 1.8- fold, *MEP1* 3- fold, *ATO5* 4.7- fold, *TOP2* 1.8- fold, *TPO4* 1.6- fold, *FLU1* 2.6-fold, *RTA2* 6.8-fold) (Vylkova et al., 2011).

CONCLUSION

In this study, the RNA-seq technique comprehensively presented the molecular mechanisms behind the inhibitory activity of aurones SH1009 and SH9051 against *C. albicans* cells and interpreted the selectivity of SH1009 against fungal cells. The diminished trehalose levels combined with elevated intracellular ROS content synergistically contribute to cell damage, ultimately affecting RNA processing and ribosome biogenesis, which could be a promising therapeutic strategy by making *C. albicans* more vulnerable to the host immune oxidative burst. Targeting the trehalose metabolic biosynthesis pathway has been identified as an attractive target for antifungal drug development, not only because of the important role of trehalose in progressing the *Candida* infection (Perfect et al., 2017), but also because of the absence of any functional trehalose synthase gene in vertebrates (Argüelles, 2017), which makes SH1009 relatively non-toxic for human cells (Alqahtani et al., 2019). The sulfate assimilation pathway has also been recognized as a favorable antifungal target since humans cannot synthesize methionine like yeasts (Jastrzębowska & Gabriel, 2015). However, the nitrogen atom in SH9051 could increase urea levels in human cells as a nitrogenous waste product because, in mammals, excess nitrogen is excreted as urea (Wright, 1995), which could explain the low selectivity index of SH9051. The paralleled analysis of the transcriptional responses of the aurone SH1009 and SH9051 simultaneously allowed us to examine the overlapping enrichment terms between the repressed and induced transcriptomic profiles, clarifying the antifungal roles for the C ring structure and functional groups. The knowledge gathered in this work can be used for development and design of more efficient aurone compounds with highly selective

toxicity and pave the way for a better understanding of how the molecular mechanisms exerted by these compounds can be exploited for a therapeutic approach.

References

Alqahtani, F. M., Arivett, B. A., Taylor, Z. E., Handy, S. T., Farone, A. L., & Farone, M. B. (2019). Chemogenomic profiling to understand the antifungal action of a bioactive aurone compound. *PLoS One*, *14*(12), e0226068. https://doi.org/10.1371/journal.pone.0226068

Argüelles, J. C. (2017). Trehalose as antifungal target: The picture is still incomplete. *Virulence*, *8*(2), 237-238. https://doi.org/10.1080/21505594.2016.1215797

Askew, C., Sellam, A., Epp, E., Hogues, H., Mullick, A., Nantel, A., & Whiteway, M. (2009). Transcriptional regulation of carbohydrate metabolism in the human pathogen *Candida albicans*. *PLoS Pathog*, *5*(10), e1000612. https://doi.org/10.1371/journal.ppat.1000612

Baldim, J. L., de Alcântara, B. G. V., Domingos, O. D. S., Soares, M. G., Caldas, I. S., Novaes, R. D., Oliveira, T. B., Lago, J. H. G., & Chagas-Paula, D. A. (2017). The Correlation between Chemical Structures and Antioxidant, Prooxidant, and Antitrypanosomatid Properties of Flavonoids. *Oxid Med Cell Longev*, *2017*, 3789856. https://doi.org/10.1155/2017/3789856

Basenko, E. Y., Pulman, J. A., Shanmugasundram, A., Harb, O. S., Crouch, K., Starns, D., Warrenfeltz, S., Aurrecoechea, C., Stoeckert, C. J., Jr., Kissinger, J. C., Roos, D. S., & Hertz-Fowler, C. (2018). FungiDB: An Integrated Bioinformatic Resource for Fungi and Oomycetes. *J Fungi (Basel)*, *4*(1). https://doi.org/10.3390/jof4010039

Bolger, A. M., Lohse, M., & Usadel, B. (2014). Trimmomatic: a flexible trimmer for Illumina sequence data. *Bioinformatics*, *30*(15), 2114-2120. https://doi.org/10.1093/bioinformatics/btu170

Boyle, E. I., Weng, S., Gollub, J., Jin, H., Botstein, D., Cherry, J. M., & Sherlock, G. (2004). GO::TermFinder--open source software for accessing Gene Ontology information and finding significantly enriched Gene Ontology terms associated with a list of genes. *Bioinformatics*, *20*(18), 3710-3715. https://doi.org/10.1093/bioinformatics/bth456

Brown, A. J., Brown, G. D., Netea, M. G., & Gow, N. A. (2014). Metabolism impacts upon *Candida* immunogenicity and pathogenicity at multiple levels. *Trends Microbiol*, *22*(11), 614-622. https://doi.org/10.1016/j.tim.2014.07.001

Brown, G. D., Denning, D. W., Gow, N. A. R., Levitz, S. M., Netea, M. G., & White, T. C. (2012). Hidden killers: human fungal infections. *Sci. Transl. Med.*, *4*(165), 165rv113, 110 pp. https://doi.org/10.1126/scitranslmed.3004404

Carillo, P., Feil, R., Gibon, Y., Satoh-Nagasawa, N., Jackson, D., Bläsing, O. E., Stitt, M., & Lunn, J. E. (2013). A fluorometric assay for trehalose in the picomole range. *Plant Methods*, *9*(1), 21. https://doi.org/10.1186/1746-4811-9-21

Chakravarti, A., Camp, K., McNabb, D. S., & Pinto, I. (2017). The Iron-Dependent Regulation of the *Candida albicans* Oxidative Stress Response by the CCAAT-Binding Factor. *PloS one*, *12*(1), e0170649-e0170649. https://doi.org/10.1371/journal.pone.0170649

Chaves, G. M., Bates, S., Maccallum, D. M., & Odds, F. C. (2007). *Candida albicans* GRX2, encoding a putative glutaredoxin, is required for virulence in a murine model. *Genet Mol Res*, *6*(4), 1051-1063.

Chebaro, Y., Lorenz, M., Fa, A., Zheng, R., & Gustin, M. (2017). Adaptation of *Candida albicans* to Reactive Sulfur Species. *Genetics*, *206*(1), 151-162. https://doi.org/10.1534/genetics.116.199679

Chen, C., Pande, K., French, S. D., Tuch, B. B., & Noble, S. M. (2011). An iron homeostasis regulatory circuit with reciprocal roles in *Candida albicans* commensalism and pathogenesis. *Cell Host Microbe*, *10*(2), 118-135. https://doi.org/10.1016/j.chom.2011.07.005

Coulomb, B., Robert-Peillard, R., Palacio, E., Di Rocco, R., & Boudenne, J.-L. (2017). Fast microplate assay for simultaneous determination of thiols and dissolved sulfides in wastewater. *Microchemical Journal*, *132*, 205 - 210. https://doi.org/10.1016/j.microc.2017.01.022

Dantas, A. S., Patterson, M. J., Smith, D. A., Maccallum, D. M., Erwig, L. P., Morgan, B. A., & Quinn, J. (2010). Thioredoxin regulates multiple hydrogen peroxide-induced signaling pathways in *Candida albicans*. *Mol Cell Biol*, *30*(19), 4550-4563. https://doi.org/10.1128/mcb.00313-10

Eghbaliferiz, S., & Iranshahi, M. (2016). Prooxidant Activity of Polyphenols, Flavonoids, Anthocyanins and Carotenoids: Updated Review of Mechanisms and Catalyzing Metals. *Phytother Res*, *30*(9), 1379-1391. https://doi.org/10.1002/ptr.5643

Fourie, R., Kuloyo, O. O., Mochochoko, B. M., Albertyn, J., & Pohl, C. H. (2018a). Iron at the Centre of. *Front Cell Infect Microbiol*, *8*, 185. https://doi.org/10.3389/fcimb.2018.00185

Fourie, R., Kuloyo, O. O., Mochochoko, B. M., Albertyn, J., & Pohl, C. H. (2018b). Iron at the Centre of *Candida albicans* Interactions. *Front Cell Infect Microbiol*, *8*, 185. https://doi.org/10.3389/fcimb.2018.00185

Gammella, E., Recalcati, S., & Cairo, G. (2016). Dual Role of ROS as Signal and Stress Agents: Iron Tips the Balance in favor of Toxic Effects. *Oxid Med Cell Longev*, *2016*, 8629024. https://doi.org/10.1155/2016/8629024

Gencer, H. K., Kivanç, M., & Turkel, S. (2018). Genetic and biochemical analysis of the reserve carbohydrate metabolism in *Candida albicans* and *Candida rugosa*. *Advanced Studies in Biology*, *10*, 61 - 77

Goecks, J., Nekrutenko, A., Taylor, J., & Team, G. (2010). Galaxy: a comprehensive approach for supporting accessible, reproducible, and transparent computational research in the life sciences. *Genome Biol*, *11*(8), R86. https://doi.org/10.1186/gb-2010-11-8-r86

Gong, Y., Li, T., Yu, C., & Sun, S. (2017). Heat Shock Proteins and Hsps-Associated Signaling Pathways as Potential Antifungal Targets. *Front Cell Infect Microbiol*, *7*, 520. https://doi.org/10.3389/fcimb.2017.00520

González-Párraga, P., Hernández, J. A., & Argüelles, J. C. (2003). Role of antioxidant enzymatic defences against oxidative stress H(2)O(2) and the acquisition of oxidative tolerance in *Candida albicans*. *Yeast*, *20*(14), 1161-1169. https://doi.org/10.1002/yea.1029

Halder, V., Porter, C. B. M., Chavez, A., & Shapiro, R. S. (2019). Design, execution, and analysis of CRISPR-Cas9-based deletions and genetic interaction networks in the fungal pathogen *Candida albicans*. *Nat Protoc*, *14*(3), 955-975. https://doi.org/10.1038/s41596-018-0122-6

Harrison, C., Katayama, S., Dhut, S., Chen, D., Jones, N., Bähler, J., & Toda, T. (2005). SCF(Pof1)-ubiquitin and its target Zip1 transcription factor mediate cadmium response in fission yeast. *EMBO J*, *24*(3), 599-610. https://doi.org/10.1038/sj.emboj.7600536

Hassani, R. A., & Dupuy, C. Detection of Intracellular Reactive Oxygen Species (CM-H 2 DCFDA)

Hennicke, F., Grumbt, M., Lermann, U., Ueberschaar, N., Palige, K., Böttcher, B., Jacobsen, I. D., Staib, C., Morschhäuser, J., Monod, M., Hube, B., Hertweck, C., & Staib, P. (2013). Factors supporting cysteine tolerance and sulfite production in *Candida albicans*. *Eukaryot Cell*, *12*(4), 604-613. https://doi.org/10.1128/EC.00336-12

Hess, D. C., Lu, W., Rabinowitz, J. D., & Botstein, D. (2006). Ammonium toxicity and potassium limitation in yeast. *PLoS Biol*, *4*(11), e351. https://doi.org/10.1371/journal.pbio.0040351

Hsu, P. C., Yang, C. Y., & Lan, C. Y. (2011). *Candida albicans* Hap43 is a repressor induced under low-iron conditions and is essential for iron-responsive transcriptional regulation and virulence. *Eukaryot Cell*, *10*(2), 207-225. https://doi.org/10.1128/EC.00158-10

Hwang, C. S., Baek, Y. U., Yim, H. S., & Kang, S. O. (2003). Protective roles of mitochondrial manganese-containing superoxide dismutase against various stresses in *Candida albicans*. *Yeast*, *20*(11), 929-941. https://doi.org/10.1002/yea.1004

Hébert, A., Forquin-Gomez, M. P., Roux, A., Aubert, J., Junot, C., Heilier, J. F., Landaud, S., Bonnarme, P., & Beckerich, J. M. (2013). New insights into sulfur metabolism in yeasts as revealed by studies of Yarrowia lipolytica. *Appl Environ Microbiol*, *79*(4), 1200-1211. https://doi.org/10.1128/AEM.03259-12

Issi, L., Farrer, R. A., Pastor, K., Landry, B., Delorey, T., Bell, G. W., Thompson, D. A., Cuomo, C. A., & Rao, R. P. (2017). Zinc Cluster Transcription Factors Alter Virulence in *Candida albicans*. *Genetics*, *205*(2), 559-576. https://doi.org/10.1534/genetics.116.195024

Jastrzębowska, K., & Gabriel, I. (2015). Inhibitors of amino acids biosynthesis as antifungal agents. *Amino Acids*, *47*(2), 227-249. https://doi.org/10.1007/s00726-014-1873-1

Jiménez-López, C., Collette, J. R., Brothers, K. M., Shepardson, K. M., Cramer, R. A., Wheeler, R. T., & Lorenz, M. C. (2013). *Candida albicans* induces arginine biosynthetic genes in response to host-derived reactive oxygen species. *Eukaryot Cell*, *12*(1), 91-100. https://doi.org/10.1128/EC.00290-12

Jomová, K., Hudecova, L., Lauro, P., Simunkova, M., Alwasel, S. H., Alhazza, I. M., & Valko, M. (2019). A Switch between Antioxidant and Prooxidant Properties of the Phenolic Compounds Myricetin, Morin, 3',4'-Dihydroxyflavone, Taxifolin and 4-Hydroxy-Coumarin in the Presence of Copper(II) Ions: A Spectroscopic, Absorption Titration and DNA Damage Study. *Molecules*, *24*(23). https://doi.org/10.3390/molecules24234335

Kaba, H. E., Nimtz, M., Müller, P. P., & Bilitewski, U. (2013). Involvement of the mitogen activated protein kinase Hog1p in the response of *Candida albicans* to iron availability. *BMC Microbiol*, *13*, 16. https://doi.org/10.1186/1471-2180-13-16

Kagkli, D. M., Bonnarme, P., Neuvéglise, C., Cogan, T. M., & Casaregola, S. (2006). L-methionine degradation pathway in Kluyveromyces lactis: identification and functional analysis of the genes encoding L-methionine aminotransferase. *Appl Environ Microbiol*, *72*(5), 3330-3335. https://doi.org/10.1128/AEM.72.5.3330-3335.2006

Kim, D., Langmead, B., & Salzberg, S. L. (2015). HISAT: a fast spliced aligner with low memory requirements. *Nat Methods*, *12*(4), 357-360. https://doi.org/10.1038/nmeth.3317

Kullberg, B. J., & Arendrup, M. C. (2015). Invasive candidiasis. *N. Engl. J. Med.*, *373*(15), 1445-1456. https://doi.org/10.1056/NEJMra1315399

Lage, P., Sampaio-Marques, B., Ludovico, P., Mira, N. P., & Mendes-Ferreira, A. (2019). Transcriptomic and chemogenomic analyses unveil the essential role of Com2-regulon in response and tolerance of. *Microb Cell*, *6*(11), 509-523. https://doi.org/10.15698/mic2019.11.697

Landaud, S., Helinck, S., & Bonnarme, P. (2008). Formation of volatile sulfur compounds and metabolism of methionine and other sulfur compounds in fermented food. *Appl Microbiol Biotechnol*, *77*(6), 1191-1205. https://doi.org/10.1007/s00253-007-1288-y

Law, C. W., Chen, Y., Shi, W., & Smyth, G. K. (2014). voom: Precision weights unlock linear model analysis tools for RNA-seq read counts. *Genome Biol*, *15*(2), R29. https://doi.org/10.1186/gb-2014-15-2-r29

Leggett, R. M., Ramirez-Gonzalez, R. H., Clavijo, B. J., Waite, D., & Davey, R. P. (2013). Sequencing quality assessment tools to enable data-driven informatics for high throughput genomics. *Front Genet*, *4*, 288. https://doi.org/10.3389/fgene.2013.00288

Liao, Y., Smyth, G. K., & Shi, W. (2014). featureCounts: an efficient general purpose program for assigning sequence reads to genomic features. *Bioinformatics*, *30*(7), 923-930. https://doi.org/10.1093/bioinformatics/btt656

Lin, C. J., & Chen, Y. L. (2018). Conserved and Divergent Functions of the cAMP/PKA Signaling Pathway in. *J Fungi (Basel)*, *4*(2). https://doi.org/10.3390/jof4020068

Ljungdahl, P. O., & Daignan-Fornier, B. (2012). Regulation of amino acid, nucleotide, and phosphate metabolism in Saccharomyces cerevisiae. *Genetics*, *190*(3), 885-929. https://doi.org/10.1534/genetics.111.133306

Mayer, F. L., Wilson, D., Jacobsen, I. D., Miramón, P., Slesiona, S., Bohovych, I. M., Brown, A. J., & Hube, B. (2012). Small but crucial: the novel small heat shock protein Hsp21 mediates stress adaptation and virulence in *Candida albicans*. *PLoS One*, *7*(6), e38584. https://doi.org/10.1371/journal.pone.0038584

Miramón, P., & Lorenz, M. C. (2017). A feast for Candida: Metabolic plasticity confers an edge for virulence. *PLoS Pathog*, *13*(2), e1006144. https://doi.org/10.1371/journal.ppat.1006144

Mishra, B. B., & Tiwari, V. K. (2011). Natural products: An evolving role in future drug discovery. *European Journal of Medicinal Chemistry*, *46*(10), 4769-4807. https://doi.org/10.1016/j.ejmech.2011.07.057

Missall, T. A., Lodge, J. K., & McEwen, J. E. (2004). Mechanisms of resistance to oxidative and nitrosative stress: implications for fungal survival in mammalian hosts. *Eukaryot Cell*, *3*(4), 835-846. https://doi.org/10.1128/EC.3.4.835-846.2004

Monteiro, P. T., Oliveira, J., Pais, P., Antunes, M., Palma, M., Cavalheiro, M., Galocha, M., Godinho, C. P., Martins, L. C., Bourbon, N., Mota, M. N., Ribeiro, R. A., Viana, R., Sá-Correia, I., & Teixeira, M. C. (2020). YEASTRACT+: a portal for cross-species comparative genomics of transcription regulation in yeasts. *Nucleic Acids Res*, *48*(D1), D642-D649. https://doi.org/10.1093/nar/gkz859

Monteiro, P. T., Pais, P., Costa, C., Manna, S., Sá-Correia, I., & Teixeira, M. C. (2017). The PathoYeastract database: an information system for the analysis of gene and genomic transcription regulation in pathogenic yeasts. *Nucleic Acids Res*, *45*(D1), D597-D603. https://doi.org/10.1093/nar/gkw817

Ogasawara, A., Iino, Y., Sato, K., Nakajima, Y., Bessho, S., Watanabe, T., Mikami, T., & Matsumoto, T. (2008). Anti-*Candida* activity of sodium sulfite. *Biol Pharm Bull*, *31*(6), 1101-1103. https://doi.org/10.1248/bpb.31.1101

Pedreño, Y., González-Párraga, P., Conesa, S., Martínez-Esparza, M., Aguinaga, A., Hernández, J. A., & Argüelles, J. C. (2006). The cellular resistance against oxidative stress (H2O2) is independent of neutral trehalase (Ntc1p) activity in *Candida albicans*. *FEMS Yeast Research*, *6*(1), 57-62. https://doi.org/10.1111/j.1567-1364.2005.00025.x

Perfect, J. R., Tenor, J. L., Miao, Y., & Brennan, R. G. (2017). Trehalose pathway as an antifungal target. *Virulence*, *8*(2), 143-149. https://doi.org/10.1080/21505594.2016.1195529

Pertea, M., Kim, D., Pertea, G. M., Leek, J. T., & Salzberg, S. L. (2016). Transcript-level expression analysis of RNA-seq experiments with HISAT, StringTie and Ballgown. *Nat Protoc*, *11*(9), 1650-1667. https://doi.org/10.1038/nprot.2016.095

Pertea, M., Pertea, G. M., Antonescu, C. M., Chang, T. C., Mendell, J. T., & Salzberg, S. L. (2015). StringTie enables improved reconstruction of a transcriptome from RNA-seq reads. *Nat Biotechnol*, *33*(3), 290-295. https://doi.org/10.1038/nbt.3122

Petti, A. A., McIsaac, R. S., Ho-Shing, O., Bussemaker, H. J., & Botstein, D. (2012). Combinatorial control of diverse metabolic and physiological functions by transcriptional regulators of the yeast sulfur assimilation pathway. *Mol Biol Cell*, *23*(15), 3008-3024. https://doi.org/10.1091/mbc.E12-03-0233

Prasad, R., Nair, R., & Banerjee, A. (2019). Emerging Mechanisms of Drug Resistance in *Candida albicans*. In I. Sá-Correia (Ed.), *Yeasts in Biotechnology and Human Health: Physiological Genomic Approaches* (pp. 135-153). Springer International Publishing. https://doi.org/10.1007/978-3-030-13035-0_6

Pratelli, R., & Pilot, G. (2014). Regulation of amino acid metabolic enzymes and transporters in plants. *J Exp Bot*, *65*(19), 5535-5556. https://doi.org/10.1093/jxb/eru320

Rajendra, P. (2017). *Candida albicans : Cellular and Molecular Biology* (2nd ed.). Springer Nature.

Rio, D. C., Ares, M., Hannon, G. J., & Nilsen, T. W. (2010). Purification of RNA using TRIzol (TRI reagent). *Cold Spring Harb Protoc*, *2010*(6), pdb.prot5439. https://doi.org/10.1101/pdb.prot5439

Robertson, L. S., Causton, H. C., Young, R. A., & Fink, G. R. (2000). The yeast A kinases differentially regulate iron uptake and respiratory function. *Proc Natl Acad Sci U S A*, *97*(11), 5984-5988. https://doi.org/10.1073/pnas.100113397

Sabina, J., & Brown, V. (2009). Glucose sensing network in *Candida albicans*: a sweet spot for fungal morphogenesis. *Eukaryot Cell*, *8*(9), 1314-1320. https://doi.org/10.1128/EC.00138-09

Serneels, J., Tournu, H., & Van Dijck, P. (2012). Tight control of trehalose content is required for efficient heat-induced cell elongation in *Candida albicans*. *J Biol Chem*, *287*(44), 36873-36882. https://doi.org/10.1074/jbc.M112.402651

Shcherbik, N., & Pestov, D. G. (2019). The Impact of Oxidative Stress on Ribosomes: From Injury to Regulation. *Cells*, *8*(11). https://doi.org/10.3390/cells8111379

Shenton, D., Smirnova, J. B., Selley, J. N., Carroll, K., Hubbard, S. J., Pavitt, G. D., Ashe, M. P., & Grant, C. M. (2006). Global translational responses to oxidative

stress impact upon multiple levels of protein synthesis. *J Biol Chem*, *281*(39), 29011-29021. https://doi.org/10.1074/jbc.M601545200

Shrestha, S. K., Fosso, M. Y., & Garneau-Tsodikova, S. (2015). A combination approach to treating fungal infections. *Sci Rep*, *5*, 17070. https://doi.org/10.1038/srep17070

Singh, R. P., Prasad, H. K., Sinha, I., Agarwal, N., & Natarajan, K. (2011). Cap2-HAP complex is a critical transcriptional regulator that has dual but contrasting roles in regulation of iron homeostasis in *Candida albicans*. *J Biol Chem*, *286*(28), 25154-25170. https://doi.org/10.1074/jbc.M111.233569

Sutton, C. L., Taylor, Z. E., Farone, M. B., & Handy, S. T. (2017). Antifungal activity of substituted aurones. *Bioorg. Med. Chem. Lett.*, *27*(4), 901-903. https://doi.org/10.1016/j.bmcl.2017.01.012

Tao, L., Zhang, Y., Fan, S., Nobile, C. J., Guan, G., & Huang, G. (2017). Integration of the tricarboxylic acid (TCA) cycle with cAMP signaling and Sfl2 pathways in the regulation of CO2 sensing and hyphal development in *Candida albicans*. *PLoS Genet*, *13*(8), e1006949. https://doi.org/10.1371/journal.pgen.1006949

Thammahong, A., Puttikamonkul, S., Perfect, J. R., Brennan, R. G., & Cramer, R. A. (2017). Central Role of the Trehalose Biosynthesis Pathway in the Pathogenesis of Human Fungal Infections: Opportunities and Challenges for Therapeutic Development. *Microbiology and Molecular Biology Reviews*, *81*(2), e00053-00016. https://doi.org/10.1128/mmbr.00053-16

Truong, D. H., Nhung, N. T., & Dao, D. Q. (2020). Iron ions chelation-based antioxidant potential vs. pro-oxidant risk of ferulic
acid: A DFT study in aqueous phase *1185*.

Vylkova, S., Carman, A. J., Danhof, H. A., Collette, J. R., Zhou, H., & Lorenz, M. C. (2011). The fungal pathogen *Candida albicans* autoinduces hyphal morphogenesis by raising extracellular pH. *mBio*, *2*(3), e00055-00011. https://doi.org/10.1128/mBio.00055-11

Wright, P. A. (1995). Nitrogen excretion: three end products, many physiological roles. *J Exp Biol*, *198*(Pt 2), 273-281.

Wysong, D. R., Christin, L., Sugar, A. M., Robbins, P. W., & Diamond, R. D. (1998). Cloning and sequencing of a *Candida albicans* catalase gene and effects of disruption of this gene. *Infect Immun*, *66*(5), 1953-1961. https://doi.org/10.1128/IAI.66.5.1953-1961.1998

Xu, N., Dong, Y., Cheng, X., Yu, Q., Qian, K., Mao, J., Jia, C., Ding, X., Zhang, B., Chen, Y., Zhang, B., Xing, L., & Li, M. (2014). Cellular iron homeostasis mediated by the Mrs4–Ccc1–Smf3 pathway is essential for mitochondrial function, morphogenesis and virulence in *Candida albicans*. *Biochimica et Biophysica Acta (BBA) - Molecular Cell Research*, *1843*(3), 629-639. https://doi.org/https://doi.org/10.1016/j.bbamcr.2013.12.009

Xu, Y. H., Jia, K. Z., & Tang, Y. J. (2018). Regulatory Networks Governing Methionine Catabolism into Volatile Organic Sulfur-Containing Compounds in Clonostachys. *Appl Environ Microbiol*, *84*(22). https://doi.org/10.1128/AEM.01840-18

Zhou, X., Liao, W. J., Liao, J. M., Liao, P., & Lu, H. (2015). Ribosomal proteins: functions beyond the ribosome. *J Mol Cell Biol*, *7*(2), 92-104. https://doi.org/10.1093/jmcb/mjv014

Zinskie, J. A., Ghosh, A., Trainor, B. M., Shedlovskiy, D., Pestov, D. G., & Shcherbik, N. (2018). Iron-dependent cleavage of ribosomal RNA during oxidative stress

in the yeast. *J Biol Chem*, *293*(37), 14237-14248. https://doi.org/10.1074/jbc.RA118.004174

APPENDICES

APPENDIX A

List of gene drive construct and primers.

Name	Seq (5'->3')	Note	Reference
TYE7_ Gene_ Drive	GAGATCCAGAAAACTGAATTGTGCTTGAATACCACTTGTTT AGCCATGAGTTCATTCCAGCAAGAAAATCAATTGAACGCT AACAACAACAACAACAACAATGTCATGAATGAATATATTAGCT ATTCGGTTCCATTATCTCCTGTCACTACAAACGAAAACCCT CAAGATTATTGGATGAACGGTTTGATTGCAAATTCTGTTCC GATCTCGCAAACCACAAGCAACTCCGATATCAATTATAGC CAACCACCAAATCCTATTAACTTCAATTAAAAGTCATTGGT CAATAACTATACTCGAGTATTGCCTCATCAAAGAAACAAT CAAATATTATAGATACTCACTCCATCACGTGATAATTTCAC TGGTATGGAAAAGTGGAAAATTTTATAAAAAAAAAATTTGA TGCCTTTGGCATAGCTGAAACTTCGGCCCAATAGGATTGGA GAATATGTTTTCGCAGCGTTCTTACAATTAAATTGTGGTGG AAGTTCGAGACTTGCGTAAACTATTTTTAATTTGTTGCGCA ATACTGTCTGATGGTTTTAGAGCTAGAAATAGCAAGTTAA AATAAGGCTAGTCCGTTATCAACTTGAAAAAGTGGCACCG AGTCGGTGGTGCGCTCATAACAAAATTGAAAAGGTTTTAG AGCTATGCTGAAAAGCATAGCAAGTTAAAATAAGGCAGTG ATTTTTAATCCAGTCCGTACACAACTTGAAAAAGTGCGCAC CGATTCGGTGCTTTTTTTTGCTTTTGAAAAGACTGCTTTTGA AACTGGTGAAGAAAATGAAACTGAAGCTGAAGCCAAGAA TAATACTAGACTTAATAAGTCGATGATCTTGGAGAAAGCT ACTGAGTATATTCTTCATTTACAGAAAAAGGAAGAAGAAT ACATGGCTGAAAATCAAAAATTAAGAGAACAAGTTATTAA ATTGGGTGGTGAAATATGAGGCGAACGTGGCGAGAAAGG AAGGGAAGAAAGCGAAAGGAGCGGGCGCTAG	gene drive construct to clone the plasmid	This study
PAC6725_F	TCAGTAACATCAAGAGAAAGAAACTGA	Forward universal primer Sanger sequencing to validate gene drive integration into plasmid	Shapiro et al, 2019
PAC6389_R	ACAGTTGCGTAGCCTGAATG	Reverse universal primer Sanger sequencing to validate gene drive integration into plasmid	
oRS110_F	ACTATTAAAGAACGTGGACTCCAACGTCA	Forward primer to test for NEUT5L integration of the plasmid	Shapiro et al, 2019
oRS118_R	CAAGTTTGCACTCTTTTGTCTA	Reverse primer to test for NEUT5L 59 integration of the plasmid	
oRTYE7OUT_F	GGCCATGCATAAAACTCTTGCT	Forward primer to test for TYE7 deletion placed outside the ORF	Primer Blast
oRTYE7OUT_R	TCTCTGTTAACCCTGAACGAGT	Reverse primer to test for TYE7 deletion placed outside the ORF	
oRTYE7-in_F	GCTTTGGAATTCGCTTTTGA	Forward primer to test for TYE7 deletion placed inside the ORF	Asekw et al, 2009
oRTYE7-in_R	CCACCCAAGGAATGATTTTC	Reverse primer to test for TYE7 deletion placed inside the ORF	
oRMET4-in_F	CAGGAAATTGGCAGTAGC	Forward primer to test for MET4 deletion placed inside the ORF	Li et al, 2013
oRMET4-in_R	GTGAAGCAAGAAGGGAAG	Reverse primer to test for MET4 deletion placed inside the ORF	

APPENDIX B

Selectivity index of SH9051.

Table 1: The CC_{50} (cytotoxicity concentration of aurone SH9051 that results in 50% cell inhibition) and the selectivity index (SI) as a fraction between the CC_{50} for the human cell lines divided by the IC_{50} value (91.05 μM) against *C. albicans* SC5314.

Human cell line	**CC_{50}(μM)**	**SI**
THP-1 (ATCC, TIB-202)	**111.2±3.4***	**1.22**
HepG2 (ATCC, HB-8065)	**115.4±1.16**	**1.26**
A549 (ATCC, CCL-185)	**199.2±0.6**	**2.18**

*Mean±SEM.

APPENDIX C

Cytotoxicity assay of SH9051.

The cytotoxic effects of aurone SH9051 on *C. albicans* SC5314 and human cell lines (THP-1, HepG2, and A549). **A)** Significance was calculated using two-way ANOVA to compare the cell viability of *C. albicans* to the viability of human cell lines. *P* values (*** $P \leq 0.001$), (** $P \leq 0.01$), (* $P \leq 0.05$). **B)** Dose-response curves of SH9051 (logarithmic form of molar concentrations) treatment against *C. albicans* SC5314 and human cell lines (THP-1, HepG2, and A549) by graphing the cell viability reading as nonlinear regression using GraphPad Software.

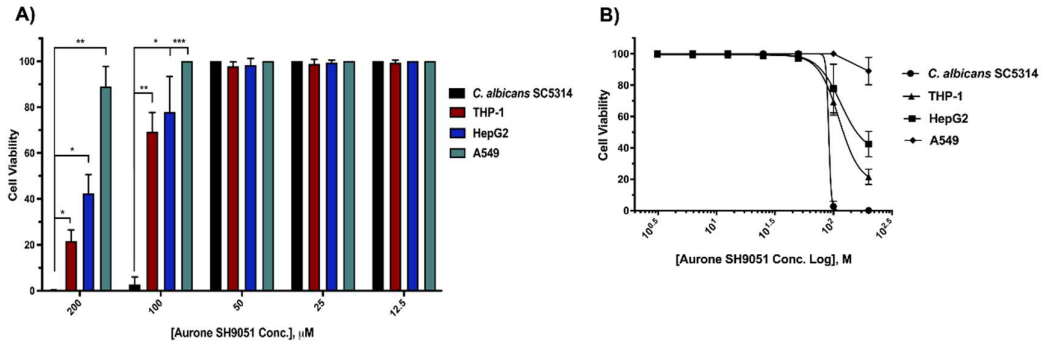

APPENDIX D

RNA samples quantity and integrity.

A) 1% agarose along with 1% v/v bleach TAE gel. Each well was loaded with 2 µL 6× DNA Loading dye + 10 µL of ≥ 1.5 µg of total RNA isolated from SH1009- and SH9051-treated, and untreated *Candida albicans* SC5314 cells. All samples were run for ~30 min at a constant 120V in 1% TAE buffer. The presence of clean 2:1 ratios of 28S and 18S ribosomal RNA (rRNA) bands suggested intact RNA samples without DNA contamination. **B)** Agilent Bioanalyzer analysis of RNA integrity. The fluorescence signal generated by the Agilent Bioanalyzer instrument indicated intact RNA samples with RIN (RNA Integrity Number) values range from 9.7 to 10 with two discrete peaks corresponding to 18S and 28S rRNA bands on the gel.

A)

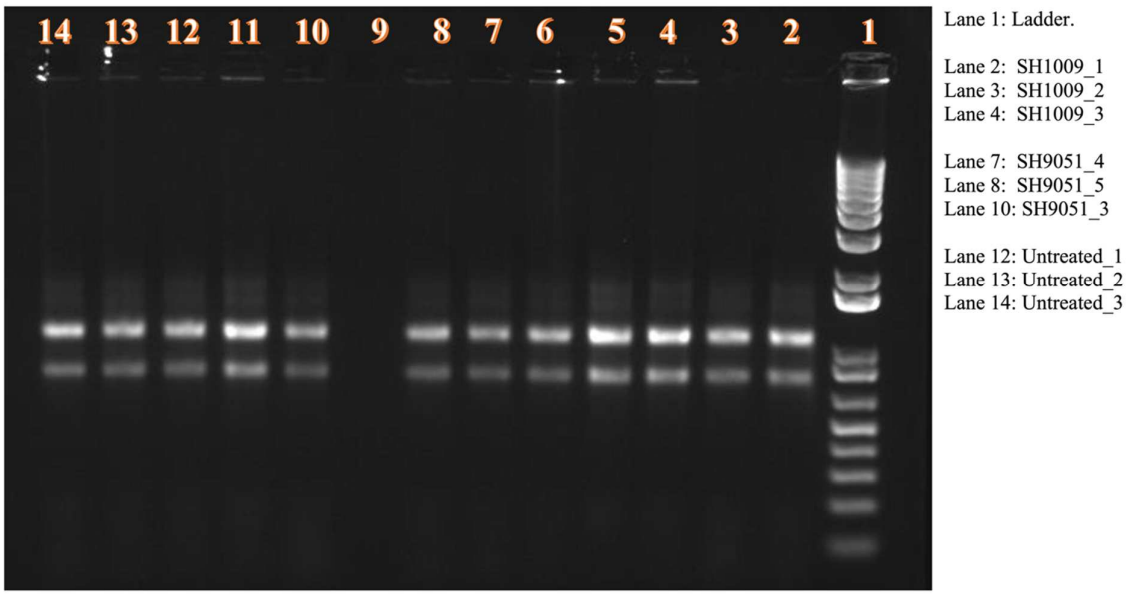

B)

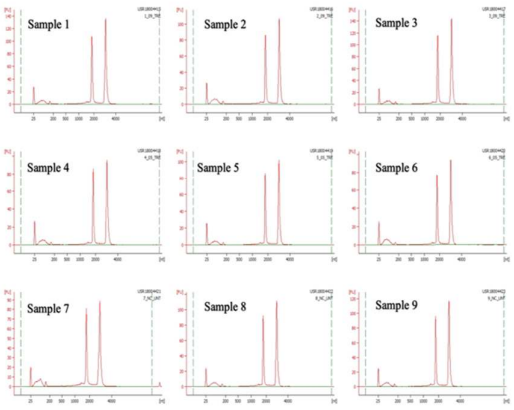

Sample Nr.	Sample Name	Amt. (µg)	$260/280_{ratio}$	RIN
1	SH1009_1	2.550	2.09	10
2	SH1009_2	1.890	2.06	10
3	SH1009_3	2.340	2.10	10
4	SH9051_1	1.750	2.08	9.9
5	SH9051_2	1.550	2.00	10
6	SH9051_3	1.630	2.03	10
7	Untreated_1	2.620	2.10	9.7
8	Untreated_2	1.770	2.00	10
9	Untreated_3	1.900	2.06	10

APPENDIX E

Diagnosis plots of RNA-seq data quality.

A) The quality assessment of mapped reads showed high alignment accuracy with an average of 94.88% mapping rate, HISAT2 tool. **B)** The distribution of fragment coverage for all the 9 samples showed that < 10% of sampled base pairs have up to 1000 overlapping reads, indicating a uniformly sufficient sequencing depth, plotCoverage tool. **C)** The distribution of filtered counts, using a counts per million (CPM) threshold of one to remove low-count genes, showed consistent frequency profiles for all the samples, indicating high quality of RNA purification and library preparation steps with no difference in RNA composition among the samples, Limma-voom tool. **D)** The distribution of normalized counts showed a straight blue line crosses the gene expression at the median level evenly, indicating a proper normalization method, Limma-voom tool.

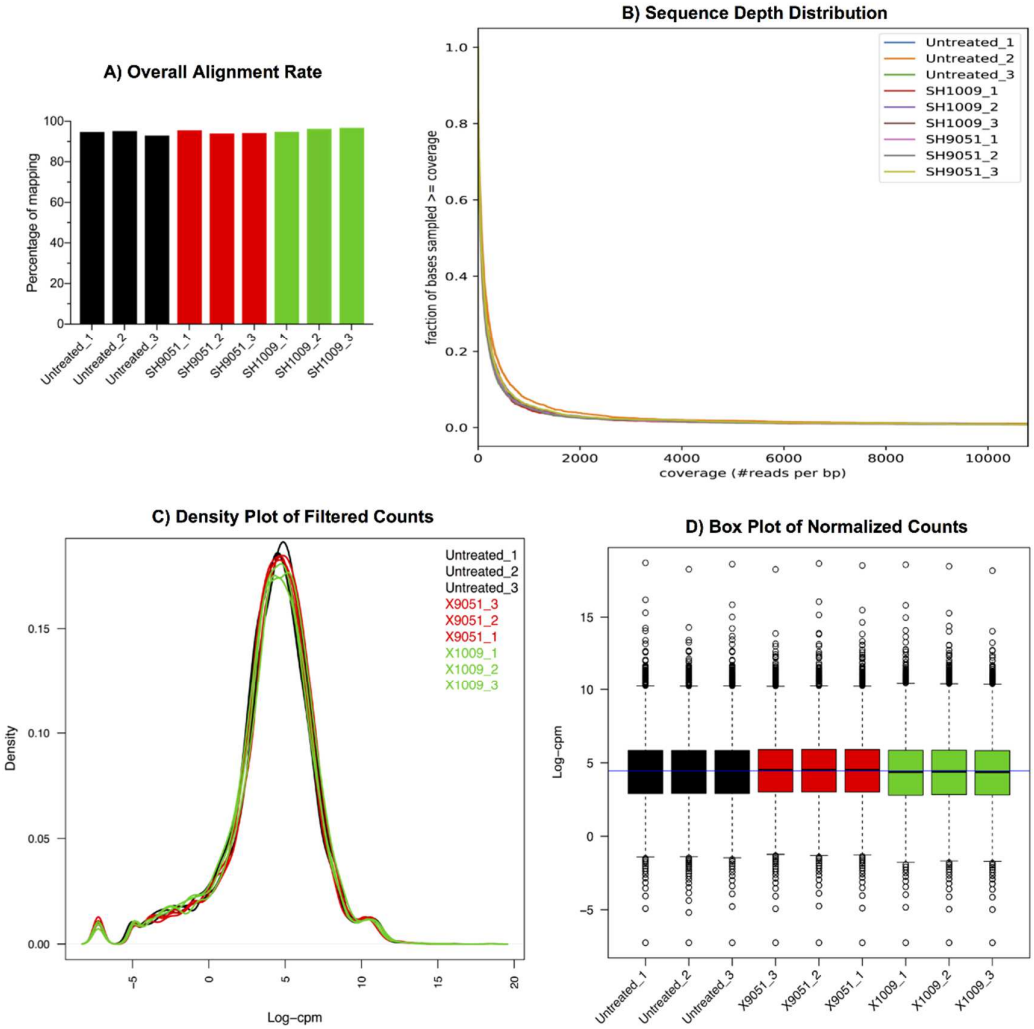

APPENDIX F

Verification of mutant genotypes.

A) Confirmation of generation of *TYE7*Δ mutant by PCR and gel electrophoresis where the *TYE7*Δ[1] band (~ 478 bp) confirmed the replacement of *TYE7* gene sequence with the gene drive cassette, WT[2] band (~ 221 bp) confirmed the presence of *TYE7* gene in wild type and the deletion of *TYE7* gene sequence in *TYE7*Δ mutant, *TYE7*Δ[3] band (~ 747 bp) confirmed the integration of Cas9 plasmid into *C. albicans* genome at the NEUT5L locus. **B)** Confirmation of *MET4*Δ genotype by PCR and gel electrophoresis where the WT[4] band (~ 224 bp) confirmed the presence of *MET4* gene in wild type and the deletion of *MET4* gene sequence in *MET4*Δ mutant. **C)** Growth of *C. albicans* SC5314 wild type and *MET4*Δ mutant in rich agar media (YPD), Minimal Media (MM), and Complete Minimal (CM) dropout media (synthetic mix minus methionine and cysteine) with or without addition of methionine and/or cysteine at 40 µg/mL final concentration. **D)** The integrated-plasmid NEUT5L did not show a defective effect on fungal fitness.

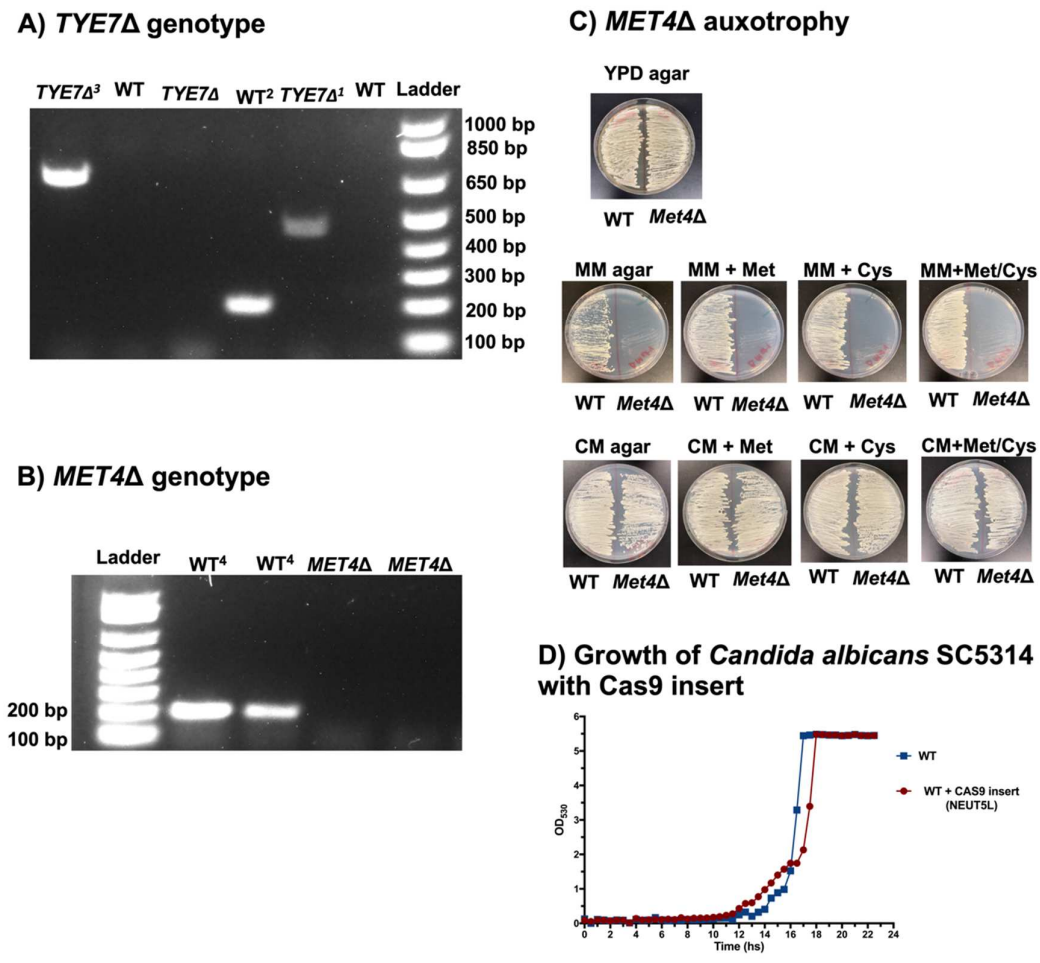

APPENDIX G

Growth curves of SH1009+$FeCl_3$ treatments.

(A, B, and **C)** The growth curves of *C. albicans* SC5314 wild-type strain and the *TYE7*Δ mutant under the IC_{50} concentration of aurone SH1009 (16 µM) with supplement of different concentrations of $FeCl_3$ (50, 25, and 12,5 µM). The growth conditions were carried out in YPD broth media using the Bioscreen C growth curve instrument and the OD_{530} reads were recorded at 30 min intervals for 24 h incubation at 30℃. **D)** The growth curves of *C. albicans* SC5314 wild-type strain and the *MET4*Δ mutant under the IC_{50} concentration of aurone SH9051 (90 µM) with supplement of 20 mM cysteine showed insignificant differences in growth for the wild type and mutant strain in contrast to treatment with 10 mM cysteine (in the main manuscript) that produced more susceptible growth for the *MET4*Δ mutant (**Figure 6F**).

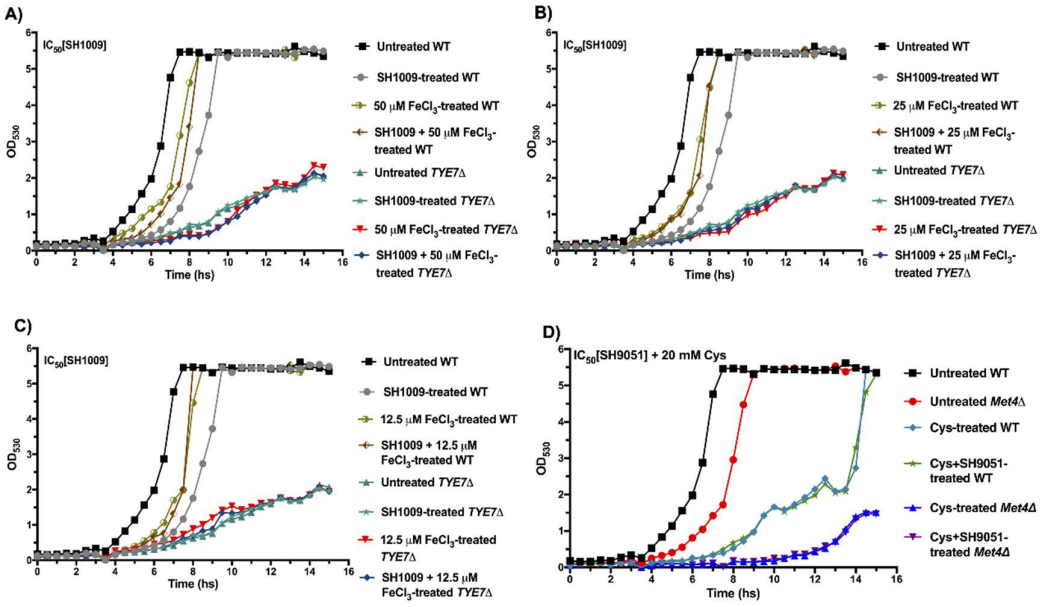

CONCLUSION

As an initial step in the drug discovery of novel antifungal agents against the most prevalent causal agents (*Candida* spp.) of healthcare-associated invasive fungal infections, this study aimed to assess the antifungal activity and selectivity of bioactive aurone compounds SH1009 and SH9051, and to study the cellular and molecular mechanisms of these aurones against *C. albicans*.

Therefore, aurone SH1009 was investigated for antifungal activity and pharmacodynamic properties to indicate selectively fungistatic-inhibitory activity against *Candida* spp., including resistant isolates. These studies highlighted this aurone as modulating the resistant mechanisms of these resistant strains. Cellular responses of haploinsufficiency and homozygous *S. cerevisiae* genome-wide mutant collections under SH1009 treatment suggested that SH1009 targets cell cycle-dependent organization of the actin cytoskeleton. Accordingly, phenotypic studies were conducted in *C. albicans*, demonstrating G1 phase-cells accumulation of abnormally depolarized actin cytoskeleton. These observations were further validated by quantifying differential expression in cell cycle and actin polarization genes under SH1009 treatment.

In the second chapter of this work, the project was expanded by including SH9051 as a bioactive aurone with a different functional group to explore the impact of different aurone derivatives on aurone inhibitory activity. First, we investigated the possibility of any antifungal synergy since both aurones possess the same chemical-core structure. The checkboard assay resulted in a neutral interaction, suggesting different mode of actions for the aurones. In addition, the toxicity rate of these aurones showed selective inhibitory activity of SH1009 toward *C. albicans* cells with high

selectivity indexes, ranging from 8.6 to more than 12 times difference in 50% cell viability loss between the fungal and human cells. In contrast, SH9051 showed poor selectivity indexes (1.22-2.18), supporting the observation from the checkboard assay of targeting different molecular pathways.

RNA-sequencing comprehensively presented the cellular effects and the molecular targets behind the inhibitory activity of aurones SH1009 and SH9051 against *C. albicans* cells, and most importantly, interpreted the selectivity differences between SH1009 and SH9051 toward fungal cells. The paralleled analysis of the transcriptional responses to aurones SH1009 and SH9051 in *C. albicans* cells allowed us to statistically examine the variability in gene expression profiles which demonstrated high variance between SH1009- and SH9051-treated groups and indicated independent transcriptional responses. Enrichment analyses showed uniquely repressed alterations in different metabolic pathways, carbon versus sulfur metabolism in SH1009 and SH9051 treatments, respectively. Furthermore, cross-transcriptomic profile analyses revealed overlapping enrichment terms between the repressed and induced genes, which aided in speculation on the molecular effects of C ring structures as the base of any aurone skeleton and the respective impact of different functional groups.

Additional genetical and biochemical experimental analyses determined that functional groups in aurone SH1009 uniquely targeted the trehalose biosynthesis pathway, rendering *C. albicans* more vulnerable to ROS and resulting in more cleavages in ribosomal RNA. However, the functional group in SH9051 uniquely increased nitrogen overabundance, leading to sulfur amino acid catabolism and increasing sulfite production. In addition to the roles of functional groups in both aurones in generating ROS, studying the phenyl aurone evidenced the central role of

the C ring structures in ROS production via catalyzing iron ions, thus highlighting prooxidative stress as a common cellular effect for aurone compounds.

The results of this project concluded that aurone SH1009 has high eligibility as a promising antifungal by selectively targeting the most desirable target in the antifungal drug discovery field, the oxidative stress protectant (trehalose biosynthesis pathway). The functional groups of aurone SH1009 and their positions can be used in the future as fundamental structures for chemical modification to increase antifungal activity and/or selective toxicity for human cells. The current study provides experimental frameworks for future mechanistic studies that could be used to investigate the bioactivity of a large number of aurone compounds with different functional groups and the search for novel molecular mechanisms in fungi with favorable selectivity for survival of human cells.

REFERENCES

One Health: Fungal Pathogens of Humans, Animals, and Plants: Report on an American Academy of Microbiology Colloquium held in Washington, DC, on October 18, 2017. Washington (DC): American Society for Microbiology; 2019. Available from:https://www.ncbi.nlm.nih.gov/books/NBK549988/ doi: 10.1128/AAMCol.18Oct.2017

Aldholmi, M., Marchand, P., Ourliac-Garnier, I., Le Pape, P., & Ganesan, A. (2019). A Decade of Antifungal Leads from Natural Products: 2010-2019. *Pharmaceuticals (Basel)*, *12*(4). https://doi.org/10.3390/ph12040182

Alexander, B. D., Johnson, M. D., Pfeiffer, C. D., Jiménez-Ortigosa, C., Catania, J., Booker, R., Castanheira, M., Messer, S. A., Perlin, D. S., & Pfaller, M. A. (2013). Increasing echinocandin resistance in Candida glabrata: clinical failure correlates with presence of FKS mutations and elevated minimum inhibitory concentrations. *Clin Infect Dis*, *56*(12), 1724-1732. https://doi.org/10.1093/cid/cit136

Alsaif, G. A., N. Hawkins, I. Taylor, Z. Knott, D. Handy, S. Altman, E. Gao, Y. (2017). Evaluation of Fourteen Aurone Derivatives as Potential Anti-Cancer Agents. In (Vol. 18, pp. 384): Current Pharmaceutical Biotechnology.

Ankhi, D. (2019). *Candidiasis. Introduction to Clinical Infectious Diseases.* . Springer, Cham.

Aldholmi, M., Marchand, P., Ourliac-Garnier, I., Le Pape, P., & Ganesan, A. (2019). A Decade of Antifungal Leads from Natural Products: 2010-2019. *Pharmaceuticals (Basel)*, *12*(4). https://doi.org/10.3390/ph12040182

Alexander, B. D., Johnson, M. D., Pfeiffer, C. D., Jiménez-Ortigosa, C., Catania, J., Booker, R., Castanheira, M., Messer, S. A., Perlin, D. S., & Pfaller, M. A. (2013). Increasing echinocandin resistance in Candida glabrata: clinical failure correlates with presence of FKS mutations and elevated minimum inhibitory concentrations. *Clin Infect Dis*, *56*(12), 1724-1732. https://doi.org/10.1093/cid/cit136

Alsaif, G. A., N. Hawkins, I. Taylor, Z. Knott, D. Handy, S. Altman, E. Gao, Y. (2017). Evaluation of Fourteen Aurone Derivatives as Potential Anti-Cancer Agents. In (Vol. 18, pp. 384): Current Pharmaceutical Biotechnology.

Bondaryk, M., KurzAtkowski, W., & Staniszewska, M. (2013). Antifungal agents commonly used in the superficial and mucosal candidiasis treatment: mode of action and resistance development. *Postepy Dermatol Alergol*, *30*(5), 293-301.

Bongomin, F., Gago, S., Oladele, R. O., & Denning, D. W. (2017). Global and Multi-National Prevalence of Fungal Diseases-Estimate Precision. *J Fungi (Basel)*, *3*(4). https://doi.org/10.3390/jof3040057

Chen, Y., He, Y., Zhang, W., Huang, Y., Fu, J., Fu, F., & Zhou, Y. (2020). Pathogenic characteristics of nosocomial infections in patients with cerebrovascular diseases and characteristics and treatment of pathogenic bacteria in different seasons. *J Infect Public Health*, *13*(5), 800-805. https://doi.org/10.1016/j.jiph.2019.11.010

Di Santo, R. (2010). Natural products as antifungal agents against clinically relevant pathogens. *Nat Prod Rep*, *27*(7), 1084-1098. https://doi.org/10.1039/b914961a

Dimopoulos, G., Ntziora, F., Rachiotis, G., Armaganidis, A., & Falagas, M. E. (2008). Candida albicans versus non-albicans intensive care unit-acquired bloodstream infections: differences in risk factors and outcome. *Anesth Analg*, *106*(2), 523-529, table of contents. https://doi.org/10.1213/ane.0b013e3181607262

Gillum, A. M., Tsay, E. Y. H., & Kirsch, D. R. (1984). Isolation of the Candida albicans gene for orotidine-5′-phosphate decarboxylase by complementation of S. cerevisiae ura3 and E. coli pyrF mutations. *Molecular and General Genetics MGG*, *198*(1), 179-182. https://doi.org/10.1007/BF00328721

Grossart, H. P., Van den Wyngaert, S., Kagami, M., Wurzbacher, C., Cunliffe, M., & Rojas-Jimenez, K. (2019). Fungi in aquatic ecosystems. *Nat Rev Microbiol*, *17*(6), 339-354. https://doi.org/10.1038/s41579-019-0175-8

Guzman, J. A., Tchokonte, R., & Sobel, J. D. (2011). Septic shock due to candidemia: outcomes and predictors of shock development. *J Clin Med Res*, *3*(2), 65-71. https://doi.org/10.4021/jocmr536w

Höfs, S., Mogavero, S., & Hube, B. (2016). Interaction of Candida albicans with host cells: virulence factors, host defense, escape strategies, and the microbiota. *J Microbiol*, *54*(3), 149-169. https://doi.org/10.1007/s12275-016-5514-0

Jahagirdar, V. L., Davane, M., Aradye, S. C., & Nagoba, B. S. (2018). Candida species as potential nosocomial pathogens – A review. *European journal of general medicine*, *15*, 71-75.

Janbon, G., Quintin, J., Lanternier, F., & d'Enfert, C. (2019). Studying fungal pathogens of humans and fungal infections: fungal diversity and diversity of approaches. *Microbes Infect*, *21*(5-6), 237-245. https://doi.org/10.1016/j.micinf.2019.06.011

Jansson, J. K., & Hofmockel, K. S. (2020). Soil microbiomes and climate change. *Nat Rev Microbiol*, *18*(1), 35-46. https://doi.org/10.1038/s41579-019-0265-7

Jones, T., Federspiel, N. A., Chibana, H., Dungan, J., Kalman, S., Magee, B. B., Newport, G., Thorstenson, Y. R., Agabian, N., Magee, P. T., Davis, R. W., & Scherer, S. (2004). The diploid genome sequence of Candida albicans. *Proc. Natl. Acad. Sci. U. S. A.*, *101*(19), 7329-7334. https://doi.org/10.1073/pnas.0401648101

Kim, J. Y. (2016). Human fungal pathogens: Why should we learn? *J Microbiol*, *54*(3), 145-148. https://doi.org/10.1007/s12275-016-0647-8

Kojic, E. M., & Darouiche, R. O. (2004). Candida infections of medical devices. *Clin Microbiol Rev*, *17*(2), 255-267. https://doi.org/10.1128/cmr.17.2.255-267.2004

Kullberg, B. J., & Arendrup, M. C. (2015). Invasive candidiasis. *N. Engl. J. Med.*, *373*(15), 1445-1456. https://doi.org/10.1056/NEJMra1315399

Köhler, J. R., Casadevall, A., & Perfect, J. (2014). The spectrum of fungi that infects humans. *Cold Spring Harb Perspect Med*, *5*(1), a019273. https://doi.org/10.1101/cshperspect.a019273

Lamoth, F., Lockhart, S. R., Berkow, E. L., & Calandra, T. (2018). Changes in the epidemiological landscape of invasive candidiasis. *J Antimicrob Chemother*, *73*(suppl_1), i4-i13. https://doi.org/10.1093/jac/dkx444

Li, Y., Ren, L., & Zou, J. (2019). Risk Factors and Prevention Strategies of Nosocomial Infection in Geriatric Patients. *Can J Infect Dis Med Microbiol*, *2019*, 6417959. https://doi.org/10.1155/2019/6417959

Morrell, M., Fraser, V. J., & Kollef, M. H. (2005). Delaying the empiric treatment of candida bloodstream infection until positive blood culture results are obtained:

a potential risk factor for hospital mortality. *Antimicrob Agents Chemother*, *49*(9), 3640-3645. https://doi.org/10.1128/AAC.49.9.3640-3645.2005

Méan, M., Marchetti, O., & Calandra, T. (2008). Bench-to-bedside review: Candida infections in the intensive care unit. *Crit Care*, *12*(1), 204. https://doi.org/10.1186/cc6212

Park, H. S., Nelson, D. E., Taylor, Z. E., Hayes, J. B., Cunningham, K. D., Arivett, B. A., Ghosh, R., Wolf, L. C., Taylor, K. M., Farone, M. B., Handy, S. T., & Farone, A. L. (2017). Suppression of LPS-induced NF-κB activity in macrophages by the synthetic aurone, (Z)-2-((5-(hydroxymethyl) furan-2-yl) methylene) benzofuran-3(2H)-one. *Int Immunopharmacol*, *43*, 116-128. https://doi.org/10.1016/j.intimp.2016.12.004

Perfect, J. R. (2016). "Is there an emerging need for new antifungals?". *Expert Opin Emerg Drugs*, *21*(2), 129-131. https://doi.org/10.1517/14728214.2016.1155554

Prasad, R., Nair, R., & Banerjee, A. (2019). Emerging Mechanisms of Drug Resistance in Candida albicans. In I. Sá-Correia (Ed.), *Yeasts in Biotechnology and Human Health: Physiological Genomic Approaches* (pp. 135-153). Springer International Publishing. https://doi.org/10.1007/978-3-030-13035-0_6

Rajendra, P. (2017). *Candida albicans : Cellular and Molecular Biology* (2nd ed.). Springer Nature.

Shor, E., & Perlin, D. S. (2015). Coping with stress and the emergence of multidrug resistance in fungi. *PLoS Pathog*, *11*(3), e1004668. https://doi.org/10.1371/journal.ppat.1004668

Singh, G., & Wulansari, S. G. (2018). Pattern of bacterial and fungal pathogen in patients with high risk for invasive fungal disease in an indonesian tertiary care hospital: an observational study. *Pan Afr Med J*, *29*, 60. https://doi.org/10.11604/pamj.2018.29.60.11931

Skrzypek, M. S., Binkley, J., & Sherlock, G. (2018). Using the Candida Genome Database. *Methods Mol Biol*, *1757*, 31-47. https://doi.org/10.1007/978-1-4939-7737-6_3

Sutton, C. L., Taylor, Z. E., Farone, M. B., & Handy, S. T. (2017). Antifungal activity of substituted aurones. *Bioorg. Med. Chem. Lett.*, *27*(4), 901-903. https://doi.org/10.1016/j.bmcl.2017.01.012

Taylor, L. H., Latham, S. M., & Woolhouse, M. E. (2001). Risk factors for human disease emergence. *Philos Trans R Soc Lond B Biol Sci*, *356*(1411), 983-989. https://doi.org/10.1098/rstb.2001.0888

Treml, J., & Šmejkal, K. (2016). Flavonoids as Potent Scavengers of Hydroxyl Radicals. *Compr Rev Food Sci Food Saf*, *15*(4), 720-738. https://doi.org/10.1111/1541-4337.12204

Vidyasagar, G. M. (2016). Plant-Derived Antifungal Agents: Past and Recent Developments. In A. Basak, R. Chakraborty, & S. M. Mandal (Eds.), *Recent Trends in Antifungal Agents and Antifungal Therapy* (pp. 123-147). Springer India. https://doi.org/10.1007/978-81-322-2782-3_5

Wickes, B. L. (2020). Analysis of a Candida auris Outbreak Provides New Insights into an Emerging Pathogen. *J Clin Microbiol*, *58*(4). https://doi.org/10.1128/JCM.02083-19

Wickes, B. L., & Wiederhold, N. P. (2018). Molecular diagnostics in medical mycology. *Nat Commun*, *9*(1), 5135. https://doi.org/10.1038/s41467-018-07556-5

Bondaryk, M., KurzAtkowski, W., & Staniszewska, M. (2013). Antifungal agents commonly used in the superficial and mucosal candidiasis treatment: mode of action and resistance development. *Postepy Dermatol Alergol*, *30*(5), 293-301.

Bongomin, F., Gago, S., Oladele, R. O., & Denning, D. W. (2017). Global and Multi-National Prevalence of Fungal Diseases-Estimate Precision. *J Fungi (Basel)*, *3*(4). https://doi.org/10.3390/jof3040057

Brown, G. D., Denning, D. W., Gow, N. A. R., Levitz, S. M., Netea, M. G., & White, T. C. (2012). Hidden killers: human fungal infections. *Sci. Transl. Med.*, *4*(165), 165rv113, 110 pp. https://doi.org/10.1126/scitranslmed.3004404

Chen, Y., He, Y., Zhang, W., Huang, Y., Fu, J., Fu, F., & Zhou, Y. (2020). Pathogenic characteristics of nosocomial infections in patients with cerebrovascular diseases and characteristics and treatment of pathogenic bacteria in different seasons. *J Infect Public Health*, *13*(5), 800-805. https://doi.org/10.1016/j.jiph.2019.11.010

Di Santo, R. (2010). Natural products as antifungal agents against clinically relevant pathogens. *Nat Prod Rep*, *27*(7), 1084-1098. https://doi.org/10.1039/b914961a

Dimopoulos, G., Ntziora, F., Rachiotis, G., Armaganidis, A., & Falagas, M. E. (2008). Candida albicans versus non-albicans intensive care unit-acquired bloodstream infections: differences in risk factors and outcome. *Anesth Analg*, *106*(2), 523-529, table of contents. https://doi.org/10.1213/ane.0b013e3181607262

Gillum, A. M., Tsay, E. Y. H., & Kirsch, D. R. (1984). Isolation of the Candida albicans gene for orotidine-5′-phosphate decarboxylase by complementation of S. cerevisiae ura3 and E. coli pyrF mutations. *Molecular and General Genetics MGG*, *198*(1), 179-182. https://doi.org/10.1007/BF00328721

First meeting of the WHO Antifungal Expert Group on Identifying Priority Fungal Pathogens: meeting report. Geneva: World Health Organization; 2020. Licence: CC BY-NC-SA 3.0 IGO.

Grossart, H. P., Van den Wyngaert, S., Kagami, M., Wurzbacher, C., Cunliffe, M., & Rojas-Jimenez, K. (2019). Fungi in aquatic ecosystems. *Nat Rev Microbiol*, *17*(6), 339-354. https://doi.org/10.1038/s41579-019-0175-8

Guzman, J. A., Tchokonte, R., & Sobel, J. D. (2011). Septic shock due to candidemia: outcomes and predictors of shock development. *J Clin Med Res*, *3*(2), 65-71. https://doi.org/10.4021/jocmr536w

Höfs, S., Mogavero, S., & Hube, B. (2016). Interaction of Candida albicans with host cells: virulence factors, host defense, escape strategies, and the microbiota. *J Microbiol*, *54*(3), 149-169. https://doi.org/10.1007/s12275-016-5514-0

Jahagirdar, V. L., Davane, M., Aradye, S. C., & Nagoba, B. S. (2018). Candida species as potential nosocomial pathogens – A review. *European journal of general medicine*, *15*, 71-75.

Janbon, G., Quintin, J., Lanternier, F., & d'Enfert, C. (2019). Studying fungal pathogens of humans and fungal infections: fungal diversity and diversity of approaches. *Microbes Infect*, *21*(5-6), 237-245. https://doi.org/10.1016/j.micinf.2019.06.011

Jansson, J. K., & Hofmockel, K. S. (2020). Soil microbiomes and climate change. *Nat Rev Microbiol*, *18*(1), 35-46. https://doi.org/10.1038/s41579-019-0265-7

Jones, T., Federspiel, N. A., Chibana, H., Dungan, J., Kalman, S., Magee, B. B., Newport, G., Thorstenson, Y. R., Agabian, N., Magee, P. T., Davis, R. W., & Scherer, S. (2004). The diploid genome sequence of Candida albicans. *Proc.*

Natl. Acad. Sci. U. S. A., *101*(19), 7329-7334. https://doi.org/10.1073/pnas.0401648101

Kim, J. Y. (2016). Human fungal pathogens: Why should we learn? *J Microbiol*, *54*(3), 145-148. https://doi.org/10.1007/s12275-016-0647-8

Kojic, E. M., & Darouiche, R. O. (2004). Candida infections of medical devices. *Clin Microbiol Rev*, *17*(2), 255-267. https://doi.org/10.1128/cmr.17.2.255-267.2004

Kullberg, B. J., & Arendrup, M. C. (2015). Invasive candidiasis. *N. Engl. J. Med.*, *373*(15), 1445-1456. https://doi.org/10.1056/NEJMra1315399

Köhler, J. R., Casadevall, A., & Perfect, J. (2014). The spectrum of fungi that infects humans. *Cold Spring Harb Perspect Med*, *5*(1), a019273. https://doi.org/10.1101/cshperspect.a019273

Lamoth, F., Lockhart, S. R., Berkow, E. L., & Calandra, T. (2018). Changes in the epidemiological landscape of invasive candidiasis. *J Antimicrob Chemother*, *73*(suppl_1), i4-i13. https://doi.org/10.1093/jac/dkx444

Li, Y., Ren, L., & Zou, J. (2019). Risk Factors and Prevention Strategies of Nosocomial Infection in Geriatric Patients. *Can J Infect Dis Med Microbiol*, *2019*, 6417959. https://doi.org/10.1155/2019/6417959

Morrell, M., Fraser, V. J., & Kollef, M. H. (2005). Delaying the empiric treatment of candida bloodstream infection until positive blood culture results are obtained: a potential risk factor for hospital mortality. *Antimicrob Agents Chemother*, *49*(9), 3640-3645. https://doi.org/10.1128/AAC.49.9.3640-3645.2005

Méan, M., Marchetti, O., & Calandra, T. (2008). Bench-to-bedside review: Candida infections in the intensive care unit. *Crit Care*, *12*(1), 204. https://doi.org/10.1186/cc6212

Park, H. S., Nelson, D. E., Taylor, Z. E., Hayes, J. B., Cunningham, K. D., Arivett, B. A., Ghosh, R., Wolf, L. C., Taylor, K. M., Farone, M. B., Handy, S. T., & Farone, A. L. (2017). Suppression of LPS-induced NF-κB activity in macrophages by the synthetic aurone, (Z)-2-((5-(hydroxymethyl) furan-2-yl) methylene) benzofuran-3(2H)-one. *Int Immunopharmacol*, *43*, 116-128. https://doi.org/10.1016/j.intimp.2016.12.004

Perfect, J. R. (2016). "Is there an emerging need for new antifungals?". *Expert Opin Emerg Drugs*, *21*(2), 129-131. https://doi.org/10.1517/14728214.2016.1155554

Prasad, R., Nair, R., & Banerjee, A. (2019). Emerging Mechanisms of Drug Resistance in Candida albicans. In I. Sá-Correia (Ed.), *Yeasts in Biotechnology and Human Health: Physiological Genomic Approaches* (pp. 135-153). Springer International Publishing. https://doi.org/10.1007/978-3-030-13035-0_6

Rajendra, P. (2017). *Candida albicans : Cellular and Molecular Biology* (2nd ed.). Springer Nature.

Shor, E., & Perlin, D. S. (2015). Coping with stress and the emergence of multidrug resistance in fungi. *PLoS Pathog*, *11*(3), e1004668. https://doi.org/10.1371/journal.ppat.1004668

Singh, G., & Wulansari, S. G. (2018). Pattern of bacterial and fungal pathogen in patients with high risk for invasive fungal disease in an indonesian tertiary care hospital: an observational study. *Pan Afr Med J*, *29*, 60. https://doi.org/10.11604/pamj.2018.29.60.11931

Skrzypek, M. S., Binkley, J., & Sherlock, G. (2018). Using the Candida Genome Database. *Methods Mol Biol*, *1757*, 31-47. https://doi.org/10.1007/978-1-4939-7737-6_3

Sutton, C. L., Taylor, Z. E., Farone, M. B., & Handy, S. T. (2017). Antifungal activity of substituted aurones. *Bioorg. Med. Chem. Lett.*, *27*(4), 901-903. https://doi.org/10.1016/j.bmcl.2017.01.012

Taylor, L. H., Latham, S. M., & Woolhouse, M. E. (2001). Risk factors for human disease emergence. *Philos Trans R Soc Lond B Biol Sci*, *356*(1411), 983-989. https://doi.org/10.1098/rstb.2001.0888

Treml, J., & Šmejkal, K. (2016). Flavonoids as Potent Scavengers of Hydroxyl Radicals. *Compr Rev Food Sci Food Saf*, *15*(4), 720-738. https://doi.org/10.1111/1541-4337.12204

Vidyasagar, G. M. (2016). Plant-Derived Antifungal Agents: Past and Recent Developments. In A. Basak, R. Chakraborty, & S. M. Mandal (Eds.), *Recent Trends in Antifungal Agents and Antifungal Therapy* (pp. 123-147). Springer India. https://doi.org/10.1007/978-81-322-2782-3_5

Wickes, B. L. (2020). Analysis of a Candida auris Outbreak Provides New Insights into an Emerging Pathogen. *J Clin Microbiol*, *58*(4). https://doi.org/10.1128/JCM.02083-19

Wickes, B. L., & Wiederhold, N. P. (2018). Molecular diagnostics in medical mycology. *Nat Commun*, *9*(1), 5135. https://doi.org/10.1038/s41467-018-07556-5